Complementary tracer tests – SWIW, CEC and multi-hole reciprocal cross flow tests at the TRUE-1 site

TRUE-1 Continuation project
TRUE-1 Completion

Rune Nordqvist, Johan Byegård, Calle Hjerne

Geosigma AB

December 2014

SKB

Complementary tracer tests – SWIW, CEC and multi-hole reciprocal cross flow tests at the TRUE-1 site

TRUE-1 Continuation project
TRUE-1 Completion

Rune Nordqvist, Johan Byegård, Calle Hjerne

Geosigma AB

Abstract

The Tracer Retention Understanding Experiments (TRUE) project at the Äspö HRL (Hard Rock Laboratory) comprise a number of field tracer experiments performed in order to increase the understanding of transport of solutes, especially sorbing radioactive tracers, in fractured rock.

Processes such as diffusion and sorption have been of particular interest. The various experiments within the TRUE project have been performed in laboratory scale (< 0.5 m), detailed scale (5–10 m) and in block scale (10–50 m). Tracer tests at the TRUE-1 site have also been carried out within the TRUE-1 Continuation project. TRUE-1 Continuation is a follow-up to the first TRUE-1 project.

Complementing the TRUE-1 Continuation experimental programme, the TRUE-1 Completion was performed at the TRUE-1 site. The main activity within TRUE-1 Completion has been the injection of epoxy with subsequent over-coring of relevant parts of Feature A and analysis of pore structure and identification of sorption sites. Furthermore, a number of complementary *in situ* experiments were performed prior to epoxy injection in order to collect important additional information about Feature A and the TRUE-1 site before the epoxy injection and subsequent destruction of the site.

This report describes three complementary *in situ* experiments, including pre-tests, performed as part of TRUE-1 Completion: a SWIW test (Single-Well Injection-Withdrawal), a CEC test (Cation Exchange Capacity) and COM tests (multi-hole reciprocal cross flow tests). The target structure for all these tests was Feature A at the TRUE-1 site. Six boreholes intercepting Feature A were used in the experiments.

The experimental configuration for the SWIW test is somewhat unique for studies in fractured rock insofar that it included four peripheral borehole sections for observation of the radially diverging tracer transport. One unexpected result is a very low tracer recovery in the central SWIW borehole section. A hypothetical explanation for this is that the tracer was pushed out too far into the formation during the injection phase and was thereafter lost to groundwater flow in other directions. However, irrespective of the low recovery in the SWIW section, the results from the observation sections clearly demonstrate the heterogeneous nature of the radial solute spreading in the fracture during the water injection phase. Although the distances between the SWIW section and the observation sections are fairly similar, tracer residence times as well as peak tracer concentrations vary over about one magnitude.

The CEC experiment was carried out with the aim of saturating the sorption sites within the transport path. The experiment was carried out with a constant tracer injection concentration in three steps with increasingly higher concentrations. The intention was that the first step would be performed with no or small effects of sorption site limitation and the last step would result in significant sorption site-limitation and preferably site saturation. Although results indicate that effects of site-limitation occur at higher injection concentrations, it is also concluded that the sorption capacity within the flow path was underestimated and that site saturation was not attained during the experiment.

Multi-hole reciprocal cross-flow tests (COM tests) were performed with the purpose of examining and evaluating effects of possible channelling in Feature A. The COM tests consist of a number of hydraulic interference tests with measurements of both pressure and flow responses. The pumping hole was alternated in order to evaluate the hydraulic interference in several directions and whether the responses were corresponding with a reversed flow direction. The flow responses were measured by means of the tracer dilution method under both ambient and pumped conditions.

The COM test resulted in an interpretation of the hydraulic conductivity distribution and connectivity within Feature A. It also shows that the approach of systematic alteration of pumping borehole in combination with registration of both pressure and flow responses may provide a good foundation for a detailed modelling of a feature or site.

Sammanfattning

TRUE-projektet (Tracer Retention Understanding Experiments) vid Äspölaboratoriet innefattar en serie spårämnesförsök i syfte att öka förståelsen av lösta ämnen, i synnerhet sorberande radio-aktiva ämnen, i sprickigt berg. Processer som t.ex. diffusion och sorption är av särskilt intresse. Spårämnesförsöken inom TRUE har gjorts i tre olika skalor: laboratorieskala (< 0.5 m), detaljskala (5–10 m) och blockskala (10–50 m).

En serie med uppföljande spårförsök har genomförts inom projektet TRUE-1 Continuation. Som ytterligare komplement till detta har en rad försök gjorts inom TRUE-1 Completion. Den huvudsakliga aktiviteten inom TRUE-1 Completion har varit injicering av epoxy och efterföljande överborrning av utvalda delar av den s k Feature A. Dessutom har ett antal fältexperiment gjorts innan injiceringen av epoxy i syfte att säkerställa ytterligare information av Feature A innan denna borras ut efter epoxyinjiceringen.

Denna rapport beskriver tre fältförsök utförda som en del av TRUE-1 Completion: ett s k SWIW-test (Single-Well Injection-Withdrawal), ett CEC-försök (Cation Exchange Capacity) samt ett s k COM-test (multi-hole reciprocal cross flow tests). Samtliga fältförsök gjordes inom Feature A. Sex borrhål, borrade genom Feature A, användes för fältförsöken.

Den experimentella konfigurationen för SWIW-försöket är tämligen unik för liknande försök i sprickigt berg såtillvida att fyra omgivande borrhålssektioner finns tillgängliga för att följa den radiellt divergerande spårämnestransporten runt själva SWIW-sektionen. Ett oväntat resultat var ett mycket lågt s k recovery (återvinningsgrad av spårämne) i SWIW-sektionen. En möjlig förklaring är att spårämnet trycks ut alltför långt i berget och därefter förlorats. Bortsett från detta visar dock resultat från de omliggande observationshålen tydligt på en heterogen spridning av spårämnen i sprickan. Trots att avstånden till observationshålen är likartade varierar uppehållstider och maximala koncentrationer med över en storleksordning.

CEC-experimentet strävade efter att mätta sorptionsplatserna i transportvägen för det sorberande spårämnet. Detta försök genomfördes med injicering av spårämne med konstant koncentration i tre steg, med successivt ökad injiceringskoncentration. Intentionen var att det första steget inte skulle ge några tydliga effekter av begränsning av sorptionsplatser medan det sista steget helst skulle innebära mättnad av sorptionsplatser. Resultaten indikerar att effekter av platsbegränsning uppstår vid högre koncentrationer. Dock är en slutsats även att transportvägens sorptionskapacitet var underskattad och att full mättnad av sorptionsplatser inte uppnåddes.

COM-testerna gjordes i syfte att undersöka och utvärdera effekter av möjlig kanalbildning inom Feature A. Testerna består av en serie hydrauliska interferenstester med mätningar av tryck- och flödesresponser. Pumphålen alternerades för att studera interferens i olika riktningar samt att undersöka responsernas överensstämmelse vid ombytt riktning av vattenflödet. Flödesresponserna mättes med hjälp av utspädningsmätningar under både befintliga och pumpade förhållanden. Testerna resulterade in en tolkning av fördelning av hydraulisk konduktivitet och konnektivitet inom Feature A. Dessutom visar försöket att metoden i allmänhet kan vara av stor användning för detaljerad hydraulisk modellering av liknande formationer.

Contents

1   Introduction

The Tracer Retention Understanding Experiments (TRUE) project included several field tracer experiments performed in order to increase the understanding of transport of solutes, especially sorbing radioactive tracers, in fractured rock. Processes such as diffusion and sorption have been of particular interest. The various experiments within the TRUE project have been performed in laboratory scale (<0.5 m), detailed scale (5–10 m) and in block scale (10–50 m). Presently, the First TRUE Stage (TRUE-1) (Winberg et al. 2000), and the TRUE Block Scale parts (Andersson et al. 2002a, b, 2007, Poteri et al. 2002, Winberg et al. 2003) of the programme have been completed. A closely related project is the Long Term Diffusion Experiment (LTDE) (Widestrand et al. 2006, 2010, Byegård et al. 2010).

Tracer tests at the TRUE-1 site have also been carried out within the TRUE-1 Continuation project as reported by Andersson et al. (2002a). TRUE-1 Continuation is a follow-up to the first TRUE-1 project.

As part of the TRUE-1 Continuation experimental programme, it was decided that TRUE-1 Completion should be performed at the TRUE-1 site, see Figure 1-1, complementing already performed experiments. The main activity within TRUE-1 Completion is the injection of epoxy in the fracture with subsequent over-coring of relevant parts of Feature A and analysis of pore structure and identification of sorption sites. Furthermore, a number of complementary *in situ* experiments were performed in order to gather important information from Feature A and the TRUE-1 site before the epoxy injection and subsequent destruction of the site. Prior to the execution of the complementary *in situ* tracer tests, boreholes KXTT3 and KXTT4 were re-instrumented in order to restore the site to the same packer configuration as employed during the STT-tests (Winberg et al. 2000) and to make it possible to conduct the complementary tracer test, epoxy injection and subsequent over-coring. The re-instrumentation, epoxy injection and over-coring are described in Sigurdsson and Hjerne (2014).

This report describes the complementary *in situ* experiments: SWIW test (Single Well Injection Withdrawal test), CEC test (Cation Exchange Capacity test) and COM tests (multi-hole reciprocal cross flow tests), including pre-tests, performed within TRUE-1 Completion mainly during 2006. The target structure for all these tests was Feature A at the TRUE-1 site. Feature A is intercepted by six boreholes, see Figure 1-2. All of the six borehole sections located in Feature A were used in the experiments. However, the flow path between KXTT3:S3 and KXTT4:T3, as illustrated in Figure 1-3, was the only one that was included in all of the experiments. Feature A is interpreted as a single fracture in KXTT3:S3 and as one major (Feature A) and one minor (Feature A') fracture in KXTT4:T3. The flow path in Feature A between KXTT3 and KXTT4 is well characterized in earlier investigations at the TRUE-1 site and reported by Winberg et al. (2000) and Andersson et al. (2002a).
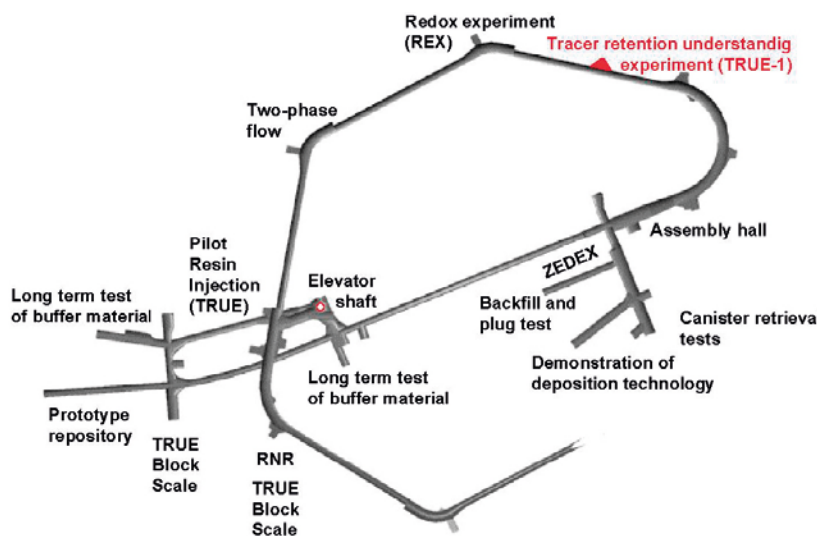
Figure 1-1. Plan view of main experimental level at the Äspö HRL showing the location of the TRUE-1 experiment in red (taken from Winberg et al. 2000).
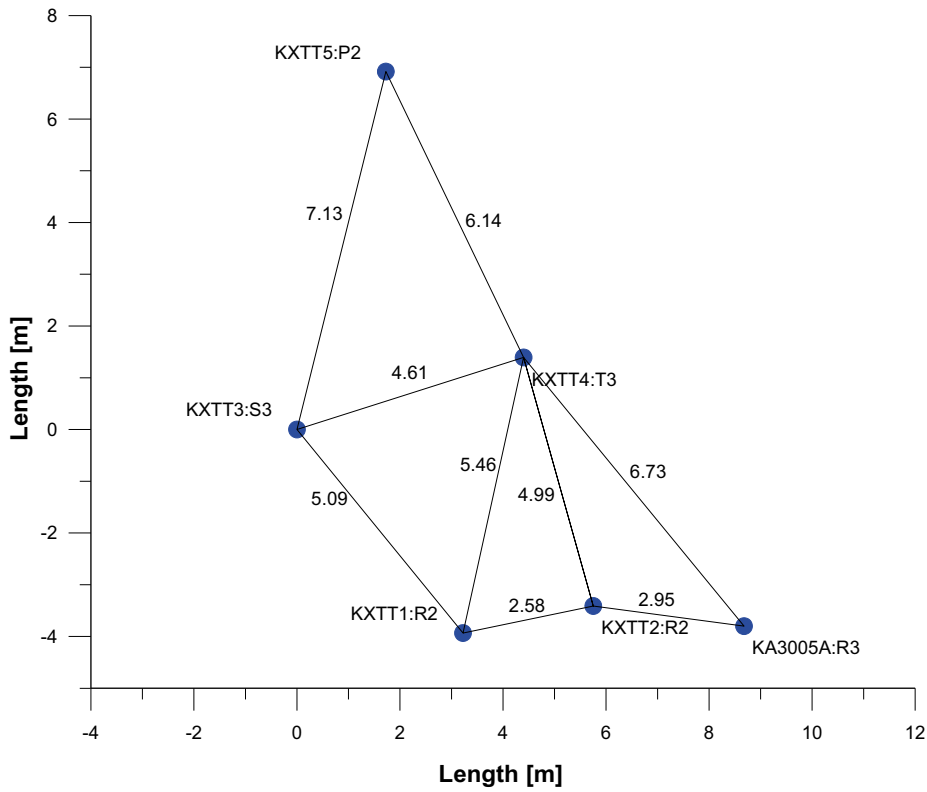
Figure 1-2. *Borehole intersection pattern with Feature A (view normal to the plane of the fracture). Euclidian distances in meters between the boreholes are shown in the figure.*
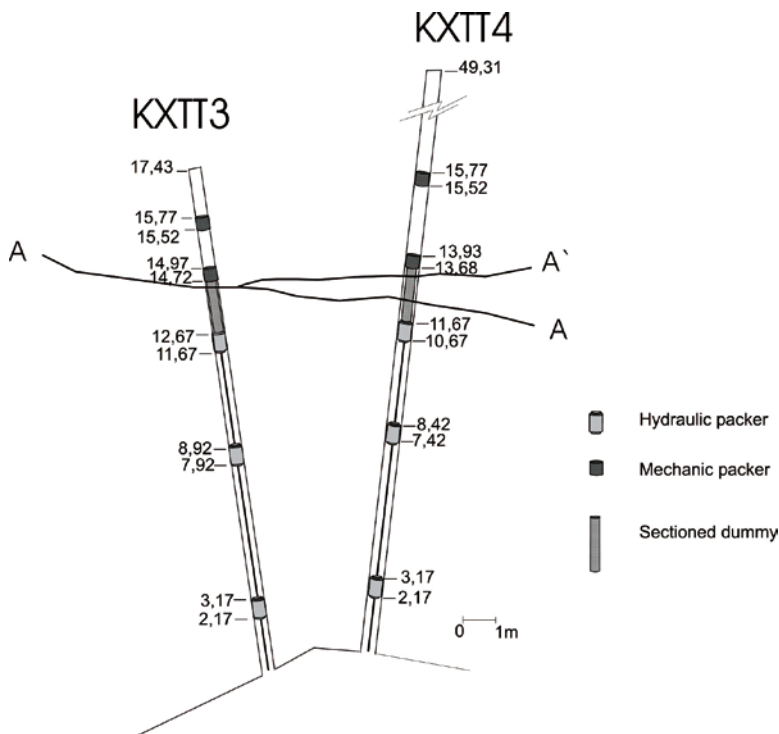
Figure 1-3. *Schematic drawing (plan view) of the test sections and flow path used in the TRUE-1 completion campaign after the re-instrumentation in October 2005.*
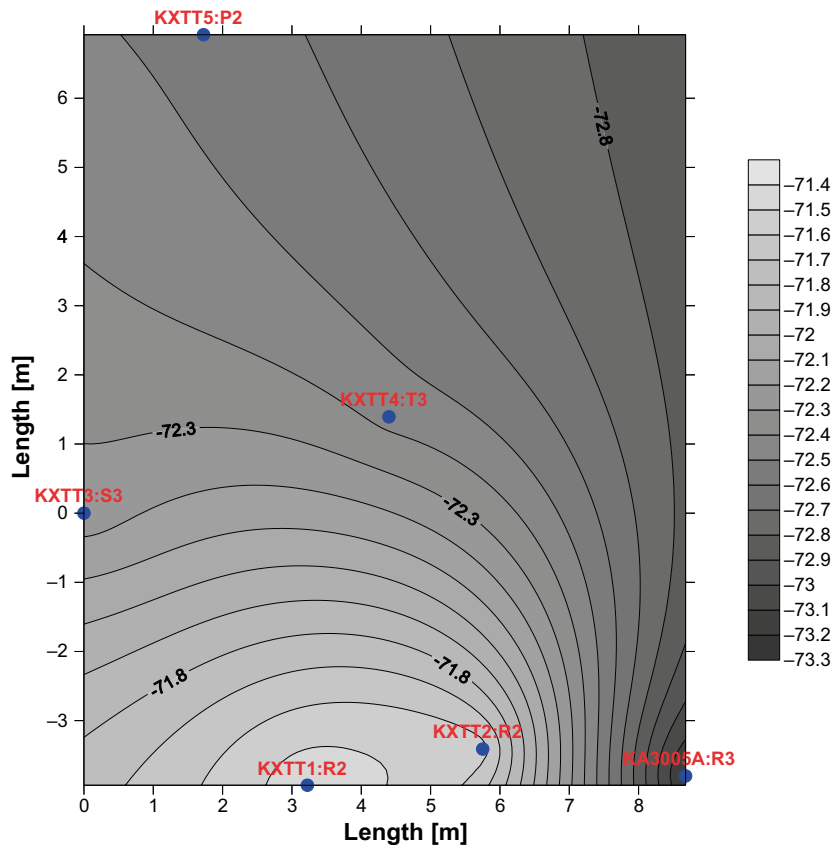
Figure 1-4. *Hydraulic head in Feature A during ambient conditions 2006-08-14 (view normal to the plane of the fracture).*

2 Objectives and scope

2.1 General objectives

The general objectives of the TRUE-1 Completion were to:

1) improve the knowledge of the inner structure of Feature A through epoxy injection and subsequent analyses, including improvement of the identification and description of the immobile zone(s) that are involved in observed retention effects,

2) perform complementary test useful to the SKB Site Investigations (PLU), including *in situ K_d* and SWIW tests,

3) improve the description of zones of immobile water that contributes to observed retention effects. The approach is identification and mineralogical-chemical characterisation of the sites where Cs is sorbed. Before over-coring the fracture, the Cs-signature must be enhanced,

4) update the conceptual microstructure and sorption models of Feature A.

2.2 Specific objectives

The specific objectives of the activities described in this report were:

- to perform a SWIW test in order to:
    - study the tracer distribution surrounding the SWIW-test borehole by passive sampling in the surrounding multi-borehole array intersecting Feature A,
    - evaluate the SWIW test and to compare the results to previously performed tracer tests at the TRUE-1 site.

- to perform a CEC test in order to:
    - study the cation exchange capacity (CEC) *in situ* and study the de-sorption of the previously injected ^{134}Cs and ^{137}Cs in the flow path, possibly making the drill cores more manageable for image analysis and microscopy (radiation safety aspects),
    - enhance the Cs signature in Feature A, i.e., to make it possible to study adsorbed non-radio-active Cs instead of the radioactive ^{134}Cs and ^{137}Cs, which are suspected to be present in rather low amounts.

- to perform COM tests in order to:
    - examine and evaluate effects of possible channelling in a single fracture (Feature A).

3   Performance and evaluation procedure

3.1   Test principles

3.1.1   Groundwater flow

Two methods were used to estimate the groundwater flow through a borehole section: dilution test and continuous injection.

Dilution test

Dilution tests are employed to determine the flow rate through a borehole section by dilution of a tracer by the ambient groundwater flow. The principle is to inject a tracer solution into a borehole section and then monitor the decrease in tracer concentration over time as illustrated in Figure 3-1. A number of dilution tests were performed within the SWIW, CEC and COM experiments, either as a part of the main test or as a pre-test (to help define experimental conditions to be employed in the main test).

Continuous injection

The groundwater flow may also be estimated with a simple mass balance calculation when a continuous injection with constant concentration is employed and the concentration in the borehole section reaches a stable level. This was the case for the CEC tests, both pre-tests and the main test.
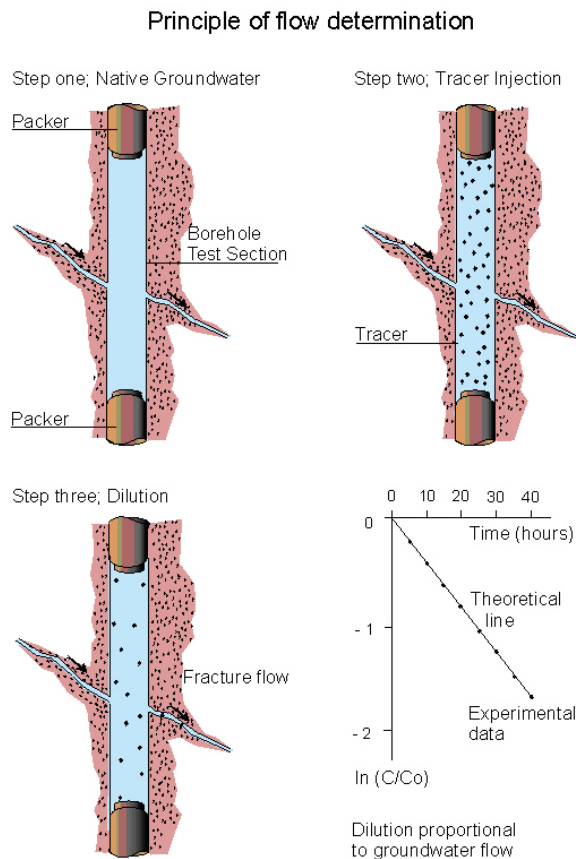
Figure 3-1. *General principle of the dilution method.*

3.1.2 SWIW

The principle of a Single-Well Injection-Withdrawal (SWIW) test is that one or several tracers are injected into the rock formation and are later pumped back. The breakthrough during the pumping phase may then provide information about solute transport properties of the rock formation. A SWIW test may consist of the following phases:

1. Pre injection: only water is injected.

2. Tracer injection: water and tracers are injected.

3. Chaser phase: only water is injected in order to push the tracers further out into the rock formation.

4. Pumping phase: the water is pumped back and the tracer concentrations are measured.

In addition to the experimental phases listed above, there may be waiting periods when the water is neither injected nor pumped.

The tracer breakthrough data that are eventually used for evaluation is obtained from the pumping phase. The injection of chaser fluid has theoretically the effect of pushing the tracer out as a concentric "ring" in the formation surrounding the tested section. An advantage of this is that when the tracer is pumped back both the ascending as well as the descending parts in the recovery breakthrough curve are obtained. A schematic example of a resulting breakthrough curve during a SWIW test is shown in Figure 3-2.

In the SWIW tests performed within the SKB site investigations (Nordqvist 2008), there were no other borehole section in the vicinity where it was possible to observe the propagation of the tracer into the rock formation. However, during the present SWIW test at the TRUE-1 site several boreholes were present where one may be used as the SWIW test borehole (injection and pumping hole) whiles the others may be used as observation holes. In this way it will be possible to study the tracer distribution surrounding the SWIW-test borehole by passive sampling.
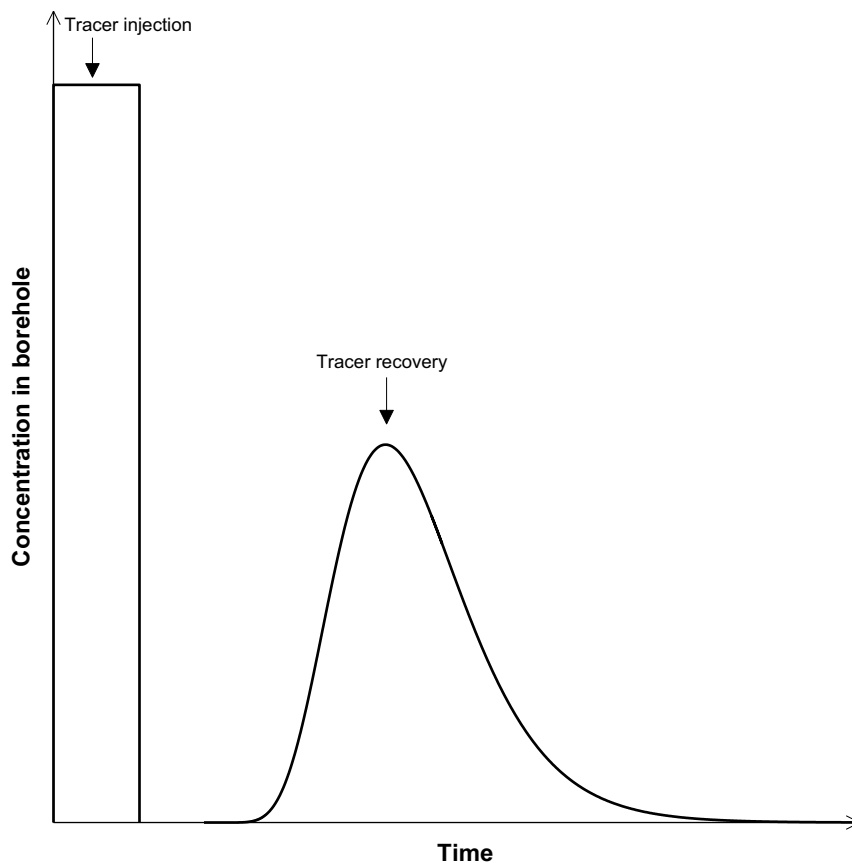
Figure 3-2 Schematic tracer concentration sequence during a SWIW test.

The principal objectives for the SWIW tests were initially formulated as follows:

- to verify the tracer distribution surrounding the SWIW test borehole by passive sampling in the surrounding multi-borehole array intersecting Feature A,

- to evaluate the SWIW test and to compare the results to previously performed tracer test at the TRUE site.

The first of the above objectives were considered especially valuable for the SWIW tests performed within the SKB site investigations (Nordqvist 2008). In these SWIW tests, no other surrounding borehole sections were available where it was possible to observe the propagation of the tracer into the rock formation. At the TRUE-1 test site several boreholes are available of which one may be used as a SWIW test borehole (injection and pumping hole) while the others may be used as observation holes.

A number of scoping calculations were carried out prior to the SWIW test in order to obtain an understanding of tracer (sorbing and non-sorbing) behaviour in peripheral boreholes and to provide support for experimental design. The specific purpose of the scoping calculations was to indicate suitable experimental flows and duration of various phases. These scoping calculations are presented in more detail below.

The original experimental plan for the TRUE-1 Completion SWIW tests included use of sorbing and radioactive tracers. First, a pre-test was to be carried out with only a fluorescent dye tracer in order to optimize experimental such as injection flow rates, pressures, etc. The pre-test was to be followed by a main SWIW tests with injection of a relatively large number of conservative, sorbing (weakly and strongly) and radioactive tracers.

However, the planned main test with sorbing and radioactive tracers was never carried out. Because of very low tracer (Uranine) recovery (about two percent) during the pre-test., the pre-test was repeated with a modified (shorter) chaser injection period in order to increase tracer recovery. The repeated test resulted in improved tracer recovery, but still with a very low recovery (about 11 percent). Because of this, it was decided to not proceed with radioactive/sorbing tracers.

Despite the reduced experimental plan, an interesting set of data from the two tracer injections (herein called SWIW 1 and SWIW 2, only differing in the amounts of chaser fluid volume) was obtained. Tracer breakthrough curves were obtained in all of the four peripheral boreholes sections as well as in the central SWIW section (although with low tracer recovery, as already mentioned). This is further discussed in section 4.1.2.

SWIW test scoping calculations

The scoping calculations are made based on the assumption of a homogenous radial flow and advective-dispersive transport, with outer boundary conditions located at a radial distance of 50 m from the central SWIW-section. Observation sections are placed at distances of 3, 6 and 8 m. The only transport processes considered are advection, dispersion and linear retardation; matrix diffusion effects are not modelled.

Assuming that the dispersion effect can be described with a constant dispersivity a_L [L] and that molecular diffusion is negligible the governing equation for radial solute transport with advection, dispersion and linear retardation as the only transport processes may be written as (Lee 1999):

$$R\frac{\partial C}{\partial t} = -\frac{B}{r}\frac{\partial C}{\partial r} + \frac{a_L B}{r}\frac{\partial^2 C}{\partial r^2} \qquad\qquad \text{Equation 3-1}$$

where $B = Q/(2\pi\delta)$, R is the retardation factor [–] and δ is the aperture [L].

The injection and recovery pumping flows were set to 140 ml/min (about $2.3\cdot10^{-6}$ m³/s). Tracer injection takes place during the first hour, followed by a chaser injection phase for 90 hours.

Fracture flow and transport parameters were somewhat arbitrarily selected but intended to be plausible generic values and set as follows:

- Thickness of formation (b) = 2.0 m.

- Flow porosity (p) = $3 \cdot 10^{-3}$ (i.e. corresponding to a flow volume in one or several plane-parallel fractures with a total aperture of 0.006 m).

- Longitudinal dispersivity (aL) = 0.1 m (an arbitrarily selected "small" value).

- Retardation factors (R) are set to 1, 1.5 and 2.0, respectively.

Note that the flow and transport parameters are required as separate input variables to the employed simulation model (SUTRA), but that simulation results actually only depends on effective parameters that are a combination of the above. For example, Q/(bp) determines the radial travel time in the simulated domain. In addition, the shape of recovery breakthrough in the SWIW section only depends on a single effective parameter that is a combination of porosity and dispersivity.

Simulation of tracer recovery in the SWIW-section

Simulated tracer recovery breakthrough curves in the central injection-withdrawal section are shown in Figure 3-3, for tracers with different retardation factors. Because of the reversible nature of a SWIW experiment, tracers with different retardation factors arrive approximately simultaneously. Retardation of tracers only affects the shape of the breakthrough curve in the presence of dispersion.
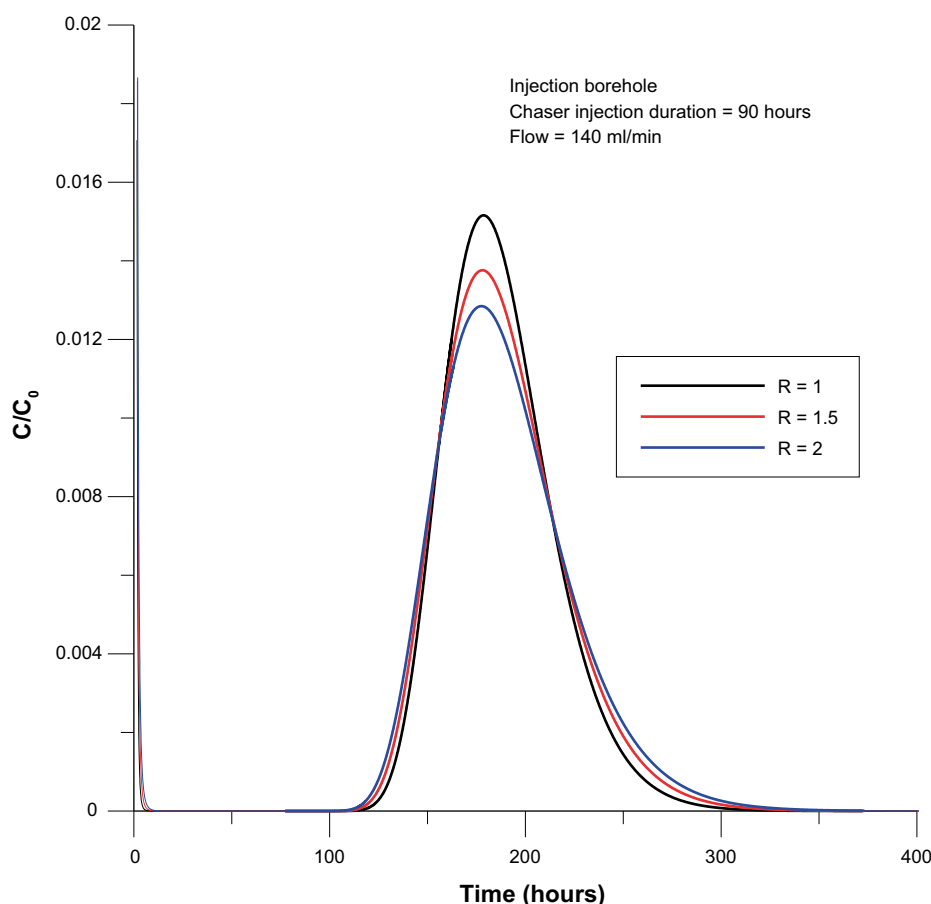
Figure 3-3. *Simulated tracer recovery breakthrough curves in the SWIW-section for non-sorbing and sorbing tracers.*

Tracer breakthrough in peripheral boreholes.

Tracer breakthrough in borehole section at various radial distances from the SWIW-section can be regarded as results from a radially diverging tracer experiment. The additional feature of the presently proposed experiment is that tracer also is pumped back after a radially diverging phase. Thus, it is conceivable that double peaks or otherwise complex breakthrough in the peripheral borehole sections occur as a result of the flow reversal. Figure 3-4 shows tracer breakthro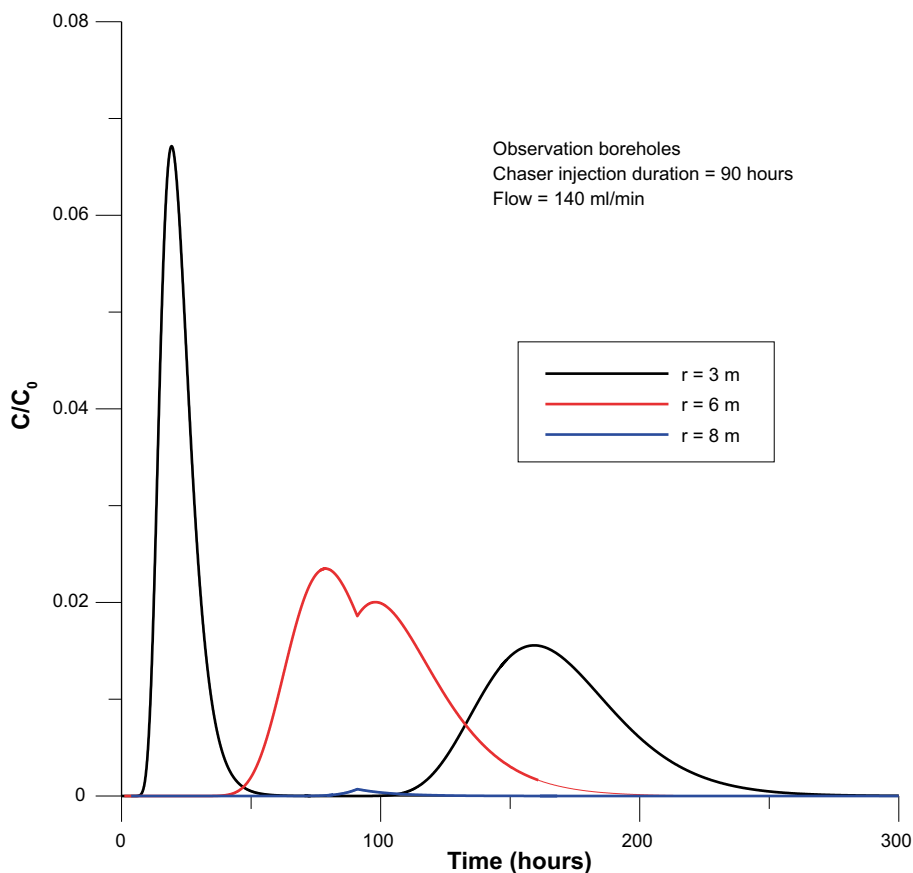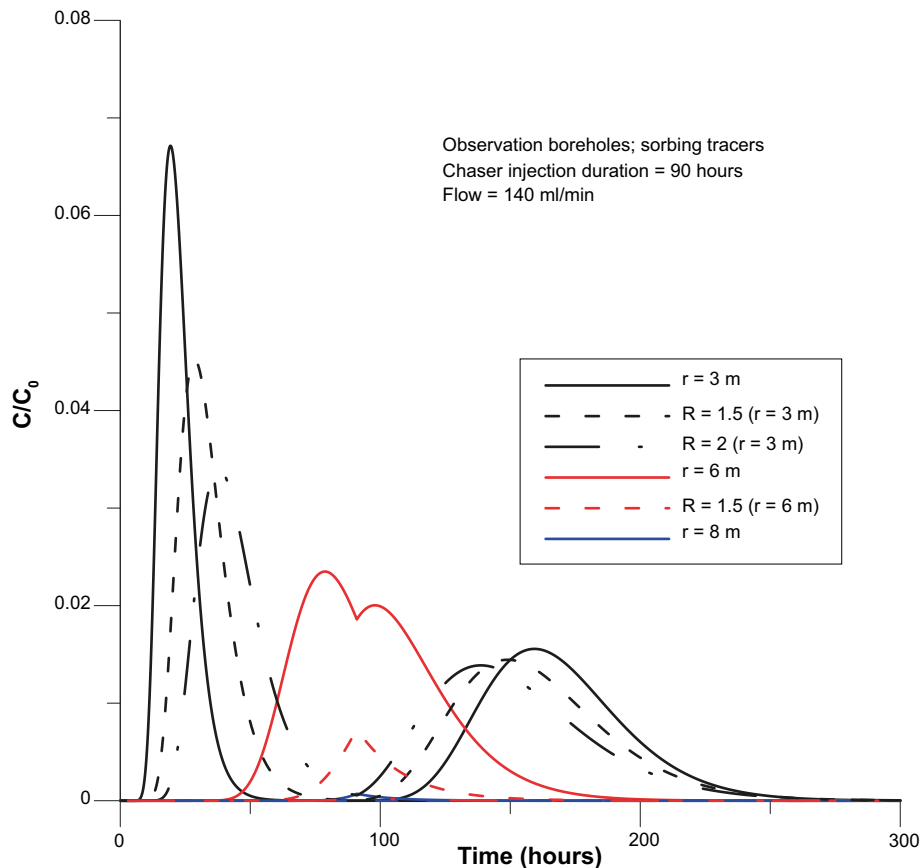ugh curves for non-sorbing tracers at three radial distances of 3, 6 and 8 m, respectively. The figure shows that the appearance of the breakthrough curves is very sensitive to the radial distance from the SWIW-section. The closest observation section at 3 m shows two peaks, well separated in time. The second peak occurs when the tracer travels back during the recovery phase. At a distance of 6 m, the peaks are not fully separated, but the start of the recovery pumping phase is clearly seen just after the peak in the breakthrough curve. At a radial distance of 8 m, tracer breakthrough is barely visible. Here, only the leading front edge of the tracer "cloud" enters the borehole section before the recovery pumping starts.

In Figure 3-5, sorbing tracers have been added to the preceding case. In this case, clearly visible effects of retardation may be seen at the closest observation section at a radial distance of 3 metres. The breakthrough of a retarded tracer is delayed during the injection/chaser phases and occurs earlier during the pumping phase, compared with the non-sorbing tracer. At a radial distance where the tracer cloud have only partially passed the observation borehole, as for a distance of 6 metres in this case, a small truncated peak is observed for $R = 1.5$. For a radial distance of 8 metres, there are no visible effects of the sorbing tracers.

The implication of these results is that, in order to observe clear effects of tracer retardation, sufficient volumes of injection and chaser fluid must be used so that the tracer cloud can pass through the observation section. Because dilution increases with distance in a diverging tracer test, detection of sorbing tracers becomes even more difficult at increasing distances, than for non-sorbing tracers.

Figure 3-4. *Simulated tracer breakthrough curves for non-sorbing tracers at various radial distances.*

Figure 3-5. *Simulated tracer breakthrough curves for non-sorbing and sorbing tracers at various radial distances. Solid lines represent non-sorbing tracers. For a radial distance of 8 m, none of the sorbing tracers are visible.*

Concluding remarks for the SWIW scopings

- Tracer breakthrough in observation sections is sensitive to the radial distance away from the central SWIW section and is dependent on that sufficient chaser volume is applied.

- For the expected hydraulic conditions at the site, it is feasible to obtain breakthrough curves in adjacent borehole sections of interest.

- For some boreholes, the tracer may pass the section completely and a second peak may appear during the recovery phase. In other sections, the tracer may only partly pass through the sections before the recovery pumping starts, which might produce relatively complex tracer breakthrough curves.

- Tracer breakthrough for sorbing tracer is more sensitive to dilution effects. However, it should be possible to study moderately retarded tracers in observation sections, provided that sufficient chaser fluid volume is applied.

3.1.3 CEC

The basic objective of this CEC test is to quantify the amount of cations that can adsorb on the fracture walls in a transport path of a natural fracture; i.e., to evaluate the cation exchange capacity (CEC). This test is thus performed by injecting both a strongly sorbing and a non-sorbing tracer in a borehole section and study the breakthrough curve in a pumping section in another borehole section, connected to the injection section by way of the fracture. The concentration of the tracers in the injection section would preferable be held at a constant level, i.e., a continuous injection of both a sorbing and a non-sorbing tracer. Assuming that the sorbing tracer used is exposed to a sorption that is strong enough to out-compete all other cations, CEC may then be evaluated from the area difference of the breakthrough curves, visualized as the shaded area in Figure 3-6.
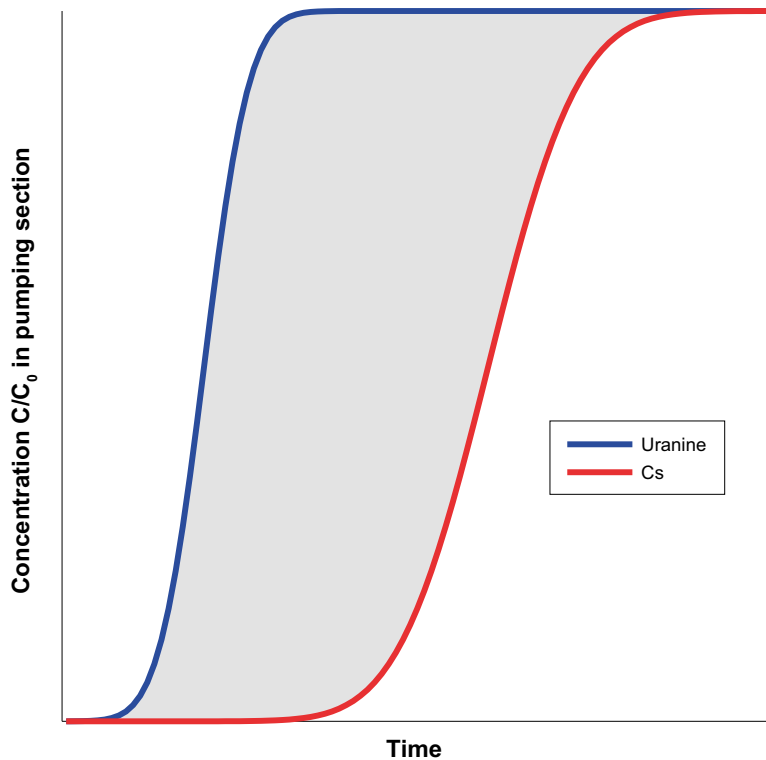
Figure 3-6. Principle character of the breakthrough curve in the CEC test. Both Cs (strongly sorbing) and Uranine (non-sorbing) are injected continuously and pumping is performed until both tracers have reached an outlet concentration corresponding to the inlet concentrations, i.e., C/C0=1. The integrated difference between the two curves are representative for the amount of Cs that have adsorbed on the fracture wall and (provided that the sorption strength of Cs is enough to outcompete all other cations in binding to the cation exchange sites) will therefore represent the Cation Exchange Capacity, CEC.

The main approach addressed in this investigation is based on the assumption that the transport takes place in a system where all sorption sites are located on the fracture surface and directly available for adsorption, i.e., a surface sorption model. In real systems and especially for low flow rates, the diffusion of tracers in to the microfractures and/or the intragranular porosity will have a significant impact of the result.

CEC test scoping

One of the prerequisites in the CEC tracer experiment is that the injected amount of cation tracer is sufficient to more or less fully saturate the sorption capacity of the transport pathway. Sorption will then become site-limited and the commonly assumed linear sorption isotherm ("K_d-sorption") is not applicable at high solute concentrations.

In the case of applying a cation exchange model for the sorption, the following expression can be formulated:

$$M_t^{x+} + (x/y)M_b\text{-}S_y \text{ D } (x/y)M_b^{y+} + M_t\text{-}S_x \qquad \text{Equation 3-2}$$

where M_t^{x+} is the tracer cation with the number of x positive charges, M_b^{y+} is the bulk cation with the number of y positive charge and $-S$ is a cation exchange site. Following the terminology formulated by Gaines and Thomas (1953), a selectivity coefficient for the reaction, K_c, can be formulated as:

$$K_c = \frac{\dfrac{x[M_t - S_x]}{CEC} \cdot \left[M_b^{y+}\right]^{\frac{x}{y}}}{\left(\dfrac{y[M_b - S_y]}{CEC}\right)^{\frac{x}{y}} \cdot \left[M_t^{x+}\right]} \qquad \text{Equation 3-3}$$

where the CEC thus is defined as the total number of cation exchange sites ($-S$).

It can easily be realized that under conditions where $[M_t] << CEC$ and $[M_t] << [M_b]$, the sorption of M_t can be described using a linear isotherm. However, when approaching saturation cases (xM_t-$S_x \approx CEC$) the proportion of the tracer cation bound to the solid phase compared to the proportion in the aqueous phase will decrease.

A common way of accounting for adsorption influenced by saturation is the Langmuir isotherm. Given the conditions that only the total concentration of the cation tracer is varied in Equation 3-3, the complicated relationships involved in a total cation exchange model can be simplified to a Langmuir model. The scoping calculations applied in this work were therefore based on the Langmuir isotherm. It should also be noted that the Langmuir isotherm is, just as linear sorption, based on equilibrium assumptions, i.e. sorption is instantaneous.

In this section, the Langmuir sorption isotherm and some of its properties are briefly discussed followed by a description of the scoping calculation results for the planned experiment.

The Langmuir sorption isotherm

The Langmuir sorption isotherm describes non-linear equilibrium sorption where the sorption capacity is limited by the number of available sorption sites. The basic difference between this model and the CEC model is that the Langmuir sorption model only treats sorption only as a function of the number of sorption sites and the concentration of the tracer in the aqueous phase; the CEC model also includes the influence of the competing cation on the sorption. The Langmuir isotherm is usually based on sorption per unit solid mass:

$$C_s = \frac{b_1 N_{max} C}{1 + b_1 C} \qquad \text{Equation 3-4}$$

where C_s is sorbed solute per unit solid (e.g. [M/M]), C is the solute concentration (e.g. $[M/L^3]$), b_1 [e.g. $[L^3/M]$]) is an adsorption coefficient related to the binding energy and N_{max} is the maximum amount that can be sorbed per unit solid (e.g. [M/M]). An illustration of a comparison of the of the Langmuir equation to the CEC model can be made by assuming a binary system with two monovalent cations competing for the cation exchange sites (i.e., CEC being the sum of $[M_t$-S] and $[M_b$-S]. Equation 3-3 can in this case be developed to:

$$[M_t - S] = \frac{K_c CEC [M_t]}{M_b + K_c [M_t]} \qquad \text{Equation 3-5}$$

which shows the close relationship between the two models and the two equations, i.e., CEC is equivalent to N_{max} describing the number available sorption sites and K_c and b_1 being the parameters determining the sorption strength of the tracer.

The effect of the Langmuir isotherm is illustrated in Figure 3-7, where breakthrough curves are generated from one-dimensional advective-dispersive transport simulations with varying injection concentrations (C_0). For very low C_0, the sorption becomes linear ("K_d-sorption"). One characteristic feature of the Langmuir isotherm is the front-sharpening effect with increasing C_0-values, which is clearly visible in Figure 3-7. This effect occurs because there is a larger sorption effect for the relatively low concentrations at the leading edge of the solute plume.

In porous media studies, C_s and Langmuir constants are usually expressed per unit solid mass, as in Equation 3-4. If flow in a fracture is considered, then the sorption may be formulated per unit area basis instead (the form of the Langmuir isotherm is still the same). The retardation factor, R_{LM}, for a Langmuir isotherm on a per-unit-surface-area basis is given by (modified from Fetter 1999):

$$R_{LM} = 1 + A \left[\frac{b_1 N_{max}}{(1 + b_1 C)^2} \right] \qquad \text{Equation 3-6}$$

where A is the surface area to void-space ratio $[L^{-1}]$. Nmax is the maximum amount of solute that can be sorbed per unit area $[M/L^2]$ and b1 has the units of $[L^3/M]$. Because the retardation factor for the Langmuir isotherm depends on the solute concentration, this factor may only be regarded as a "local" coefficient.
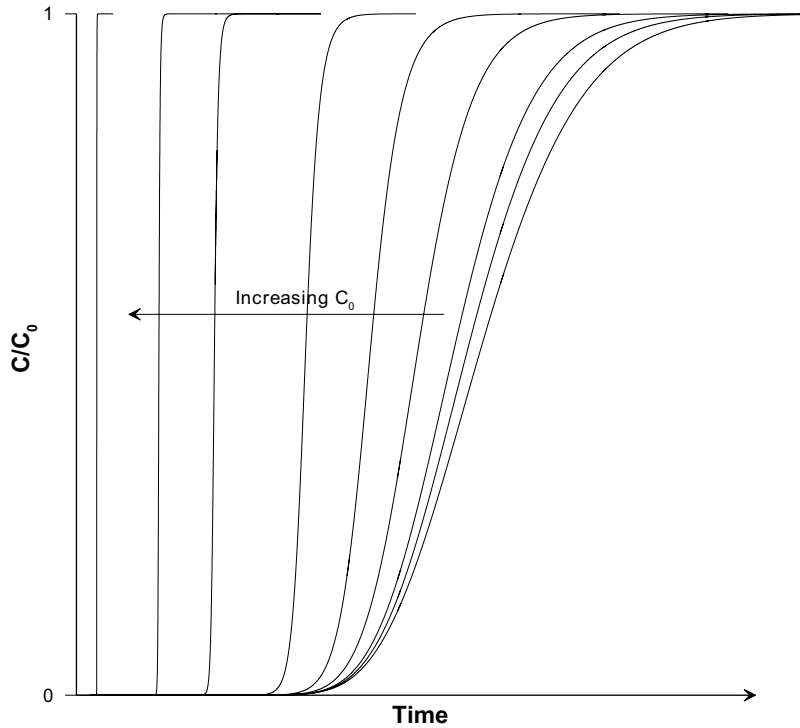
Figure 3-7. *Illustration of effects of equilibrium sorption with a Langmuir isotherm using results from simulations with a one-dimensional advective-dispersive transport model. For very low injection concentrations, C_0, the sorption becomes linear.*

At very low concentrations, the Langmuir isotherm approaches the isotherm for linear sorption; R_{LIN}. For very low concentrations, $b_1 C << 1$ and Equation 3-6 can instead be written as:

$$R_{LM} = 1 + A b_1 N_{max}$$
Equation 3-7

Which can be compared to the R explicitly for the case of linear sorption , i.e.;

$$R_{LIN} = 1 + A K_A$$
Equation 3-8

where K_A [L] is the distribution coefficient for surface sorption. If the assumption is made that transport occurs in an ideal plane-parallel fracture with smooth fracture walls, then the parameter A is given by:

$$A = \frac{2}{\delta}$$
Equation 3-9

where δ is the fracture aperture [L].

An example of the dependence of the retardation coefficient in the Langmuir isotherm (Equation 3-4) on the solute concentration is given in Figure 3-8. Here, A is chosen, somewhat arbitrarily, so that a retardation coefficient of about 100 is obtained at very low concentrations. If plane-parallel fracture flow is assumed, this corresponds to a fracture aperture of about $2.7 \cdot 10^{-4}$ m.

If the Langmuir coefficients are expressed as sorption per unit mass, i.e. as in a porous media approach, then A will have different units [M/L^3] and may be given by:

$$A = \frac{B_d}{p}$$
Equation 3-10

where B_d is the bulk density and p is the porosity.
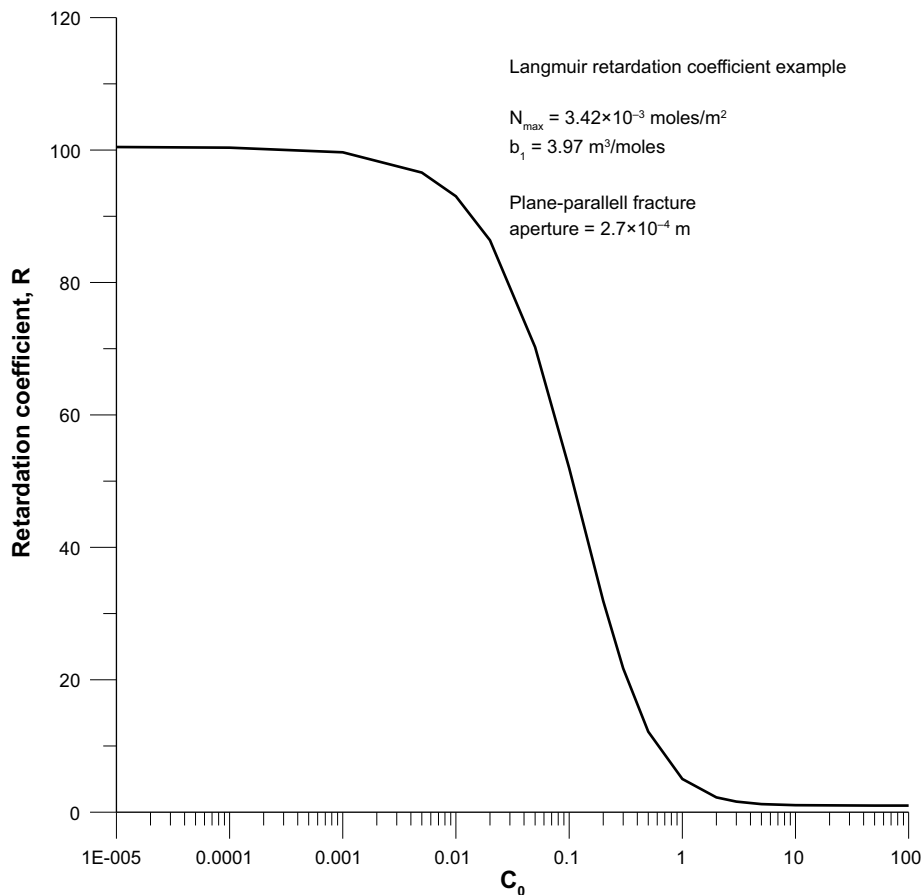
Figure 3-8. *An example of the Langmuir retardation coefficient as a function of solute concentration (Equation 3-4). The surface area to volume ratio is chosen so that a retardation coefficient of about 100 is obtained at very low concentrations. If a plane-parallel fracture is assumed, and given the values of the Langmuir coefficients, this corresponds to a fracture aperture of about $2.7 \cdot 10^{-4}$ m.*

Solute transport with equilibrium sorption

The one-dimensional advection-dispersion model with equilibrium sorption, but without matrix diffusion, is often formulated using the following governing equation:

$$R \frac{\partial C}{\partial t} = D_L \frac{\partial^2 C}{\partial x^2} - v_x \frac{\partial C}{\partial x}$$
Equation 3-11

where D_L is the longitudinal dispersion coefficient [L^2/T], v_x is the average (constant) water velocity [L/T] and R is the retardation factor [–]. The equation is valid irrespective of whether R_{LIN} or R_{LM} is used for the retardation factor.

The shape a tracer breakthrough curve is in this case only dependent on the parameters R, D_L and v_x. The dispersion coefficient, D_L, may alternatively be expressed using dispersivity, a_L ($D_L = a_L v_x$) or the Peclet number, Pe ($Pe = v_x L / D_L$; L = length of travel path). Further, v_x may be expressed using the average residence time, t_0 ($= L/v_x$). In the scoping calculations described below, a_L and t_0 are used.

If linear sorption is assumed, R is simply a constant (i.e. not dependent on concentration, see Equation 3-6). In this case, solution of Equation 3-11 is relatively simple and a number of analytical solutions are available and widely applied. In the case of Langmuir sorption, R is not a constant but a function of the concentration (see Equation 3-6). In this case the solution is more difficult and in the scoping calculations below a numerical transport code is used.

Although well known, it should be pointed out that when applying Equation 3-11 to interpret breakthrough curves from a tracer experiment only the parameters mentioned above can be uniquely

estimated. In the case of linear equilibrium sorption, a single value of R is obtained. The sorption coefficient K_A (or K_d) cannot be determined without independent knowledge of, or assumptions of, the surface/volume ratio (Equation 3-9 or Equation 3-10).

For non-linear equilibrium transport (such as Langmuir sorption), on the other hand, R as a function of concentration is obtained instead. If Langmuir sorption is assumed, the R function is effectively determined by estimating b_1 (Equation 3-6) and a combined parameter equal to Ab_1N_{max}. Thus, N_{max} may not be determined directly from tracer breakthrough curves without independent knowledge of, or assumptions of, the surface to volume ratio.

Compatibility between the CEC and the Langmuir model

Based on evaluation of the cation exchange characteristics of the Äspö rock material (Byegård et al. 1998) an attempt was made to transfer the derived model to a Langmuir model for the sorption of Cs. In this work, a cation exchange isotherm has been constructed from the literature data and Equation 3-3, which thereafter has been used to fit a Langmuir isotherm to it.

For the Cs cation exchange sorption calculation, Ca^{2+} was assumed to be the only competing ion, i.e., the sorption reaction was simplified to:

$$Cs^+ + 1/2Ca\text{-}S_2 \leftrightarrows 1/2Ca^{2+} + Cs\text{-}S \qquad\qquad \text{Equation 3-12}$$

It has been experimentally confirmed (Byegård et al. 1995) that Ca occupies $\sim75\%$ of the cation exchange capacity which, given the general uncertainties of the present concept, can motivate this simplification.

Equation 3-3 can thus be written in its simplified form:

$$K_c = \frac{\dfrac{[Cs-S]}{CEC}\cdot[Ca^{2+}]^{\frac{1}{2}}}{\left(\dfrac{2[Ca-S_2]}{CEC}\right)^{\frac{1}{2}}\cdot[Cs^+]} \qquad\qquad \text{Equation 3-13}$$

In which:

$$CEC = [Cs-S] + 2[Ca-S_2] \qquad\qquad \text{Equation 3-14}$$

The work of Byegård et al. (1998) was used to the extract numerical parameters for the calculations. From the batch sorption experiment using crushed mylonite in the 1–2 mm size fraction sampled in at the Feature A intersection at borehole KXTT2, the data in Table 3-1 was obtained.

Table 3-1. K_d and water concentration data from batch sorption experiments using 1–2 mm size fraction of mylonite from the Feature A fracture in the KXTT2 borehole (Byegård et al. 1998, p 37). For Ca^{2+}, no concentration decrease could be verified for the aqueous phase so instead the desorption K_d was used. Selectivity coefficients were calculated using the present data combined with Equation 3-13 and Equation 3-14.

Tracer	C_{aq} (M)	K_d (m3/kg)	K_c (selectivity vs Ca^{2+})
Ca^{2+}	0.03	2.7E–5	1 (–)
Cs	3.8E-8	8.0E–3	720 $M^{-1/2}$

In addition, the CEC (the total amount of cations adsorbed) was in the work of Byegård et al. (1998) estimated to 0.005 eq/kg for the crushed mylonite. Using the assumption of a spherical geometrical shape of the crushed mylonite, this value can be transformed to a surface related value of $3.4\cdot10^{-3}$ eq/m^2 which thus should be applicable for transport in a mylonite fracture. Based on these values, an adsorption isotherm was calculated (Figure 3-9) to which a Langmuir adsorption isotherm was fitted.
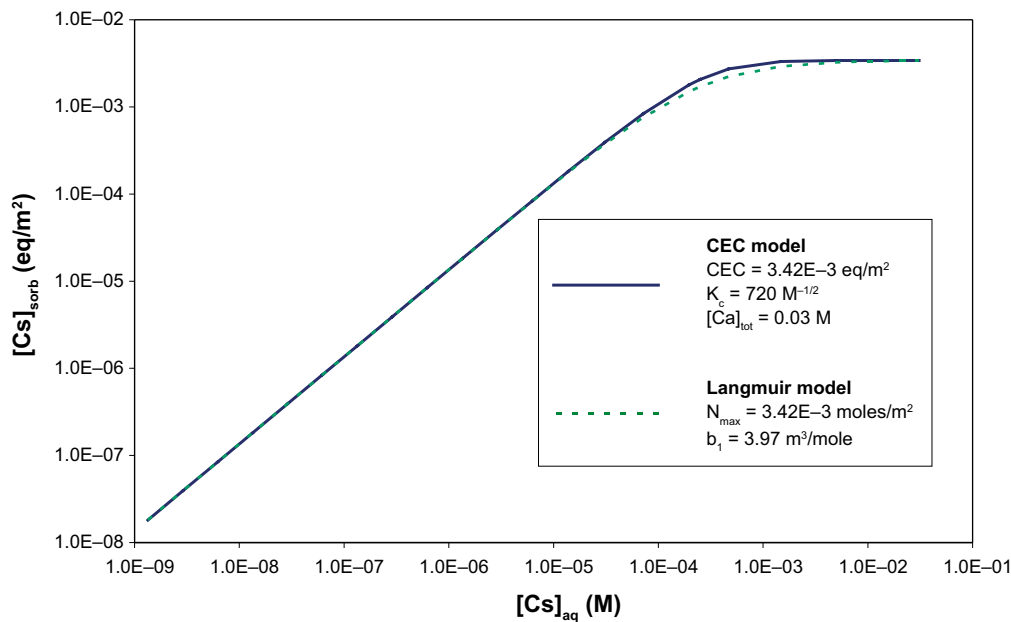
Figure 3-9. *Adsorption isotherm for Cs derived from CEC model (solid line) compared to the best fit of a Langmuir model (dashed line) to the CEC model.*

Scoping calculations for the CEC experiment

Scoping calculations for experimental design purposes were carried out prior to the experiment using a one-dimensional advection-dispersion equation with equilibrium sorption (see Equation 3-11). The simulations were carried out using SUTRA (Voss 1984). As previously discussed, the shape of calculated breakthrough curves only depend on the assumed values of average water residence time (t_0), dispersivity (a_L) and the retardation factor (R), the latter being a function of concentration in the case of Langmuir sorption.

The following assumptions were made for the advective-dispersive parameters:

- Average water residence time of 4 hours based on previously performed tracer experiments (Winberg et al. 2000).

- Longitudinal dispersivity of 0.2 m; a somewhat arbitrarily chosen "small" value in order to minimize dispersion effects on the calculated breakthrough curves.

Langmuir sorption parameters were derived from the cation exchange model, described in the preceding section, with the following values:

- $b_1 = 3.970$ m^3/moles,

- $N_{max} = 3.42 \cdot 10^{-3}$ moles/m^2.

In order to use the Langmuir parameters to obtain input for the R function to the simulation model, assumptions about the surface to void space ratio along the transport path have to be made. For these scoping calculations, two cases were simulated:

1. Plane-parallel fracture with planar fracture surfaces and a fracture aperture of 1.5 mm (Winberg et al. 2000). This corresponds to a retardation factor at low C-values of about 18 (see Equation 3-6).

2. The value of the product Ab_1N_{max} so that a retardation factor of 200 at low C-values is obtained. Note that it is arbitrary which value of A or N_{max} (or a combination of both) is changed. A value of $R = 200$ corresponds to experimentally determined linear retardation factors for Cs in the TRUE-1 experiment in Andersson et al. (1998) and this case might therefore be considered more realistic for field conditions.

The simulated tracer injection scheme is as follows:

*   1 moles/m^3 for 7 days,

*   3 moles/m^3 for 7 days,

*   10 moles/m^3 for 12 days.

The two first injection steps were intended to saturate the flow path for simulated cases 1 and 2, respectively.

In addition to the two simulation cases above, a simulation assuming conservative (non-sorbing) transport was carried out. For the purpose of comparison, the same injection concentration scheme was used as for Cs. The results from the scoping simulations are shown in Figure 3-10.

Figure 3-10 shows a clear effect of non-linear sorption effects, i.e. that sorption decreases with increasing concentration. This is obvious because the gap between the sorbing and non-sorbing tracer, respectively, decreases with increasing concentration. During the first injection step there is a clear difference between the two cases, which of course is to be expected. During the second injection step, Figure 3-10 shows visible sorption only for case 2 and during the last injection step no visible sorption for either simulation case occurs.
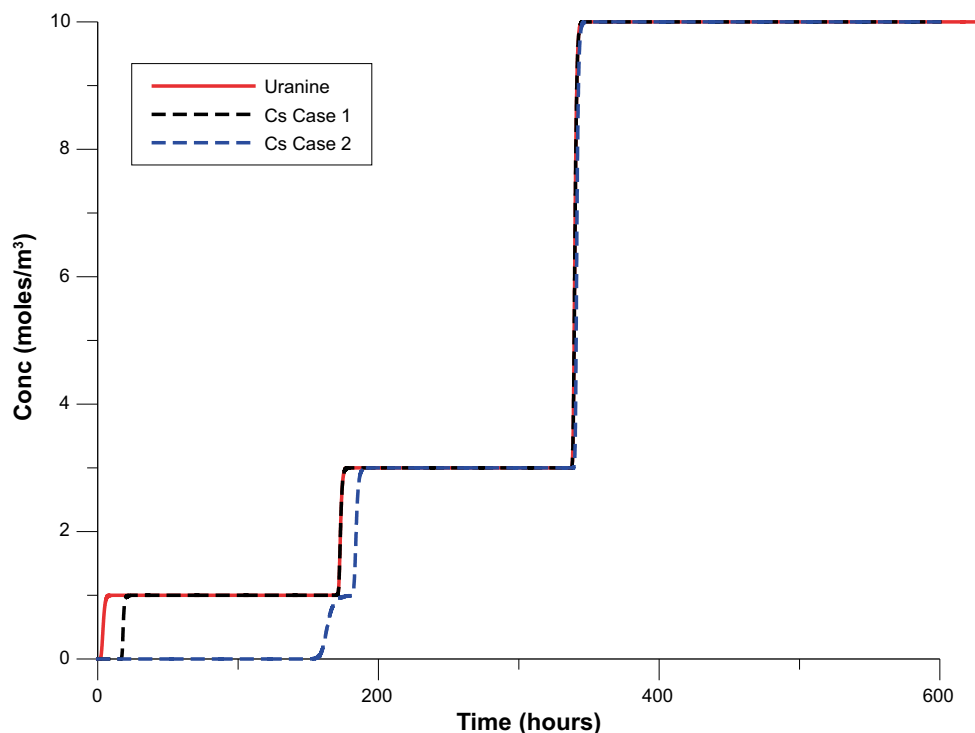
Figure 3-10. *Scoping simulation results for solute breakthrough in the pumped borehole section. The simulation cases are described in the text above.*

Matrix diffusion concept

For the case of a matrix diffusion taking place in the experiment, the numbers of interacting cation exchange sites will increase with increasing contact time, i.e., the diffusion will cause that sorption sites in the matrix will be reached and an increased sorption capacity compared to a strict surface sorption concept. Based on this process, one can can formulate a sorption model with varying apparent diffusivity depending on the degree of saturation that has been obtained. At the leading edge of the tracer diffusion pulse where the tracer concentration is low, only a minor part of the cation exchange sites will be occupied by Cs and the sorption coefficient describing the linear distribution (K_d) will be applicable, i.e. the apparent diffusivity will be comparatively low due to the limited mobility caused by the sorption. The apparent diffusion rate, D_a (m²/s) can in such a case be described as:

$$D_{a(min)} = \frac{D_e}{p + K_d B_d}$$

Equation 3-15

where D_e (m²/s) is the effective diffusivity, p (–) is the porosity and B_d (kg/m³) is the rock density. However, as the diffusion proceeds, the cation exchange sites will be saturated with the sorbing tracer and the diffusion rate will no longer be delayed due to sorption reactions. This will be obtained in a situation where the K_d term is negligible compared to the p term and the maximum apparent diffusion rate is formulated as:

$$D_{a(max)} = \frac{D_e}{p + K_d B_d} \approx \frac{D_e}{p}$$

Equation 3-16

Studying the laboratory derived sorption and diffusion parameters (Byegård et al. 1998) one can make a rough estimation of the potential amount of additional cation exchange sites available by a matrix diffusion process. This can be estimated by taking into consideration the average penetration depth, d½ (m), calculated from the different apparent diffusion rates, i.e.,

$$d_{\frac{1}{2}} = \sqrt{\frac{D_a}{t}}$$

Equation 3-17

where t (s) is the contact time applied in the experiment. The additional cation exchange sites that interacts with the Cs tracer can therefore be calculated (done in a fracture surface based concept for enabling comparison to the surface based CEC used in the previous modelling) according to:

$$CEC_{add} = CEC \cdot B_d \cdot d_{\frac{1}{2}}$$

Equation 3-18

where CEC_{add} (mole/m²) is the additional cation exchange capacity obtained per surface unit due to matrix diffusion and CEC (mole/kg) is the cation exchange capacity determined per mass unit.

The numerical parameters as well as the results of the calculations are presented in Table 3-2. Calculations have been performed for the two extremes of diffusion rates (Case 1: diffusion in the case of linear sorption and, Case 2: sorption sites saturated with sorbing tracers) and one has applied two different contact times *a)* 7 d for a singular concentration step and *b)* 26 days corresponding to the full experimental time, cf. Figure 3-10). One can see that for the case of a linear sorption, the additional CEC obtained by matrix diffusion ($2–4 \cdot 10^{-4}$ mole/m²) is low compared to the value used for the scoping calculation in the surface concept above, i.e., $3.4 \cdot 10^{-3}$ mole/m² and that one in this case can only add a very minor additional cation exchange capacity by including matrix diffusion.

However, by application of the other extreme concept of diffusion, i.e., that the penetration of the rock matrix of a sorbing tracer due to instantaneous saturation takes place in the same rate as a non-sorbing tracer, one instead obtains additional CEC in the range of $2–5 \cdot 10^{-2}$ mole/m². This is one order of magnitude higher than the comparative value applied for the surface sorption model. One must emphasize that this model is based on the assumption that the concentration of the sorbing tracer is high enough to cause an immediate saturation of the sorption sites directly in the diffusion front to enable no delay in the diffusion compared to a non-sorbing tracer. Hence this model clearly represents an overestimation of the cation capacity possible to interact in the investigation based on the laboratory determined parameters. Nevertheless, this latter calculation gives a good estimation of the maximum cation capacity that should be possible to obtain by adding the matrix diffusion mechanism.

Table 3-2. Laboratory parameters and correspond results obtained in the estimation of potential impact of the matrix diffusion in the CEC experiments, i.e., the additional CEC (last column) that would have interacted due to the diffusion mechanism. All basic parameters used in the calculation (D_e, p, K_d, B_d and CEC) are from Byegård et al. (1998) derived from sorption and diffusion experiments using mylonite sampled from the drill cores intersecting the Feature A.

Case	D_e (m²/s)	p	K_d (m³/kg)	B_d	t (s)	D_a (m²/s)	$d_{½}$ (m)	CEC (mole /kg)	Additional CEC due to matrix diffusion (mole/m²)
1a	$4\cdot10^{-14}$	0.015	$8\cdot10^{-13}$	2,700	$6\cdot10^5$ (7 d)	$1.8\cdot10^{-15}$	$3\cdot10^{-5}$	$2.2\cdot10^{-3}$	$2\cdot10^{-4}$
1b					$2\cdot10^6$ (26 d)		$6\cdot10^{-5}$		$4\cdot10^{-4}$
2a			$K_dB_d<<p$		$6\cdot10^5$ (7 d)	$2.7\cdot10^{-13}$	$4\cdot10^{-3}$		$2\cdot10^{-2}$
2b					$2\cdot10^6$ (26 d)		$8\cdot10^{-3}$		$5\cdot10^{-2}$

3.1.4 COM

Multi-hole reciprocal cross-flow tests (COM) were performed with the purpose of examining and evaluating effects of channelling in Feature A. The COM tests consist of a number of hydraulic interference tests with measurements of both pressure and flow responses. The pumping hole was alternated in order to evaluate hydraulic interference in several directions and whether the responses were corresponding with a reversed flow direction. The flow responses were measured by means of the tracer dilution method under both ambient and pumped conditions.

Several hydraulic interference tests, some also in combination with flow response estimates, have previously been performed at the TRUE-1 site (Winberg et al. 2000, Andersson et al. 2002a). The previous tests focused on distinction between features, such as Feature A and B, while the COM tests reported here focus on internal responses within Feature A.

3.2   Equipment and tracers used

3.2.1   General

The same borehole instrumentation was used during all tests described in this report. Each borehole in the TRUE-1 array was instrumented with four to five inflatable packers such that four to five borehole sections are isolated. All borehole sections are connected to the HMS-system through data loggers (Datascan). The sections planned to be used for tracer tests were equipped with three nylon hoses, two with an inner diameter of 4 mm and one with an inner diameter of 2 mm. The two 4-mm hoses were used for injection, sampling and circulation in the borehole section whereas the 2-mm hose was used for pressure monitoring. Two of the boreholes (KXTT3 and KXTT4) were re-instrumented before test start when the inflatable packers were exchanged with mechanical packers. During the re-instrumentation in KXTT4, the packers were placed so that Features A and A' were included in the same section. The packer configurations of the boreholes are given in Appendix 1 and shown in Figure 1-3 (only KXTT3 and KXTT4). The nominal volumes of water in the borehole sections, including dummies, hoses etc, are shown in Table 3-3.

The basic idea for the sampling equipment was to maintain internal circulation in the borehole section. The circulation made it possible to obtain a homogeneous tracer concentration in the borehole section and to sample the tracer concentration outside the borehole in order to monitor the tracer injection rate with time and also the dilution rate. The circulation was controlled by a pump with variable speed and measured using a flow meter.

The tracer test equipment as well as the tracers have been used earlier in the TRUE Block Scale and TRUE-1 tracer tests, see e.g. Winberg et al. (2000) and Andersson et al. (2002c). The configuration of the equipment differed between the tests as presented in Section 3.2.2 through 3.2.4.

Table 3-3. Volume of water, including circulation hoses, dummies etc, in used sections.

Borehole:Section	KXTT1:R2	KXTT2:R2	KXTT3:S3	KXTT4:T3	KXTT5:P2	KA3005A:R3
Section volume [L]	1.59	1.58	1.56	1.54	0.67	2.31

3.2.2 SWIW

The SWIW tests were performed using one equipment set-up for injection and pumping and four identical equipment set-ups for sampling in surrounding borehole sections, i.e. allowing four sections to be monitored simultaneously. A schematic drawing of the SWIW test equipment is shown in Figure 3-11 and Figure 3-12.

Tracer and water injection in the SWIW test borehole (Figure 3-11) were performed with two different piston membrane pumps (C1 & C2). Water solution was stored in two separate pressurised vessels (F) under nitrogen atmosphere. Sampling was made by continuously extracting a small volume of water from the system through a flow controller (constant leak) to a fractional sampler (D). The pumped water was collected in a 2,000 l storage tank (G). The tracer used for injection (E) was a fluorescent dye tracer, Uranine (Sodium Fluorescein) from KEBO (purum quality).

Tracer injections for dilution tests in the surrounding boreholes in two of the surrounding borehole sections (Figure 3-12) were made with one piston membrane pump (C1) and sampling was made by continuously extracting a small volume of water from the system through a flow controller (constant leak) to a fractional sampler (D). Tracer solution was injected from small bottles (E). The tracer used for the dilution tests was Rhodamine WT from Holiday Dyes Inc. (techn. quality).

3.2.3 CEC

The CEC test was performed using one equipment set-up for injection in KXTT4:T3 and another equipment set-up for pumping in KXTT3:S3. A schematic drawing of the CEC test equipment is shown in Figure 3-13 and Figure 3-14.

The pulse injection was performed with a HPLC plunger pump (C) and the continuous injection with a flow regulator (E) connected to a pressurised vessel containing tracer solution (D). Sampling was made by continuously extracting a small volume of water from the system through a flow controller (constant leak) to a fractional sampler (H). The tracers used for injection (1 and 2) were Uranine (Sodium Fluorescein, a fluorescent dye tracer) from KEBO (purum quality) and Cs^+ (inactive and radioactive Cs-131). In the pre-tests, Uranine as well as AminoG and Rhodamine Wt were used.

The pumping rate in the extraction borehole (Figure 3-14) was adjusted with a flow regulator. Sampling was made by continuously extracting a small volume of water from the system through a flow controller (constant leak) to a fractional sampler. Larger sample volumes were also collected with a magnetic valve sampler.

Cs tracer

Since the aim of the CEC experiment was to saturate the cation exchange sites of the flow path with Cs, one could easily foresee that concentrations far above the natural concentrations had to be applied. Consequently one could in this experiment analyse the non-radioactive Cs (e.g., by ICP-MS) and avoid use of any radioactive tracer. However, considering the specific conditions of this experiment, it was found that spiking non-radioactive Cs with a radioactive tracer could be advantageous. It was e.g. identified as an advantage to obtain fast measurements of the Cs injection levels (possibly stop the experiment when saturation had been obtained) during the experiment. A short-lived radioactive Cs tracer was advantageous for several other reasons:

- Radioactive measurement equipment was available at the BASLAB located in the close vicinity of the Äspö Hard Rock Laboratory.

- A general permit for use of radioactive tracer was already available at the time of the experiment.

- The use of a short-lived radioisotope would avoid radiation problem in the foreseen over-coring of the boreholes; a sufficiently short-lived tracer would thus have completely decayed at the time for the overcoring.

- Since radioactive tracers (Cs-134 and Cs-137) already had been used at the TRUE-1 Feature A, control measurements of the water samples had to be performed before any delivery to an external laboratory for ICP-MS measurement.

Based on the above, it was decided to use the Cs-131 tracer ($t_{1/2} = 9.69$ d) to spike the injection cocktails of non-radioactive Cs to a constant specific activity. Thereby, the activity of Cs-131 was used as a measure of the Cs concentration.
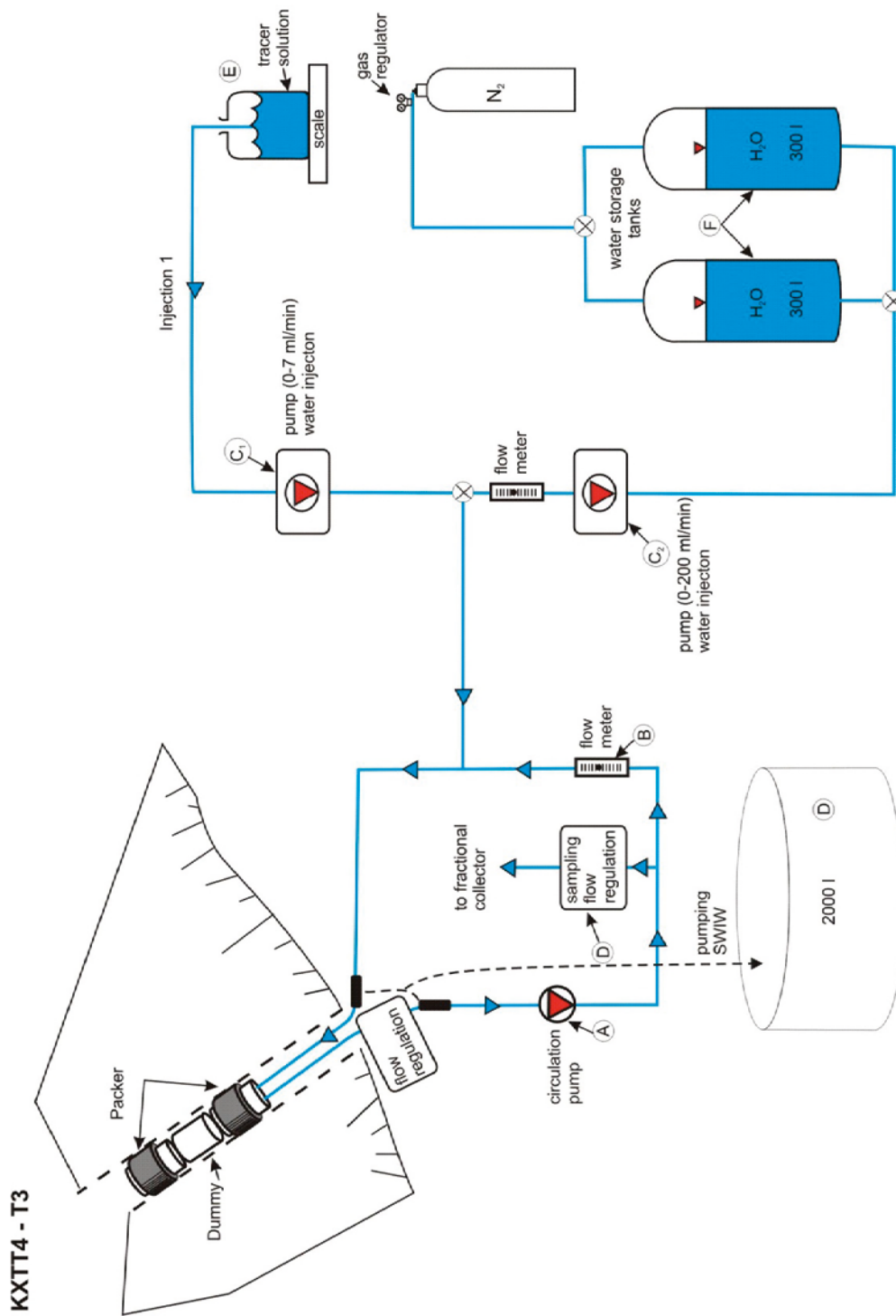
Figure 3-11. Schematic drawing of the tracer injection/sampling system used in borehole section KXTT4:T3.

KXTT5 - P2

KXTT3 - S3

KXTT1 - R2

KXTT2 - R2

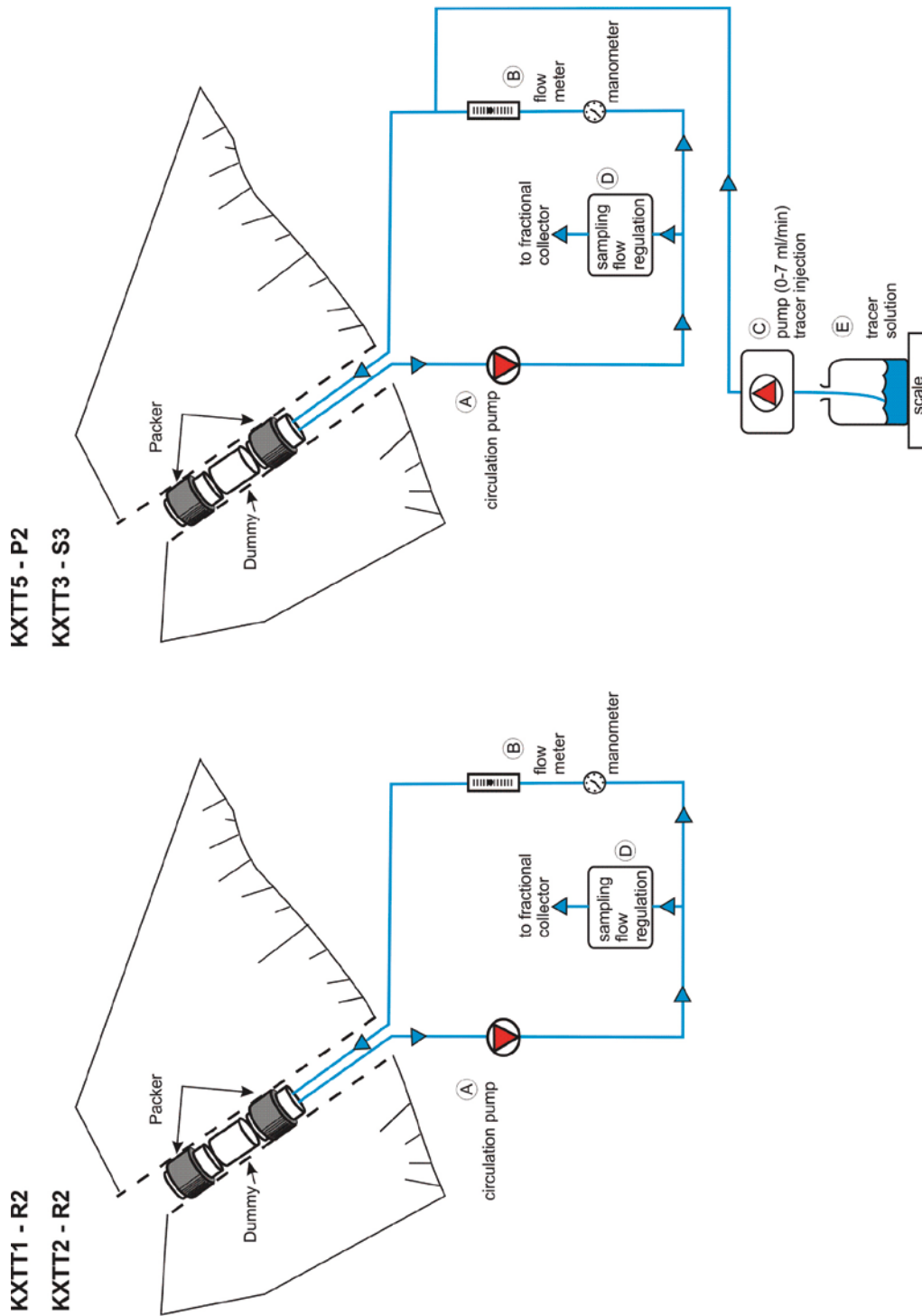*Figure 3-12. Schematic drawing of the tracer injection/sampling system used in the surrounding boreholes during the SWIW-test.*
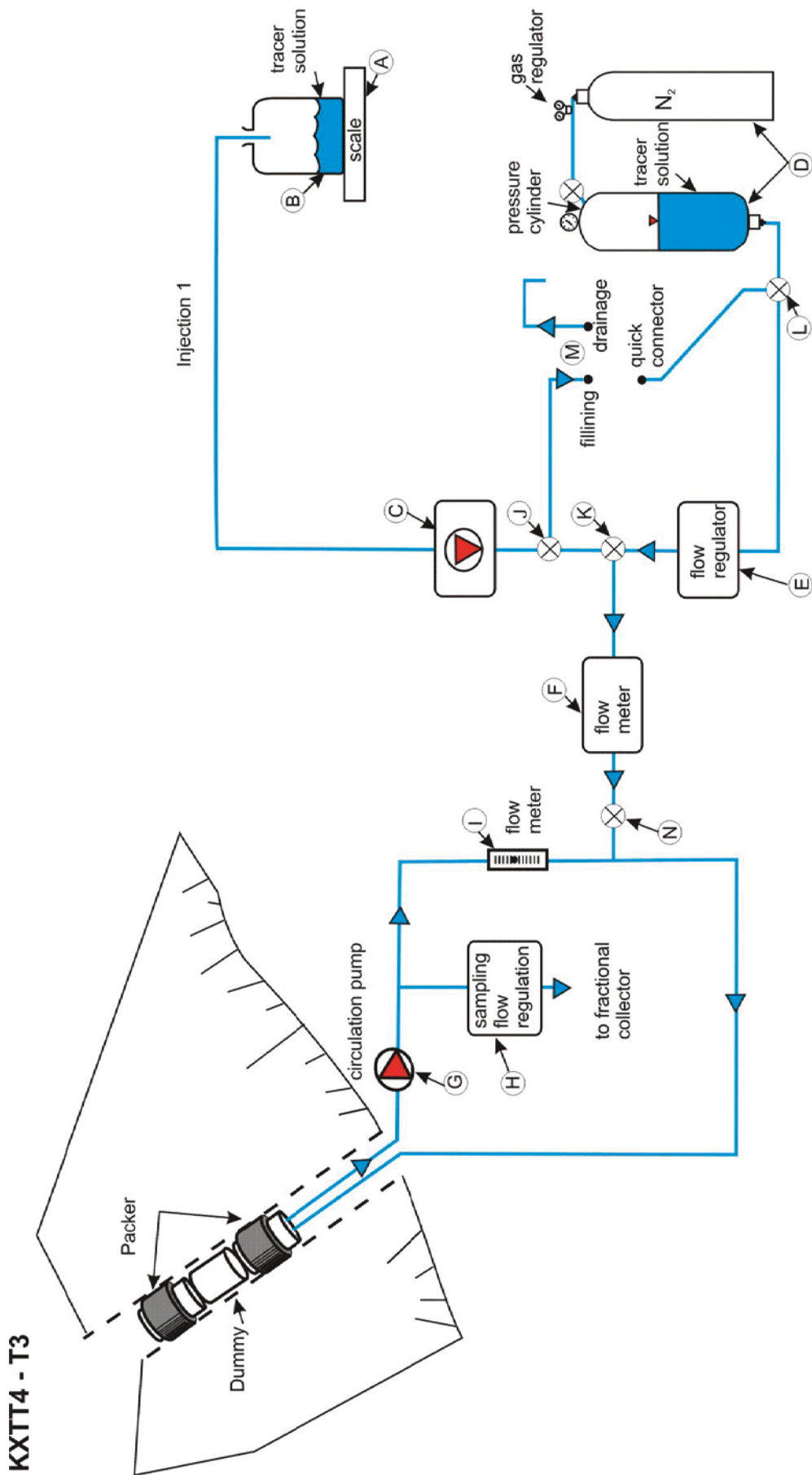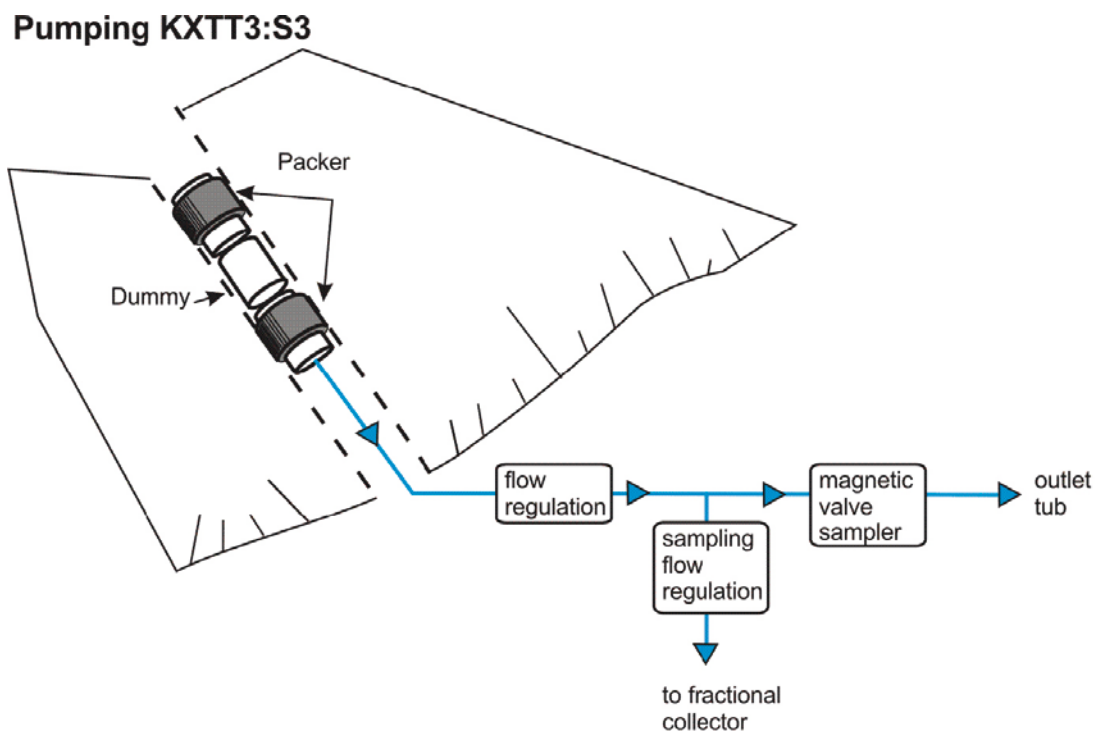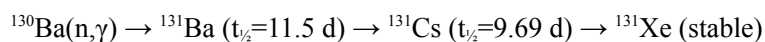
KXTT4 - T3

Figure 3-13. Schematic drawing of the tracer injection/sampling system used in the surrounding boreholes during the CEC-test.

Figure 3-14. *Schematic drawing of the tracer pumping/extraction/sampling system used in the pump boreholes during the CEC-test.*

Production

Cs-131 was produced by neutron radiation of stable $BaCO_3$ (done at Institutt for Energiteknikk, Kjeller, Norway). Cs-131 is a decay product of the radioactive Ba-131 isotope, an isotope which is produced through neutron capture of the stable isotope Ba-130 (0.1% abundance in natural Ba) i.e.;

$$^{130}Ba(n,\gamma) \rightarrow {}^{131}Ba\ (t_{1/2}=11.5\ d) \rightarrow {}^{131}Cs\ (t_{1/2}=9.69\ d) \rightarrow {}^{131}Xe\ (stable)$$

In this experiment, 7.08 g $BaCO_3$ was irradiated for 10.8 days in a neutron flux of $1.34 \cdot 10^{13}$ n/cm²/s. At the end of the irradiation, the target was allowed to cool for 6.2 days to obtain an in-growth of Cs-131 (a cooling time giving 95% of the Cs-131 activity at the optimum cooling time, 10.4 days).

The irradiated target was then carefully dissolved in concentrated hydrochloric acid where after Na_2SO_4 was added to obtain a $BaSO_4$ precipitate. Separation is thereby obtained in which the Ba-131 (and all other produced Ba isotopes) is present in the precipitate while the Cs-131 is only present in the water phase.

Measurement of Cs-131

Cs-131 decays by electron capture and no γ-energy is associated to the decay; therefore the HPGe γ-spectrometry technique (frequently used in radioactive tracer experiment, e.g., Widestrand et al. 2001) is not applicable for these measurements. Instead, X-rays associated with the decay are detected by liquid scintillation measurements, which result in the spectrum illustrated in Figure 3-15, characterised by a double peak. Liquid scintillation has the disadvantage that it has very limited nuclide specificity and lacks simultaneous detection of several nuclides, which is easily done by γ-spectrometry. However, for the present case involving only one radionuclide with activities significantly above the background level, this is not a problem.
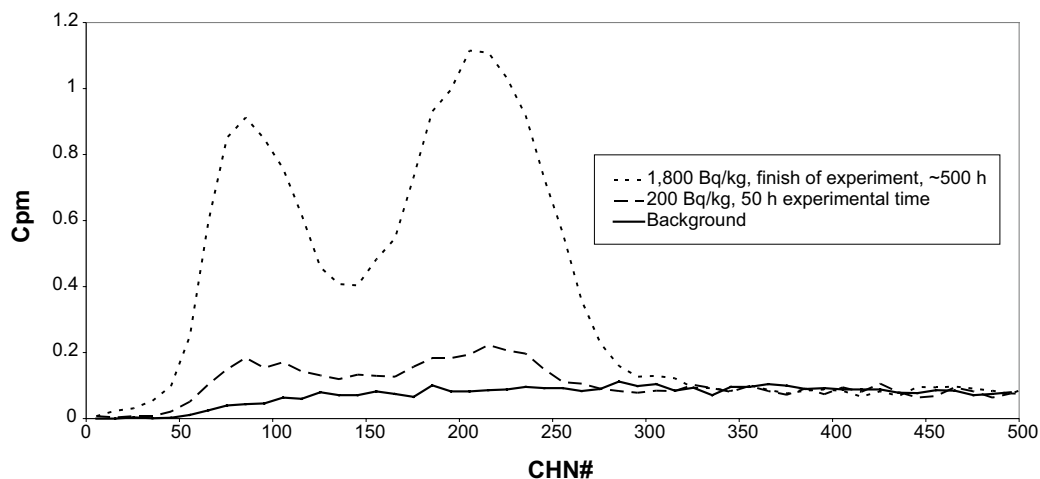
Figure 3-15. *Liquid scintillation spectrum of Cs-131. Measurements at 50 h experimental time (peak time for the first injection), 500 h experimental time (maximum for the third injection) are presented, compared to the background counting level.*

Radiochemical purity

A γ-spectrometry analysis of the eluate after the BaSO$_4$ precipitation showed that the two Cs-isotopes Cs-132 and Cs-136 were present in the obtained Cs-131 stock solution as radiochemical impurities. Their respective activity consisted of parts of less than 0.4% (Cs-132) and 0.001% (Cs-136) compared to the Cs-131 activity, cf. Table 3-4. A Ba-131 activity corresponding to 0.004% of the Cs-131 activity was also found which indicated that the separation efficiency of the BaSO$_4$ precipitation method was >99.99%.

Table 3-4. Radiochemical purity of the stock solution and the separation efficiency of the BaSO$_4$ precipitation separation method.

Isotope	Total produced amount[A] (Bq)	Activity in aqueous phase (Bq)	Separation Efficiency	Percentage of total activity in stock solution[C]
Ba-131	1.1E+8	3.3E+3	0.003%	0.004%
Cs-131	8.6E+7	(8.6E+7)[B]	(100%)[B]	99.6%[B]
Cs-132		3.3E+5	(100%)[B]	0.38%
Cs-136		1.1E+3	(100%)[B]	0.001%

[A] Calculated from irradiation data.

[B] Assumed that all Cs is transferred to the aqueos solution (i.e., no actual measurement). The assumption is justified by the fact that no insoluble Cesium sulphate is known from literature.

[C] Based on the assumption of 100% of the produced Cs-131 is present in the aqueous phase and that the liquid scintillation counting efficiency of Cs-131 is 45%.

Half-life confirmation

One sample was repeatedly measured and the counting rate was registered as a function of elapsed time. The results (Figure 3-16) show that the decrease of the counting rate perfectly followed the tabulated half-life of Cs-131, 9.69 days. This confirms the radiochemical purity of the solution; i.e., there are no reasons to believe that any other non γ-emitting radioisotope except Cs-131 is present in the stock solution.
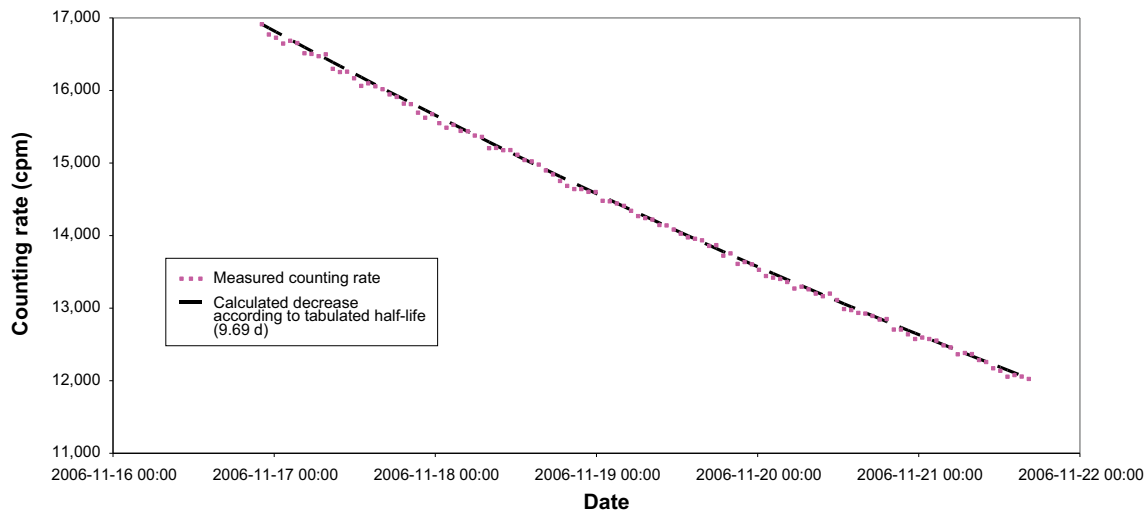
Figure 3-16. *Measured liquid scintillation counting rate of a sample from the stock solution as a function of decay time. A dashed line for the calculated decrease of the counting rate using the tabulated half-life of Cs-131 (9.69 d) is given as a comparison.*

Quenching and/or disturbances

Since liquid scintillation measurement is a process in which radiation is transformed to light transmission detected by a PM-tube, problems can arise if strongly light-absorbing chemicals are present in the samples. In this experiment, in which the strongly fluorescent tracer Uranine (Fluorescein) was present (in the injection borehole also in comparably high concentration), it was necessary to investigate potential problem of quenching.

Samples were thus prepared in which a constant level of Cs-131 activity was measured with varying amounts of Uranine. The results (Figure 3-17) indicated that quenching causes a "loss" corresponding to 10% of the counting at the highest Uranine concentration. An empirical mathematical function has been fitted in order to be used to compensate for counting rate loss due to Uranine presence in the water samples, cf. Figure 3-17. Since this equation is purely empirical, is not based on any physics and is far from perfect in its fit to the experimental data, one should acknowledge the possibility of adding an extra ~10% general uncertainty to the results.

Counting efficiency, background and detection limit

The scintillation pulses from the Cs-131 radioisotope appear as two peaks, located in the channel numbers 0–300, cf. Figure 3-15. The background counting rate in this area is 18 ± 2 count per minute (cpm) and by, somewhat arbitrarily, setting a detection limit of twice the background variation, 4 cpm can be considered to be the detection limit.

Since only relative measurements (activity in injection borehole versus activity in the sampling borehole) were necessary for this experiment, no Cs-131 calibration standard was used for absolute calibration. However, by using the results of the irradiation calculation in combination with the counting rate measurement of the stock solution, a counting efficiency of 45% ($=0.037$ Bq/cpm) was estimated. The detection limit can then be expressed as 0.15 Bq per sample; by taking in to account that 3 ml groundwater samples were measured with a detection limit of 50 Bq/kg.

γ-spectrometry measurements of radioactive Cs

As mentioned earlier, radioactive tracers have previously been used in experiments at the TRUE-1 site. As the recovery of the injected sorbing tracers Cs-137 (STT-1, June 1997, Andersson et al. 1998) and Cs-134 (STT-2, June 1998, Andersson et al. 1999) were far from complete, large amounts

of these tracers were present in the injection borehole and the fracture. Estimates of the remaining activity have been made yearly resulting in 4.4 MBq of Cs-137 and 1 MBq of Cs-134 remaining in Feature A at the start of the CEC experiment. With increased chemical concentration of Cs in the CEC experiment, one would expect de-sorption of the radioactive Cs-isotopes to occur. Studies of the breakthrough of these tracers would therefore provide information of the de-sorption characteristics of Cs. One-litre samples from the pumping boreholes were therefore regularly extracted and measured using γ-spectrometry to obtain information of any de-sorption taking place, i.e., radioactive measurements performed as a complement to the Cs-131 measurements.

3.2.4   COM

A schematic drawing of the tracer test equipment used during the COM tests is shown in Figure 3-18. Circulation is controlled by a pump with variable speed (A) and measured using a flow meter (B). Tracer injections are made with a HPLC pump (C) and sampling is made by continuously extracting a small volume of water from the system through a flow controller (constant leak) to a fractional sampler (D). The total injected mass of tracer is weighed using a balance.

The equipment described above is installed in two separate containers at the TRUE-1 site; one injection container and one pump container where the samples are collected.

In order to evaluate the dilution rate in the observation holes, the non-sorbing tracer Uranine was injected prior to each test. Sorbing tracers were also injected in the observation holes with the purpose of mapping flow paths to be traced in future excavations of Feature A.
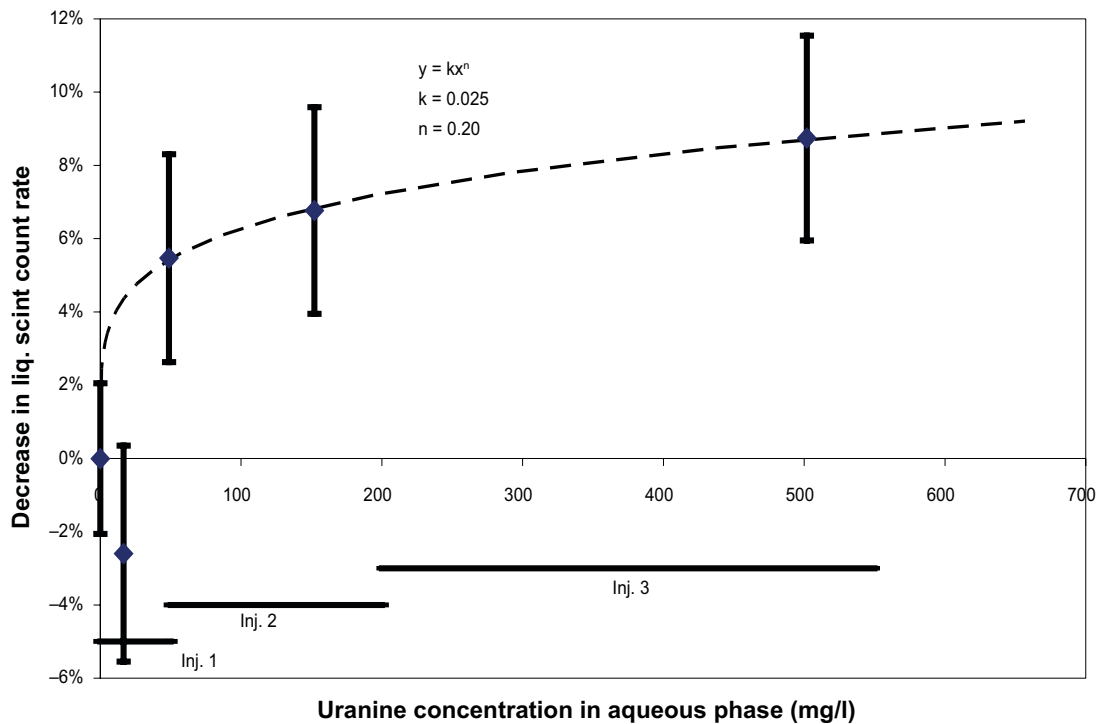
Figure 3-17. *Measured decrease in liquid scintillation counting rate as a function of Uranine concentration. The empirical fitted equation used for compensation due to the Uranine is presented in the figure together with the intervals of the Uranine concentrations used in the injection borehole during the three different injection phases of the CEC experiment.*
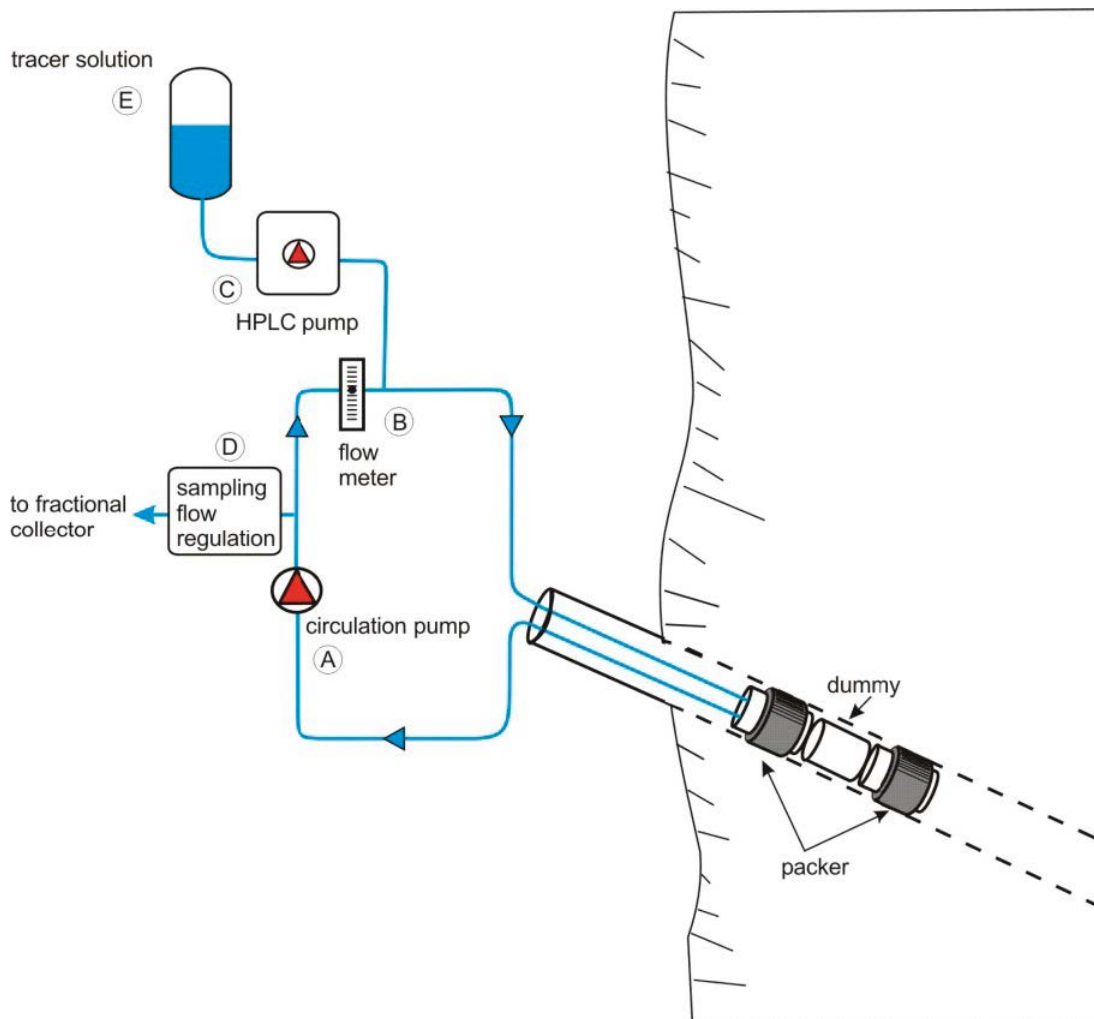
Figure 3-18. Schematic drawing of the tracer injection/sampling system used during the COM-tests.

3.3 Performance of the tests

The equipment has worked well in general and no major hydraulic disturbances have occurred. However, the pump used for injection of chaser fluid showed decreasing flow rates during the last period of water injection during SWIW test 1. Minor problems with the sampling procedure also occurred during the dilution test in KXTT3:S3 during SWIW test 2 with resulting in loss of data. A log of events during the tests is presented in Table 3-5.

3.3.1 SWIW

The borehole section used for injection and pumping during the SWIW test was KXTT4:T3 while KXTT1:R2, KXTT2:R2, KXTT3:S3 and KXTT5:P2 were used as observation sections. Two separate SWIW tests were performed, SWIW test 1 and SWIW test 2, without any radioactive tracers. The plan was to perform one SWIW test without radioactive tracers and one SWIW test with radioactive tracers. However, the total recovery in SWIW test 1 was so low that it was decided to perform an additional test without radioactive tracers. Unfortunately, the recovery in the second test was also too low to perform the radioactive SWIW test. The SWIW tests in KXTT4:T3 were

performed in three steps; tracer injection, chaser phase and withdrawal according to the log of events presented in Table 3-6. The main difference between the two tests was that chaser time in SWIW test 1 was 86 h and 21 h in SWIW test 2. In conjunction with SWIW test 2, dilution tests were performed in KXTT3:S3 and KXTT5:P2 in order to estimate flow rates through the section before the test and during injection and pumping in KXTT4:T3.

Table 3-5. Log of events in TRUE-1 Completion, November 2005–December 2006

Date	Event
051117	Water injection test in KXTT4:T3 in order to verify that the injection rate during the SWIW-test do not exceed 2 bars
051128	Start SWIW test 1 in KXTT4:T3
051212	Stop pumping in SWIW test 1 in KXTT4:T3
060214	Start SWIW test 2 in KXTT4:T3 with dilution tests in KXTT3:S3 and KXTT5:P2
060222	Stop pumping in SWIW test 2 in KXTT4:T3
060320	Start colloid test in KXTT4:T3 including three tests with different pump rates in KXTT3:S3
060424	Stop colloid test
060425	Start crosshole interference tests in TRUE-1 (for details see Table 3-10)
060509	Stop crosshole interference tests in TRUE-1 (for details see Table 3-10)
060522	Start radially converging tracer test T1 (pre-test CEC) between KXTT4:T3 and KXTT3:S3
060529	Stop radially converging tracer test T1 (pre-test CEC) between KXTT4:T3 and KXTT3:S3
060531	Start radially converging tracer test T2 (pre-test CEC) between KXTT4:T3 and KXTT3:S3
060606	Stop radially converging tracer test T2 (pre-test CEC) between KXTT4:T3 and KXTT3:S3
060608	Start tracer dilution test D1 in KXTT4:T3
060613	Stop tracer dilution test D1 in KXTT4:T3
060614	Start tracer dilution test D2 in KXTT4:T3
060616	Stop tracer dilution test D2 in KXTT4:T3
060815	Start tracer dilution test D3 in KXTT4:T3
060821	Stop tracer dilution test D3 in KXTT4:T3
060822	Start radially converging tracer test T3 (pre-test CEC) between KXTT4:T3 and KXTT3:S3
060830	Stop radially converging tracer test T3 (pre-test CEC) between KXTT4:T3 and KXTT3:S3. Continue pumping in KXTT3:S3
061115	Start CEC test between KXTT4:T3 and KXTT3:S3
061208	Stop CEC test between KXTT4:T3 and KXTT3:S3. Starts to decrease pumping rate in KXTT3:S3
061213	Stop pumping in KXTT3:S3

Table 3-6. Log of event in regarding SWIW tests in TRUE-1 Completion.

Start date	Stop date	Event
2005-08-28 18:40	2005-08-28 19:44	Injection of water and tracer solution in KXTT4:T3 (SWIW 1, tracer injection)
2005-08-28 19:44	2005-12-02 08:19	Injection of water KXTT4:T3 (SWIW 1, chaser phase)
2005-12-02 08:32	2005-12-12 08:31	Pumping of water KXTT4:T3 (SWIW 1, withdrawal)
2006-02-14 14:17	2006-02-14 15:14	Injection of water and tracer solution in KXTT4:T3 (SWIW 2, tracer injection)
2006-02-14 15:14	2006-02-15 11:10	Injection of water KXTT4:T3 (SWIW 2, chaser phase)
2006-02-15 11:19	2006-02-20 10:24	Pumping of water KXTT4:T3 (SWIW 2, withdrawal)
2006-02-20 10:24	2006-02-20 11:07	Interruption of pumping
2006-02-20 11:07	2006-02-22 13:09	Pumping of water KXTT4:T3 (SWIW 2, withdrawal)

Table 3-7. Data of injection, chaser phase and withdrawal during SWIW test 1 and 2.

Tracer injection	SWIW test 1	SWIW test 2
Injection time, t_{inj} (min)	64	57
Volume of water injected (ml)	8,970	7,980
Water injection flow rate (ml/min)	140	140
Volume of tracer injected (ml)	841	840
Initial conc. of tracer, C00 (mg/L)	10,000	10,000
Tracer injection flow rate (ml/min)	13.1	14.7
Injected mass of tracer (mg)	8,410	8,400
Chaser phase (water from KA2598A)		
Chaser time, tchaser (min)	5,080	1,200
Volume of water injected (ml)	618,000	162,000
Water injection flow rate (ml/min)	122[1]	135
Withdrawal		
Total withdrawal time (min)	14,400	10,100
Total volume withdrawn (ml)	1,990,000	1,410,000
Withdrawal rate (ml/min)	138	139

[1] Flow rate decrease during the period.

3.3.2 CEC

The CEC test was performed with a radially converging flow field with KXTT3:S3 as pumping section and KXTT4:T3 as injection section. It was preferable that the injection of tracers in KXTT4:T3 did not disturb the flow field and injection should be done without any additional pressure in the injection section. Moreover, it was desirable, from an evaluation point of view, if periods of constant concentration in KXTT4:T3 would be obtained rather quickly.

In order to achieve periods of constant injection concentration, the injection was divided into a step injection in order to reach the appropriate concentration quickly followed by continuous injection to maintain the concentration. The step injection was accomplished by injection with a relatively high flow rate of a tracer solution with high concentration during circulation of one borehole section volume. The continuous injection was carried out with a lower concentration and a lower flow rate. In order to choose the concentrations and flow rates, the groundwater flow rate through the borehole section and the previous concentration in the borehole section must be known. Furthermore, in order to not disturb the pressure, the injection flow rate must at all times be matched by a sampling flow rate.

In order to test the equipment and since the injection procedure was rather complicated, a number of pre-tests were performed prior to the main CEC test.

CEC pre-tests

The original plan was to only perform one tracer test as a dress rehearsal before the main CEC test since the groundwater flow rate in KXTT4:T3 while pumping in KXTT3:S3 was known from the COM tests performed shortly before. However, due to unexpected changes in the hydraulic characteristics of the tested rock volume and equipment problems, several pre-tests were carried out before it was found suitable to execute the main CEC test. The changes in hydraulic characteristics are discussed further on in this report. The CEC pre-tests included a total of three dilution tests and three tracer tests as displayed in Table 3-8. The type of tracers used was alternated in order to have a low background level during the tests.

During the tracer test T2, the actual injection flow rate was higher than planned, so that the pressurised vessel with the tracer solution emptied earlier than planned and nitrogen gas was accidentally injected into the system. Once the gas injection was discovered, KXXT4:T3 was drained in order to remove the injected nitrogen gas.

Table 3-8. CEC pre tests performed at the TRUE-1 site.

Test	Q_{pump} in KXTT3:S3 [ml/min]	Date	Tracer
Tracer tests T1	400	060522–060529	AminoG
Tracer tests T2	400	060531–060606	Uranine
Dilution test D1	400	060608–060613	AminoG
Dilution test D2	400	060614–060616	AminoG
Dilution test D3	400–800	060815–060821	RdWt
Tracer tests T3	800	060822–060830	AminoG

CEC main test

The CEC main test was carried out in November and December of 2006 by using Uranine and Cs^+ (inactive and Cs-131) as tracers. The pumping flow rate in KXTT3:S3 was set to 800 ml/min in order to increase the chances of obtaining a high recovery in the test. The test was carried out in three steps with an increase of concentration with about three times for each step. Due to unfortunate and unforeseen equipment failures some interruptions in the injection occurred. The time for injection start was 2006-11-15 16:14.

Table 3-9. Schedule for injection in KXTT4:T3 during CEC main test.

Time since injection start [h]		Event	Injection flow rate [ml/h]	Concentration of injection solution	
Start	Stop			Uranine [mg/l]	Cs [moles/g]
0.0	0.5	Step injection S1	100	1,797	3.29E–05
0.5	0.7	Short break between S1 and C1	0		
0.7	87.8	Continuous injection C1	4.84	590	1.15E–05
87.8	126.2	Disruption in C1 due to equipment failure	0		
126.2	141.7	C1 resumed	3.84	590	1.15E–05
141.7	142.7	Disruption in C1 due to equipment repair	0		
142.7	165.0	C1 resumed	5.02	590	1.15E–05
165.0	168.1	Short break between C1 and S2	0		
168.1	168.6	Step injection S2	100	3,261	6.74E–05
168.6	168.8	Short break between S2 and C2	0		
168.8	262.8	Continuous injection C2	5.26	1,673	3.36E–05
262.8	306.9	Disruption in C2 due to equipment failure	0		
306.9	332.8	C2 resumed	4.88	1,673	3.36E–05
332.8	335.9	Short break between C2 and S3	0		
335.9	336.4	Step injection S3	100	10,016	1.94E–04
336.4	336.6	Short break between S3 and C3	0		
336.6	545.6	Continuous injection C3	4.67	5,023	9.88E–05
545.6		Injection stop	0		

3.3.3 COM

The COM tests in TRUE-1 Completion consists of a total of eight hydraulic interference tests with measurements of both flow and pressure responses. Flow responses are measured by means of the tracer dilution method and the tests are performed under both ambient and pumped conditions. Pumping is made in all six boreholes penetrating Feature A; KXTT1 – KXTT5 and KA3005A. Table 3-10 shows the events during the COM tests.

Table 3-10. Log of event in regarding COM-tests in TRUE-1 Completion.

Start date	Stop date	Event
2006-04-27 10:00:00	2006-04-27 10:00:00	Starting time for crosshole interference test (time elapsed=0)
2006-04-27 10:00:00	2006-04-27 19:14:28	Undisturbed period 1
2006-04-27 19:14:28	2006-04-28 06:15:46	Pumping KXTT3:S3 400 ml/min
2006-04-28 06:17:42	2006-04-28 16:23:16	Pumping KXTT3:S3 2,800 ml/min
2006-04-28 16:23:16	2006-05-02 17:39:40	Undisturbed period 2
2006-05-02 17:39:40	2006-05-03 13:39:40	Pumping KXTT1:R2 350 ml/min
2006-05-03 13:39:40	2006-05-04 17:30:24	Undisturbed period 3
2006-05-04 17:30:24	2006-05-05 13:00:26	Pumping KXTT5:P2 1,540 ml/min
2006-05-05 13:00:26	2006-05-08 18:30:18	Undisturbed period 4
2006-05-08 18:30:18	2006-05-09 15:20:20	Pumping KXTT2:R2 190 ml/min
2006-05-09 15:20:20	2006-05-10 20:41:18	Undisturbed period 5
2006-05-10 20:41:18	2006-05-11 10:40:22	Pumping KXTT4:T3 200 ml/min
2006-05-11 10:43:20	2006-05-12 10:57:22	Pumping KXTT4:T3 600 ml/min
2006-05-12 10:57:22	2006-05-15 19:59:56	Undisturbed period 6
2006-05-15 19:59:56	2006-05-16 17:14:58	Pumping KA3005A 870 ml/min

3.4 Evaluation

3.4.1 Groundwater flow

Tracer dilution test – general

Flow rates were calculated from the decrease in tracer concentration versus time through dilution with natural unlabelled groundwater, cf. Andersson et al. (2002b). The so-called "dilution curves" were plotted as the natural logarithm of concentration versus time as shown in Figure 3-19. Theoretically, a straight-line relationship exists between the natural logarithm of the relative tracer concentration (c/c_0) and time (t):

$$Q_{flow} = \frac{-V \cdot \Delta \ln(c/c_0)}{\Delta t}$$

Equation 3-19

where Q_{flow} (m^3/s) is the observed groundwater flow rate through the borehole section and V (m^3) is the volume of the borehole section.

Continuous injection

If a continuous injection with a concentration, C_{00}, and a certain flow rate, Q_{inj}, is carried out and the concentration in the borehole section, C_0, reaches a stable level, the groundwater flow, Q_{flow}, may be estimated with a simple mass balance calculation according to Equation 3-20:

$$Q_{flow} = \frac{Q_{inj} \cdot C_0}{C_0} - Q_{sample}$$

Equation 3-20

where Q_{sample} is the flow rate that is withdrawn from the borehole section to monitor its concentration. Compared to the dilution method, the estimate of groundwater flow with continuous injection does not require any knowledge of the borehole section volume. On the other hand, the injection flow rate and concentration must be known.

3.4.2 Tracer tests – general

Model evaluations of tracer breakthrough curves presented in this report are generally made by performing parameter estimation using the basic one-dimensional advection-dispersion model with a single transport pathway. Applied transport models are generally fitted to the experimental tracer breakthrough curves using non-linear least squares regression (see below).
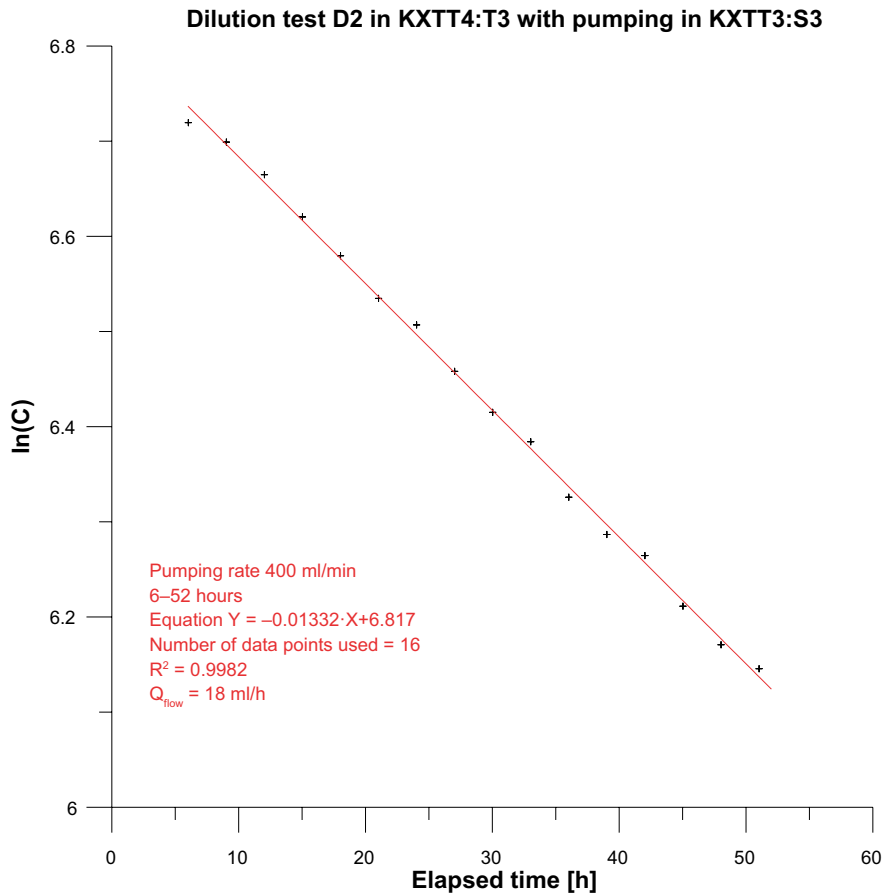
Figure 3-19. *Example of dilution tests for KXTT4:T3.*

This model is described by the standard governing equation for one-dimensional advection-dispersion transport:

$$a_L v \frac{\partial^2 C}{\partial x^2} - v \frac{\partial C}{\partial x} = R \frac{\partial C}{\partial t}$$

Equation 3-21

where C is concentration (e.q. M/L^3), x is distance along transport path (L), t is time (T), v is the average water velocity (L/T) and a_L is the longitudinal dispersivity (L) and R is the retardation factor. The latter parameter is only relevant in the cases where sorbing tracers are used (the CEC experiment).

The following initial and boundary conditions are applied:

$C(x,t) = 0$ ⠀⠀⠀⠀⠀⠀⠀⠀⠀ $t = 0$ ⠀⠀⠀⠀⠀⠀⠀⠀⠀⠀⠀⠀⠀⠀⠀⠀⠀⠀⠀⠀⠀⠀⠀ Equation 3-22

$$\frac{\partial C(x,t)}{\partial x} = 0$$ ⠀⠀⠀⠀⠀⠀ $x = \infty$ ⠀⠀⠀⠀⠀⠀⠀⠀⠀⠀⠀⠀⠀⠀⠀⠀⠀⠀⠀⠀⠀⠀ Equation 3-23

$$-a_L v \frac{\partial C}{\partial x} + vC = C_0$$ ⠀⠀⠀ $x = 0$ ⠀⠀⠀⠀⠀⠀⠀⠀⠀⠀⠀⠀⠀⠀⠀⠀⠀⠀⠀⠀⠀⠀ Equation 3-24

The above boundary and initial conditions results in a solution for a constant injection of tracer. For a tracer pulse with constant concentration of limited duration, the resulting tracer concentration may be calculated as:

$C(x,t) = M(x,t)$ ⠀⠀⠀⠀⠀⠀ $0 < t \le t_{inj}$ ⠀⠀⠀⠀⠀⠀⠀⠀⠀⠀⠀⠀⠀⠀⠀⠀⠀⠀⠀⠀ Equation 3-25

$$C(x,t) = M(x,t) - M(x, t - t_{inj})t > t_{inj} \qquad \text{Equation 3-26}$$

where $M(x,t)$ is the solution for a step-input injection with constant injection concentration. A more complex temporal variation in the tracer injection may be calculated in an analogous way by summation of a several such injection periods. Solutions of the above equations are given, for example, by Javandel et al. (1984).

In the sections describing evaluation of experimental data, estimation parameters are formulated in terms of residence time, t_0 and Peclet number, Pe. For sorbing parameters, R is estimated (see further discussion above under CEC scoping calculations). In addition, a proportionality factor, pf, is usually estimated, basically in order to account for dilution effects.

Parameter estimation method

Estimated parameter values are obtained by non-linear least-squares regression. The basic non-linear least-squares regression minimises the sum of squared differences between the modelled (Y^M) and the observed ($Y°$) variables and may be formulated as:

$$\text{Min } S = E_R^T W E_R \qquad \text{Equation 3-27}$$

where E_R is a vector of residuals ($Y^M - Y°$) and W is a vector of reliability weights on observations.

The specific method for carrying out the regression employed in this study is often referred to as the Marquardt-Levenberg method (Marquardt 1963, Levenberg 1944). This method is a Newton-type optimisation algorithm that finds the parameter values that minimises the sum of squared errors between model and measurement values in an iterative manner. A simplified version of the search algorithm used may be written as:

$$B_{r+1} = B_r + (X_r^T W X_r)^{-1} X_r^T (Y^O - Y_r^M) \qquad \text{Equation 3-28}$$

where B is a vector of parameter estimates, X is a parameter sensitivity matrix, and the subscripts r and r+1 refer to the iteration number.

Given an initial parameter estimate, Equation 3-28 is repeated until a local optimal solution is found. The local minimum is defined by some convergence criterion, for example when parameter estimates are essentially identical between iterations. Finding a local minimum does not guarantee that the global minimum is found. When this appears to be a problem, several sets of initial estimates may be tried. When some knowledge about the physical system and parameters to be estimated is already available, the initial estimates are often good enough for ensuring that a global minimum is found.

An important element of the above procedure is the matrix containing the parameter sensitivities. Parameter sensitivity is defined as the partial derivative of the dependent (simulated) variable with respect to a parameter. A sensitivity matrix contains one row for each observation and one column for each estimated parameter, as in the following example with three observations and two parameters.

$$X = \begin{pmatrix} \dfrac{\partial y_1}{\partial b_1} & \dfrac{\partial y_1}{\partial b_2} \\ \dfrac{\partial y_2}{\partial b_1} & \dfrac{\partial y_2}{\partial b_2} \\ \dfrac{\partial y_3}{\partial b_1} & \dfrac{\partial y_3}{\partial b_2} \end{pmatrix} \qquad \text{Equation 3-29}$$

Parameter sensitivities may be used to determine the precision of the estimated parameter values. Given below are two diagnostic measures regarding parameter uncertainty that may be obtained as a result of regression (Cooley 1979).

The *standard errors* of parameter estimates are obtained by taking the square roots of the diagonals in the parameter covariance matrix, which is given by:

$$s^2(\mathbf{X}^T\mathbf{W}\mathbf{X})^{-1}$$ Equation 3-30

with s^2 being the error variance:

$$s^2 = \frac{\sum_{i=1}^{N} w_i \, (y_i^O - y_i^M)^2}{N - P}$$ Equation 3-31

where N is the number of measurements, P the number of parameters and w_i the weight on observation i.

The linear correlation $r(p_1, p_2)$ between two parameters p_1 and p_2 is expressed by:

$$r(p_1, p_2) = \frac{Cov(p_1, p_2)}{\sqrt{Var(p_1) \, Var(p_2)}}$$ Equation 3-32

where the variance and covariance terms are elements of the $s^2(\mathbf{X}^T\mathbf{W}\mathbf{X})^{-1}$ matrix. The correlation is a measure of the inter-dependence between two parameter estimates and correlation values range between -1 and 1. Values close to either -1 or 1 mean that a change in one parameter value may be compensated for by a similar change in another parameter value to maintain the same fit (sum of squares) between model and measurements.

The standard errors and parameter correlation values are the main diagnostic measures used in this analysis when examining the parameter estimation results from evaluation of the tracer tests.

The regression analysis and statistical analysis has in this study been carried by using the program PAREST (Nordqvist 1994). The results are presented in Chapter 4 below.

3.4.3 SWIW

The SWIW experiments are for the peripheral observation boreholes evaluated with a one-dimensional advection-dispersion transport model and non-linear regression as described above. In the central SWIW section (KXTT4:T3), results would normally be evaluated with a similar model but with radial flow and transport. However, as discussed later in this report, the SWIW section was in this case not evaluated with a transport model due to very low tracer recovery.

3.4.4 CEC

The CEC test was evaluated by using two different methods, further on referred to as basic CEC evaluation and CEC modelling. Both methods use the difference in breakthrough curves in the evaluation but use them differently. CEC is defined as sorbed mass per surface area, often in the terms of μmoles/m^2, hence both the sorbed mass of Cs and the available sorption area must be estimated.

Available sorption area

The surface area available for sorption, A_{sorb}, may be estimated using different assumptions. During subsequent activities of TRUE-1 Completion, Feature A was injected with epoxy, then over-cored and finally analysed for available sorption area if possible. Hence, an investigation of the available sorption area will possibly be presented later on but is not available at this time.

In KXTT4:T3 two flowing fractures are interpreted (Feature A and A') while only Feature A is interpreted in KXTT3:S3. However, preliminary results from the epoxy injection and subsequent over-coring of KXTT3 and KXTT4 indicate that Feature A, at least in the interception with KXTT3, include several more or less parallel fractures. This could of course be only a local effect, so it is

reasonable to assume that the tracer transport from KXTT4:T3 to KXTT3:S3 occurs in 1–4 (or even more) fractures. Furthermore, the fractures are here assumed to be plane-parallel without any roughness so that the area of the fracture wall, A_w, is twice the area of the fracture itself, A_f, i.e. A_w/A_f is 2.

If the flow field is assumed to be radially converging, except around the injection hole where it is assumed that the flow lines converge and diverge due to a higher hydraulic conductivity within the borehole, an estimation of the available sorption area is:

$$A_{sorb} = r \cdot r_w \cdot \frac{A_w}{A_f} \cdot no_f \cdot c \qquad\qquad \text{Equation 3-33}$$

where r is the distance between the borehole sections, r_w is the radius of the injection borehole, no_f is the number of flowing fractures and c is the factor accounting for the convergence around the injection borehole. Assuming that c is 2 (Halevy et al. 1967) and no_f equals 2 the estimate for KXTT3:S3 and KXTT4:T3 is:

$$A_{sorb} = 4.6 \cdot 0.028 \cdot 2 \cdot 2 \cdot 2 = 1.0\,m^2 \qquad\qquad \text{Equation 3-34}$$

Accordingly, assuming four flowing fractures, A_{sorb} is 2 m^2 with all other parameters left unchanged.

If channel flow is assumed instead, the surface area available for sorption is:

$$A_{sorb} = L \cdot w \cdot \frac{A_w}{A_f} \cdot no_f \qquad\qquad \text{Equation 3-35}$$

where L and w are the length and width, respectively, of the flowing channels. The parameter no_f is in this case the number of flowing fractures or channels. If two flowing channels with widths equal to the borehole radius are assumed, the estimated surface area available for sorption becomes:

$$A_{sorb} = 4.6 \cdot 0.028 \cdot 2 \cdot 2 = 0.5\,m^2 \qquad\qquad \text{Equation 3-36}$$

Considering the assumptions above, it is fair to assume that the surface area available for sorption in the flow path from KXTT3:S3 and KXTT4:T3 is in the range of a couple of square metres. This is a very rough estimate of the available sorption area. For example, if accounting for surface roughness and matrix inner surfaces the surface would be much larger.

Another uncertainty about the available sorption area is if significant sorption to the borehole walls of the packed-off section occurs. If this is the case, these areas should be included in the area calculations. The area of the borehole walls, A_{bh} in KXTT3:S3 and KXTT4:T3 is:

$$A_{bh} = (2.05 + 2.00) \cdot 2 \cdot \pi \cdot 0.028 = 0.7\,m^2 \qquad\qquad \text{Equation 3-37}$$

All and all, it is reasonable to assume a surface area available for sorption in the CEC test in the range of 0.5–3 m^2 if the fractures are assumed to be plane-parallel without any roughness.

Basic CEC Evaluation

For the basic CEC evaluation the amount of non-sorbing and sorbing tracer arriving at the pumping section at the end of the test are compared. The difference between the relative concentration of these two will then indicate how much of the sorbing tracer that is left in the fracture system. First of all, the amount of Cs that has adsorbed in the fracture system ($M_{sorb,Cs}$) is calculated by using Equation 3-38:

$$M_{Sorb,Cs} = \frac{M_{pump,Uranine}}{M_{tot,uranine}} M_{tot,Cs} - M_{pump,Cs} \qquad\qquad \text{Equation 3-38}$$

where M_{sorb} is adsorbed mass, M_{pump} is the accumulated mass arriving at the pumping section and M_{tot} is the total injected mass.

An estimate of the surface related CEC (moles/m²) can then be made according to Equation 3-39, given the general uncertainties for surface estimation:

$$CEC = \frac{M_{sorb,Cs}}{A_{sorb}}$$

Equation 3-39

CEC modelling

The tracer breakthrough curves for the CEC experiments were evaluated with one-dimensional transport models and non-linear regression as described above in Section 3.4.2. In addition to advection and dispersion, sorption of Cesium was evaluated. Two types of equilibrium sorption isotherms were considered in the evaluation: a linear sorption isotherm and a Langmuir isotherm, the latter in order to account for site-limitation effects. See Section 3.1.3 for more details about Langmuir sorption.

3.4.5 COM

The evaluation of the COM tests involves calculations of groundwater flow rates, pressure response times and pressure drawdown.

Pressure responses

Pressure responses during the COM tests were observed and evaluated with respect to both time and magnitude. The qualitative evaluation has only been made on data from the drawdown phase.

From the pressure data, the response times (t_R) for each section was estimated. The response time was defined as the time after start of pumping when a drawdown of at least 1 kPa (0.1 m) is observed. This threshold pressure drop was chosen with consideration to the amplitude of the tidal effects in the boreholes, which may be in the order of 1–5 kPa. It is expected that the response time is partly dependent on the distance from the sink to the point of observation. Hence, the ratio of the response time (t_R) and the (squared) straight-line distance, r, between the sink and the observation point (t_R/r^2) was used in the analysis. The ratio is inversely related to the hydraulic diffusivity of the rock and indicates the speed of propagation in the rock of the drawdown created in the pumping section. The straight-line distances between intersects of Feature A in the boreholes are given in Appendix 3.

The final drawdown at stop of pumping (s_p) in the observation sections was determined from the pressure data. To account for the different flow rates used in the tests and to make the pressure response plots comparable between tests, the final drawdown is normalised with respect to the final flow rate (Q_{pump}) using the ratio s_p/Q_{pump} in the analysis.

The ratios s_p/Q_{pump} and t_R/r^2 may be used in so called response plots with t_R/r^2 on the x-axis and s_p/Q_{pump} on the y-axis. From such response plots, sections with anomalous, fast response times (high hydraulic diffusivity) and large (normalised) drawdown can be identified. Such sections, showing primary responses, can be assumed to have a distinct hydraulic connection to the sink and may be intersected by a channel in a fracture plane or other highly conductive structures in the rock. On the other hand, sections with delayed and weak (secondary) responses may correspond to sections in the rock mass between such structures. The ratios s_p/Q_{pump} and t_R/r^2 and their corresponding response plots have earlier been used in similar tests as for example by Andersson et al. (2002a).

The pressure responses may also be used to evaluate transmissivity values. An advantage of this compared to s_p/Q_{pump} is that the distance from the pumping hole to the observation hole is included in the calculation. Transmissivity for a single borehole, i.e. the pumping hole for a particular test, may be calculated according to Moye's equation:

$$T_M = \frac{Q_{pump} \cdot (1 + \ln(L/(2 \cdot r_w)))}{2 \cdot \pi \cdot s_p}$$

Equation 3-40

where L is the section length and r_w is the borehole radius of the pump hole. Note that s_p in this case is the drawdown in the pumped borehole itself.

To evaluate the transmissivity in between two boreholes, Thiem´s well equation may be used:

$$T_{Th} = \frac{Q_{pump} \cdot \ln(r/r_w)}{2 \cdot \pi \cdot \Delta h}$$ Equation 3-41

where Δh is the pressure difference between the pump hole and the observation hole at the end of the pumping.

The transmissivity for a flow path between two boreholes, T_{Th}, may be compared to the transmissivity of the pumping hole, T_M. For a relatively homogeneous feature, it is expected that T_{Th} is rather close to T_M. On the other hand, if T_{Th} is much higher than T_M this indicates a relatively large drawdown in the observation hole compared to the pumping hole which may be a sign of a very good flow path between the observation hole and the pumping hole. Hence, for this comparison it is natural to form the ratio T_{Th}/T_M and use this in the evaluation and interpretation.

To facilitate the interpretation of the calculated values of s_p/Q_{pump}, t_R/r^2 and T_{Th}/T_M, these responses where classified in order to visualize the results in tables and figures.

For s_p/Q_{pump}, the following class limits were used:

$s_p/Q_{pump} \geq 1 \cdot 10^6 \ s/m^2$	*Excellent (Red),*
$3 \cdot 10^5 \leq s_p/Q_{pump} < 1 \cdot 10^6 \ s/m^2$	*High (Yellow),*
$1 \cdot 10^5 \leq s_p/Q_{pump} < 3 \cdot 10^5 \ s/m^2$	*Medium (Green),*
$s_p/Q_{pump} < 1 \cdot 10^5 \ s/m^2$	*Low (Blue).*

For t_R/r^2 the following class limits were used:

$t_R/r^2 < 0.1 \ s/m^2$	*Good (G),*
$0.1 \leq t_R/r^2 < 0.3 \ s/m^2$	*Medium (M),*
$t_R/r^2 \geq 0.3 \ s/m^2$	*Bad (B).*

For T_{Th}/T_M, the following class limits were used:

$T_{Th}/T_M \geq 4$	*Excellent (Red),*
$2.00 \leq T_{Th}/T_M < 4.00$	*High (Yellow),*
$0.50 \leq T_{Th}/T_M < 2.00$	*Medium (Green),*
$T_{Th}/T_M < 0.50$	*Low (Blue).*

The classes were based on that T_{Th}/T_M close to 1 is expected for a radial homogenous feature and a higher ratio is expected for a relatively highly transmissive feature.

Flow responses

The flow rate in an observation hole may be calculated theoretically if it is assumed that the feature is two dimensional, homogenous and the flow is radially converging. Under such assumptions the flow through the observation hole is proportional to the pumping flow rate and the diameter of the observation hole divided by a circumference with a radius (r) equal to the distance between the pumping hole and the observation hole according to Equation 3-42:

$$\frac{Q_{theory}}{Q_{pump}} = \frac{2 \cdot r_o}{2 \cdot \pi \cdot r}$$ Equation 3-42

where Q_{theory} is the theoretical flow trough the observation hole and r_o is radius of the observation hole. However, it is commonly assumed that the flow lines converge in a otherwise radial flow field in the vicinity of a borehole. Hence, the effective diameter is larger than the actual. In this case we assume that the effective diameter is twice the actual diameter, resulting in the Equation 3-43 for calculation of Q_{theory}:

$$Q_{theory} = \frac{Q_{pump} \cdot 2 \cdot r_o}{r \cdot \pi}$$
<div align="right">Equation 3-43</div>

Since Qflow will be close to Qtheory if the flow field is radially and homogenous, the ratio Qflow/ Qtheory was formed and divided into the following classes for evaluation and interpretation purposes:

$Q_{flow}/Q_{theory} \geq 4$ Excellent (Red),

$2.00 \leq Q_{flow}/Q_{theory} < 4.00$ High (Yellow),

$0.50 \leq Q_{flow}/Q_{theory} < 2.00$ Medium (Green),

$Q_{flow}/Q_{theory} < 0.50$ Low (Blue).

With this concept of measuring the groundwater flow, the result is the magnitude of the flow. However, the groundwater flow also has a component of direction which this method does not give any information about. The flow direction may play a significant part in the evaluation, especially if natural flow is relatively large and flow responses are of the same order.

4 Results and interpretation

4.1 SWIW

4.1.1 General

As mentioned in section 3.3.1, two SWIW experiments with a non-sorbing tracer (Uranine) were performed, although only one was planned. The first SWIW experiment resulted in very low tracer recovery in the SWIW section as shown in Table 4-1. It was therefore decided to repeat the experiment employing a considerably shorter chaser period (the duration for injection of chaser fluid following the tracer injection) but with other experimental variables the same as during the first experiment. Thus, the main difference between the two experiments (SWIW test 1 and SWIW test 2, respectively) was that the total injected water volume was much smaller in SWIW test 2 (169 L compared to 627 L for SWIW 1). The recovery in SWIW test 2 was higher than in SWIW test 1, as shown in Table 4-1. However, the recovery was still too low for carrying out a SWIW test with radionuclides as originally planned. The recovery shown in Table 4-1 was calculated by integration of the breakthrough curve.

Table 4-1. Mass recovery during the withdrawal phase of the SWIW tests in KXTT4:T3.

	SWIW test 1	SWIW test 2
[mg]	162	934
(%)	1.92%	11.1%

An overall view of the results in the SWIW section (in KXTT4) as well as peripheral observation boreholes from both of the SWIW tests is shown in Figure 4-1, see also Figure 1-2. These results are discussed and analysed in more detail in subsequent sections. The times for first tracer arrival in the observation boreholes were fairly consistent between the two SWIW tests as shown in Table 4-2. The groundwater flow was estimated by dilution measurements in KXTT3:S3 and KXTT5:P2 during SWIW test 2. It is clear from Table 4-3 that the groundwater flow in these two sections were affected by the injection and withdrawal in KXTT4:T3. The evaluation of the dilution tests are presented in Appendix 4. In the dilution test in KXTT5:P2, the concentration was increasing prior to the SWIW injection, as seen in Figure A4-4. The reason for this is not known, but a reasonable explanation may be some kind of malfunctioning equipment that was not discovered at the time. The increasing tracer concentration is presented as a negative groundwater flow in Table 4-3 but this value should be regarded as incorrect. The value is nevertheless presented in Table 4-3 to show that the SWIW injection affects the groundwater flow in KXTT5:P2.

Table 4-2. Time (h) for first tracer arrival in observation borehole section during the SWIW tests.

| Borehole:Section	SWIW test 1	SWIW test 2
KXTT1:R2	21	21
KXTT2:R2	11	13
KXTT3:S3	3	3
KXTT5:P2	5	3–8
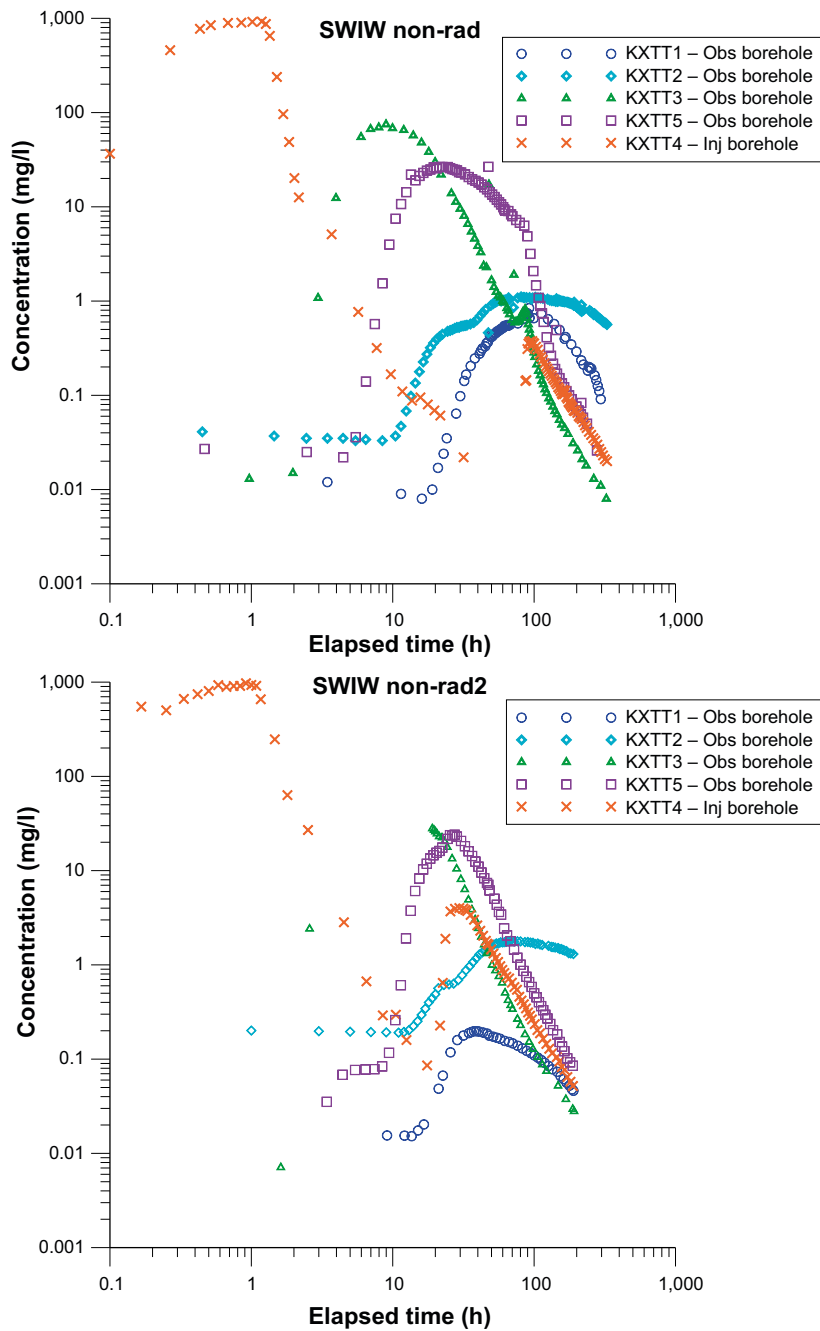
Figure 4-1. *Tracer breakthrough for test SWIW test 1 & 2 with injection in KXTT4 and observation in KXTT1, KXTT2, KXTT3 and KXTT5, logarithmic concentration- and time scales.*

Table 4-3. Groundwater flow in KXTT3:S3 and KXTT5:P2 estimated by dilution measurements prior, during and after SWIW test 2 in KXTT4:T3.

| | Groundwater flow [ml/h] | |
	KXTT3:S3	KXTT5:P2
Prior to injection	170	–220/–20[2]
During injection	[1]	2.4
During withdrawal	280	41
After withdrawal	190	8.3

[1] No evaluation due to missing samples.

[2] Increasing concentration, false value.
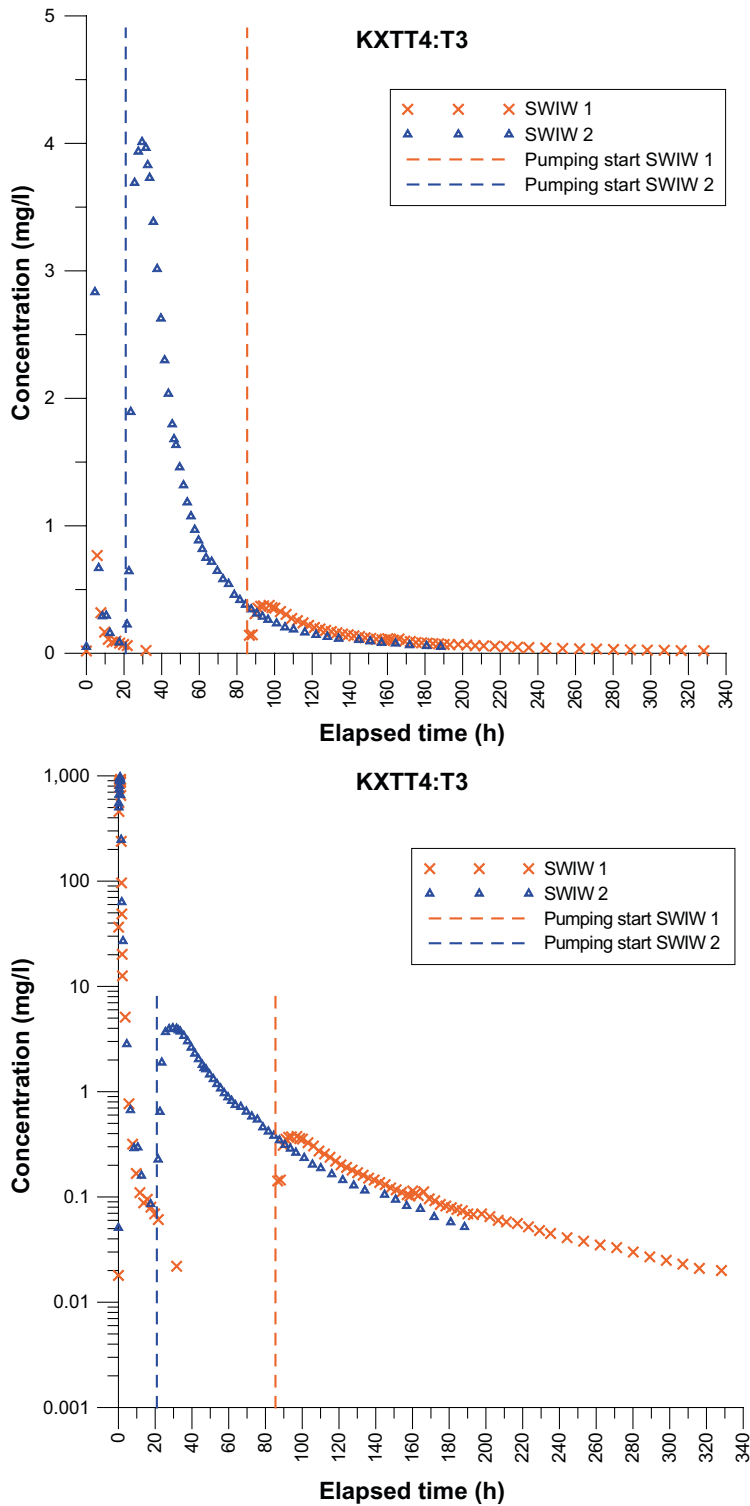
Figure 4-2. *Tracer concentration in the SWIW section (KXTT4, section T3) in linear (top) and semi-logarithmic plots (bottom). Dashed vertical line show the start of the pump-back phase for each SWIW experiment.*

4.1.2 SWIW section results – KXTT4:T3

The tracer breakthrough curves from both SWIW tests in the central injection/withdrawal borehole KXTT4, section T3, are shown in Figure 4-2.

The tracer breakthrough curves during the pump-back phase look approximately like what would be expected from a SWIW experiment. However, the tracer recovery is remarkably low in both of

the SWIW tests. In SWIW test 1, the recovery was as low as approximately two percent. This was also the main reason for repeating the experiment with a considerably shorter chaser injection phase. However, also SWIW test 2 resulted in a very low recovery, about five percent.

The low recoveries from the SWIW tests means that most of the tracer mass does not return to the SWIW section in KXTT4 during the pump-back phase. One possible explanation for this may be the influence of the ambient hydraulic background gradient, which might act to carry tracer sufficiently far away so it would not be re-captured by the recovery pumping. Such strong gradient is not indicated from available head measurement in the experimental boreholes but may nonetheless be a possibility considering the close proximity to the tunnel system.

Supporting evidence for a strong background gradient may be found in the breakthrough curves themselves. The tracer peak during the pump-back phase appears very soon after flow reversal and there is not a significant visible difference between two SWIW tests, despite that total injection time is about four times longer in SWIW test 1. Such an early peak is characteristic for a SWIW test influenced by a hydraulic gradient, as the "upstream" part of the tracer plume returns faster to the SWIW section.

Because of the low tracer recoveries, no modelling analyses of the SWIW section results were made.

4.1.3 Observation sections – peripheral boreholes

KXTT1, section R2

The tracer breakthrough curves in KXTT1:R2 for both of the SWIW tests are shown in Figure 4-3. Interpretation of the results is in this case not straight-forward. In SWIW test 1 the start of the pump-back phase occurs approximately in the middle of the breakthrough curve. One interpretation of this is that the ascending part of the curve is a result of tracer entering the borehole section as in a radially diverging tracer experiment. After water injection is stopped the breakthrough curve starts to descend, although there is some data scatter just at the injection stop. SWIW test 1 also becomes more complex to interpret because of a flow decrease after about 68 hours from 130 to about 85 ml/min. This seems to coincide with a levelling off in the breakthrough curve. The descending part of the SWIW curve could then be from tracer returning back through the observation section.

However, the results from SWIW test 2, with much shorter water injection duration, are not consistent with the interpretation of SWIW test 1. In SWIW test 2, the peak of the breakthrough clearly comes after the start of the withdrawal pumping, without any indications of an earlier peak. This means that the breakthrough curve continues to ascend well after the pumping is reversed. Because the transient storage effects are very limited (in general in this geological media) the most plausible explanations for this finding are:

- The tracer comes back along a different flow path than was taken during injection.

- Some of the tracer continues to migrate towards KXTT1 (and away from KXTT4) despite the pumping reversal, i.e. there is an ambient background gradient that is strong enough to maintain the required flow. Available pressure measurements give no indications that this would be the case, however, data is too sparse to obtain a comprehensive picture of the head distribution within the experimental volume.

Assuming that the flow through the borehole section is similar during both SWIW tests, the total tracer mass that passes KXTT1 is much smaller in SWIW test 2. One interpretation of this is that the shorter injection pumping in SWIW test 2 "pulls back" a large part of the tracer plume before it reaches, or enters into the "capture zone" of KXTT1. This seems consistent with the hypothesis of a hydraulic stagnation point during pumping between KXTT4 and KXTT1, i.e. as in bullet 2 above.

Because of the somewhat ambiguous results, further transport modelling is only presented for the SWIW test 2 breakthrough curve. Although it seems uncertain whether the breakthrough curve represents purely one-dimensional transport, at least the ascending part should be fairly reliable in this respect. Figure 4-4 shows the results from a best-fit regression analysis with a one-dimensional advection-dispersion model (see section 3.4.2).
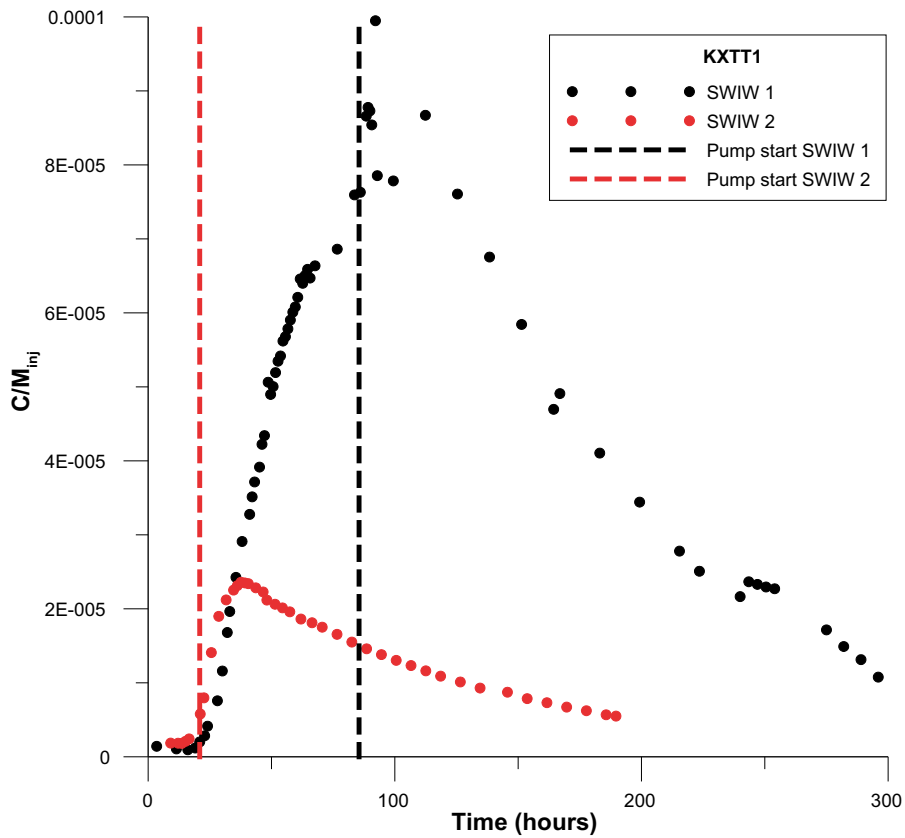
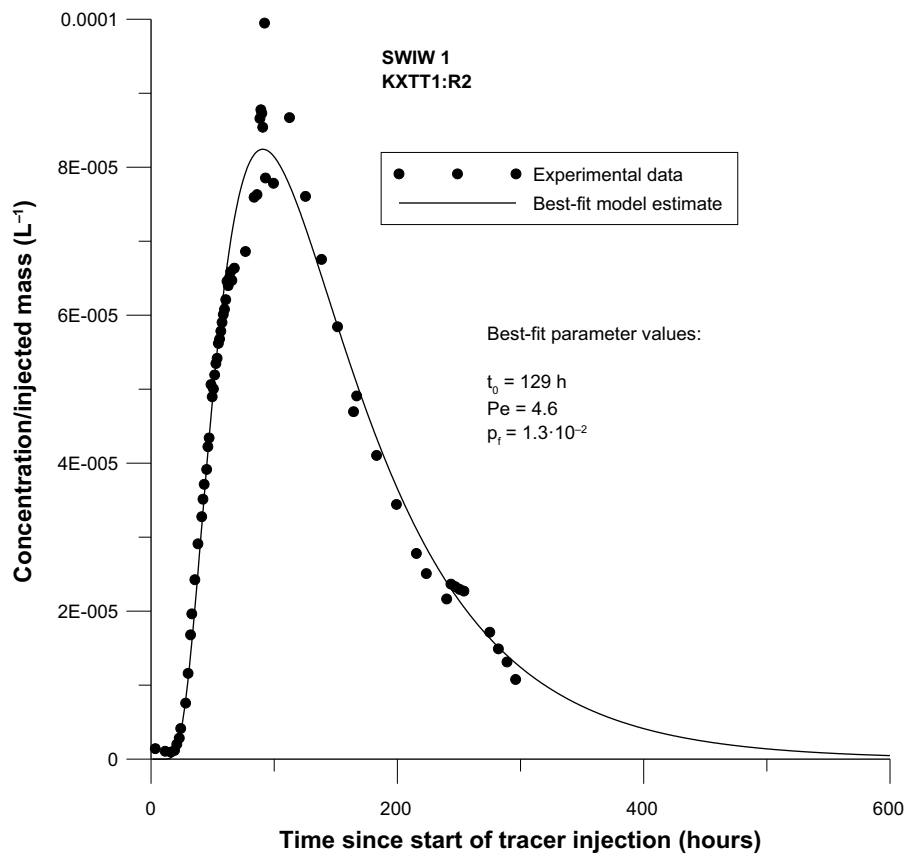*Figure 4-3.* *Tracer breakthrough in borehole KXTT1, section R2.*

Figure 4-4. *Best-fit results for KXTT1:R2 (SWIW test 1 only) breakthrough using a one-dimensional advection-dispersion model.*

KXTT2, section R2

The tracer breakthrough curves in KXTT2:R2 are shown in Figure 4-5.

As for KXTT1, the peak during SWIW test 2 occurs after the flow is reversed. In fact, KXTT1 and KXTT2 appear to behave fairly similar in response to SWIW test 2. The breakthrough curve for SWIW test 1 is lower than for SWIW test 2, but otherwise the curves appear to be approximately similar in shape. This is puzzling because of the differences in duration of chasing and is clearly inconsistent compared with the breakthrough in KXTT1.

One hypothesis for explaining the observed tracer behaviour in KXTT2 might be that the natural flow component dominates, i.e. the injection/pumping flows in the central SWIW borehole section have only minor influence on the tracer transport. Then the breakthrough curve can possibly be explained by slightly different flow regimes between SWIW tests 1 and 2 due to the different injection times. It may be possible that the tracer is more dispersed during SWIW test 2 when it passes the borehole than during SWIW test 1. Because tracer mass passing the borehole appears to be very similar for both SWIW tests, one might speculate that no or very little tracer is "pulled back" in this case during the pump-back phase. However, and as mentioned above, there is no evidence from available head measurements that such a dominating ambient flow, as speculated here, exists.

Based on the assumption that ambient background flow might dominate the tracer transport in this case, it is possible to apply a simple one-dimensional advection transport model (see section 3.4.2) to the breakthrough curves; i.e. neglecting the flow reversal effect. The results of this are shown in Figure 4-6. Because of the incomplete data for the later parts of the breakthrough curves, it is difficult to fully assess how well the model fits the experimental data.
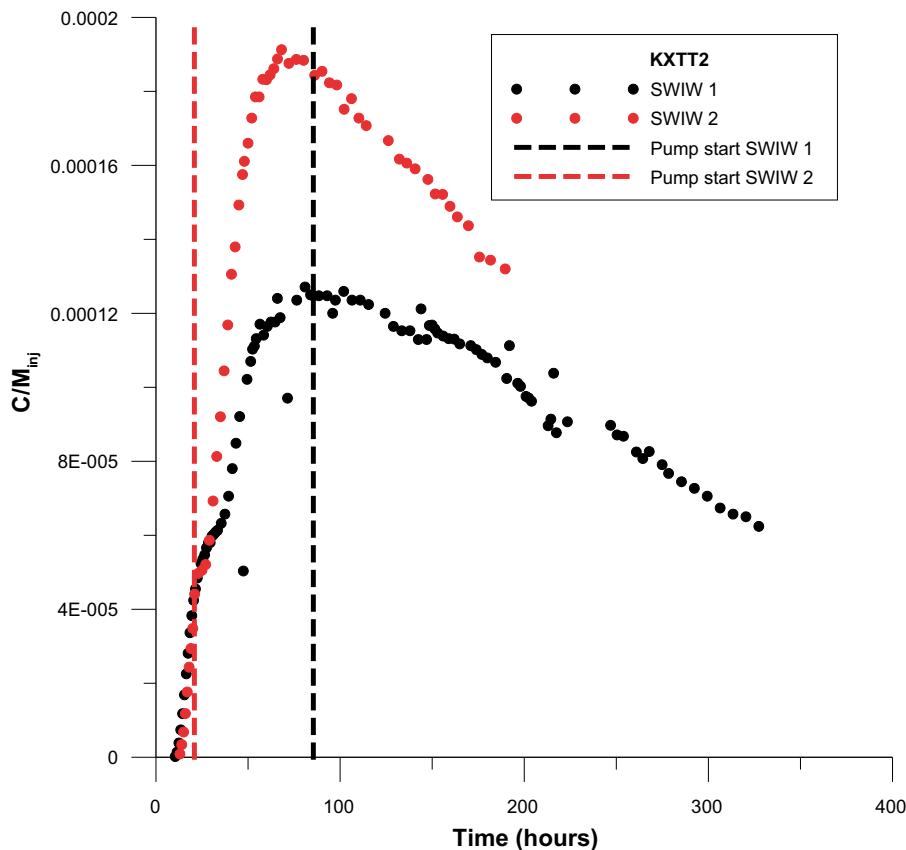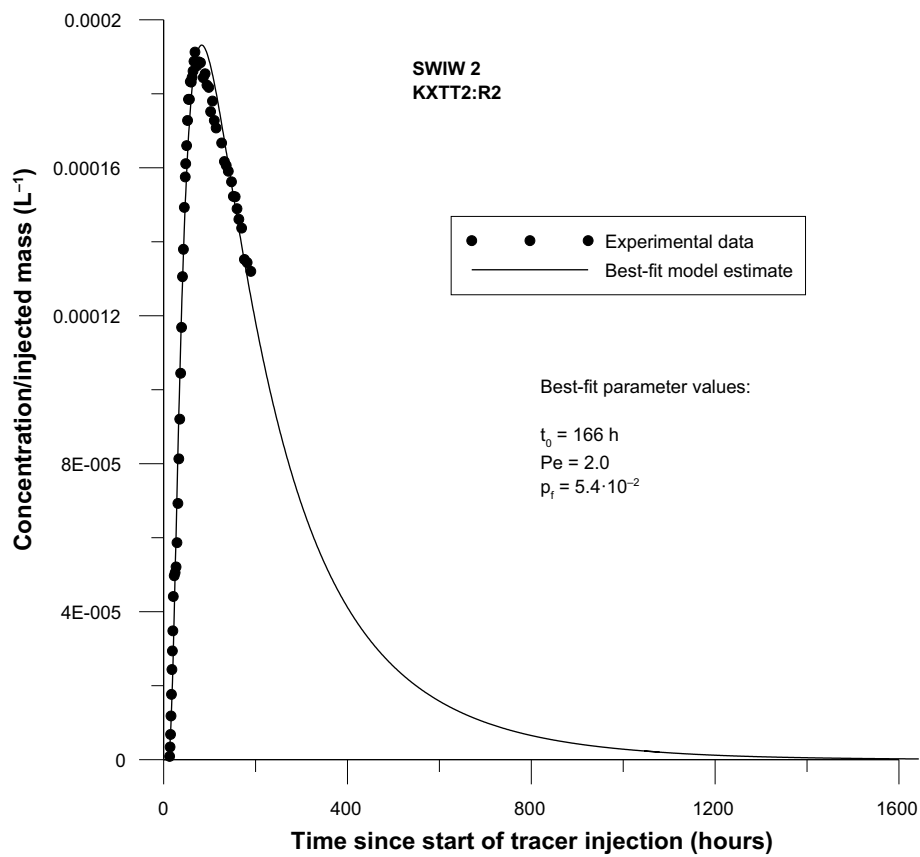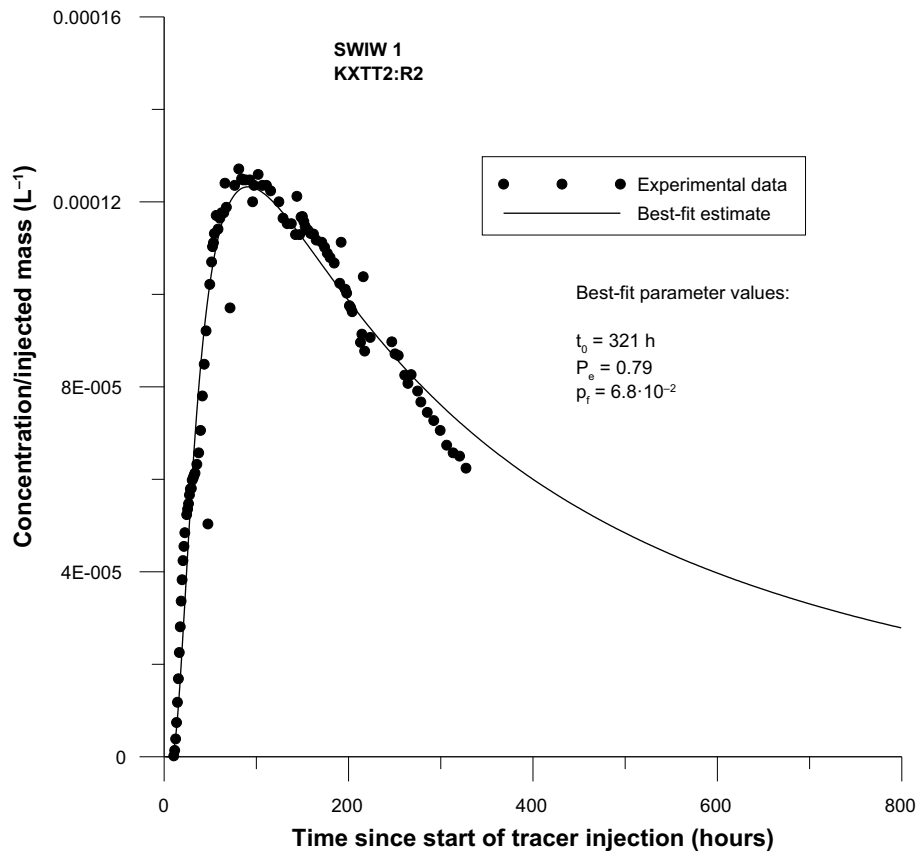

Figure 4-5. *Tracer breakthrough in borehole KXTT2, section R2.*

Figure 4-6. Best-fit results for KXTT2 breakthrough using a one-dimensional advection-dispersion model.

KXTT3, section S3

The tracer breakthrough curves in KXTT3:S3 are shown in Figure 4-7.

The tracer breakthrough in this borehole section is the fastest of all of the four peripheral observation sections. The appearance of the tracer breakthrough curves is more or less like one would expect. One might expect to observe a second peak during SWIW test 2 when the flow is reversed (vertical dashed red line). However, such a peak is not clearly visible. One-dimensional transport modelling was carried out for both of the SWIW tests, despite the fact that data are missing for a considerable portion of the SWIW test 2 curve in this borehole and the results are shown below in Figure 4-8.

In contrast to the preceding case (KXTT2), there is very good agreement between the results from the two SWIW tests. In addition, the obtained Peclet number indicates a much more moderate dispersion effect than for KXTT2. It seems reasonable to conclude that tracer breakthrough in KXTT3 is the results of a pure radially diverging test that can be well described with a one-dimensional advection-dispersion model.

KXTT5, section P2

The tracer breakthrough curves in KXTT5:P2 are shown in Figure 4-9.

As for KXTT3, relatively fast transport is indicated, peaks occur after about 20–30 hours. The breakthrough curve for SWIW test 2 is slightly lower than for SWIW test 1, which could possibly be an effect of that the tracer has not fully passed beyond the observation borehole before the pump-back phase begins (vertical dashed red line). The breakthrough curve for SWIW test 1 appears to behave much more as one might expect. The tracer goes through the observation borehole during all of the water injection phases, and then there is a clear discontinuity in the breakthrough curve when the flow is reversed (vertical dashed black line). A flow change at this time is also indicated by dilution measurements (see section 4.1.1). The breakthrough after this point would then represent tracer re-entering the borehole section.
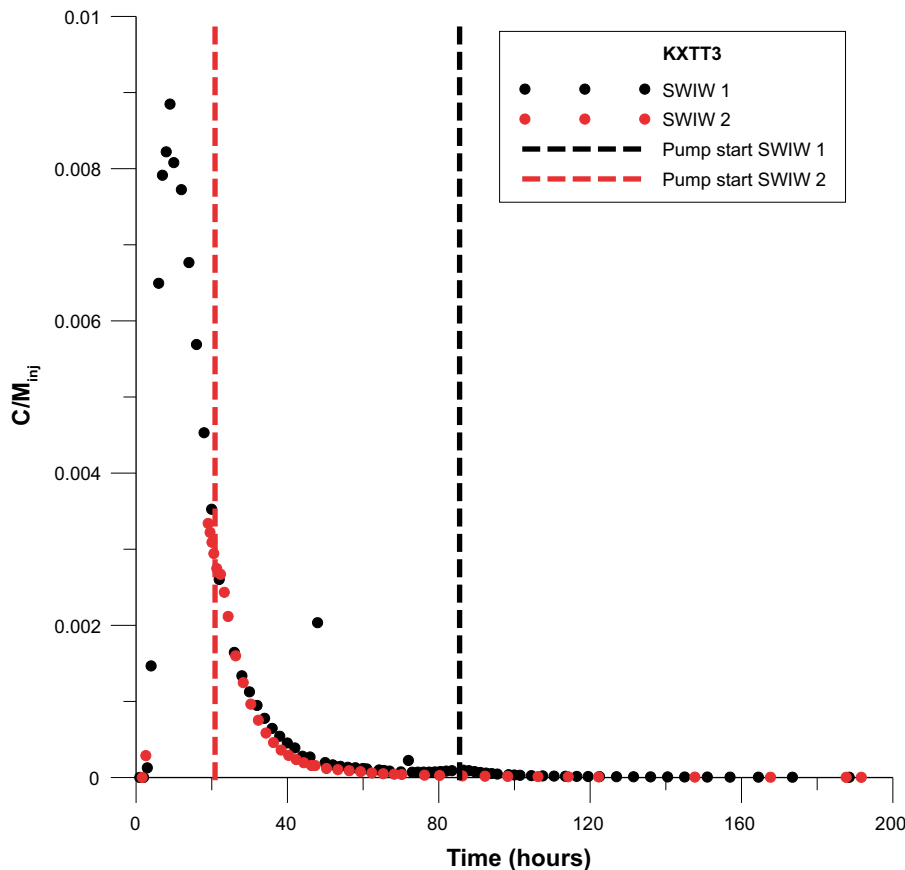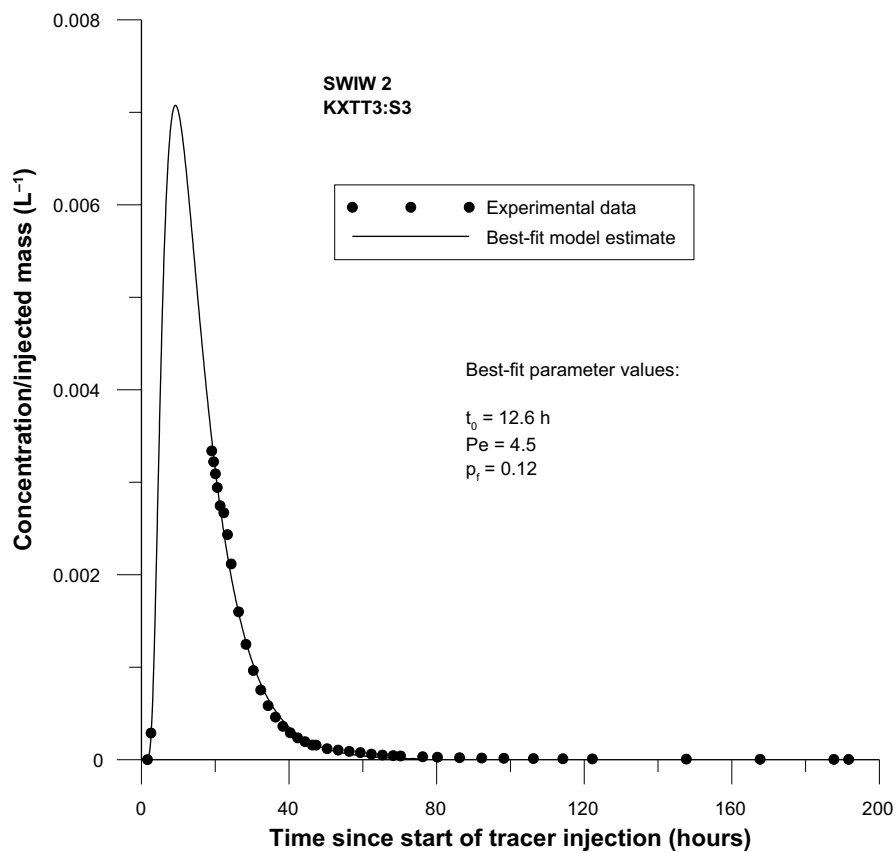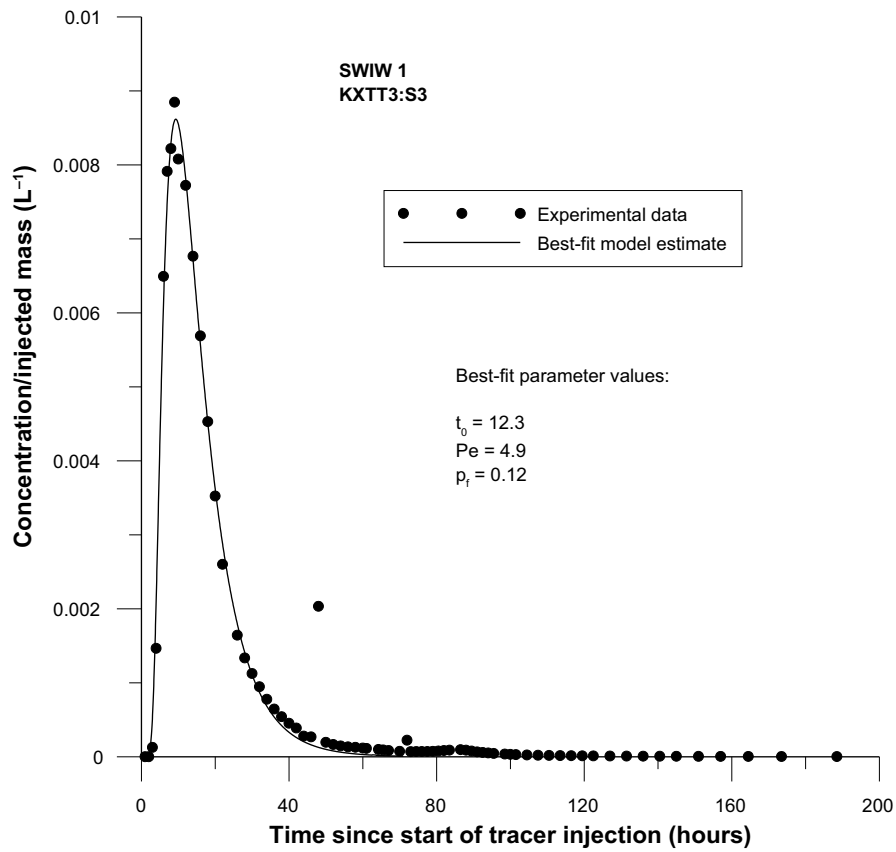

Figure 4-7. *Tracer breakthrough in borehole KXTT3, section S3.*

Figure 4-8. *Best-fit results for KXTT3 breakthrough using a one-dimensional advection-dispersion model.*
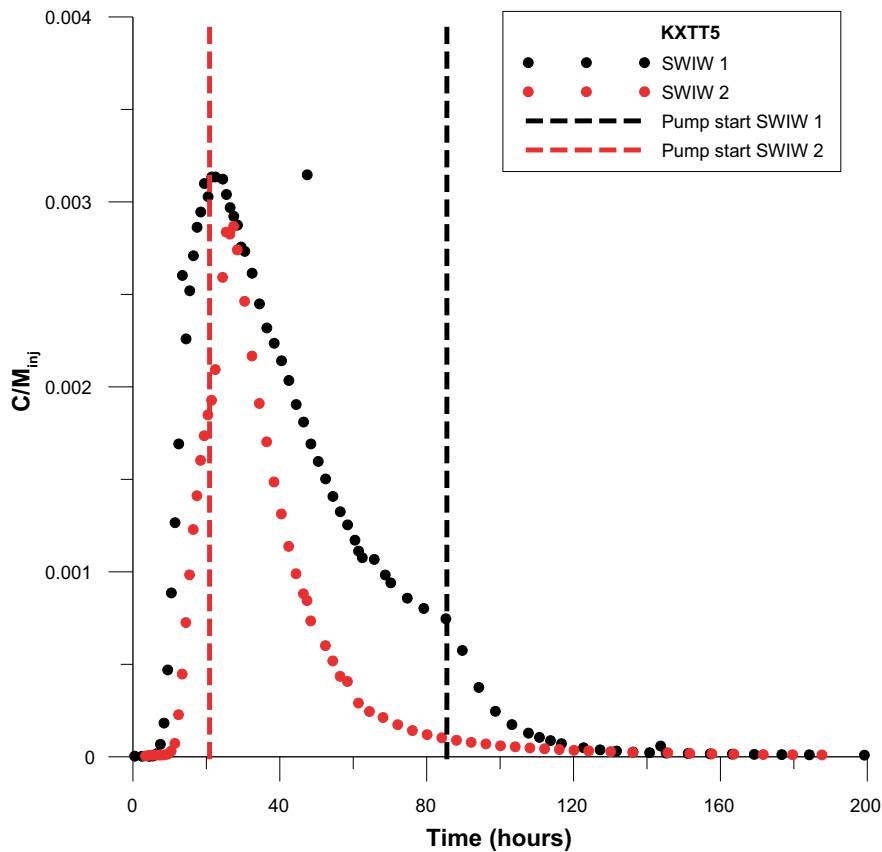
Figure 4-9. *Tracer breakthrough in borehole KXTT5, section P2.*

In this case, one-dimensional transport modelling is presented only for SWIW test 1 because tracer breakthrough during SWIW test 2 is likely affected by the switch to the pump-back phase in the middle of the breakthrough curve. The modelling result is shown in Figure 4-10.

4.1.4 Summary

The results from the observation borehole sections are summarized in Table 4-4.

Table 4-4. Summary of results from observation boreholes.

		Distance (m)	t0 (h)	Pe	pf	Max C/Minj
SWIW 1	KXTT1	5.5	129	4.6	$1.3 \cdot 10^{-2}$	0.001
	KXTT2	5.0	321	0.79	$6.8 \cdot 10^{-2}$	0.001
	KXTT3	4.6	12.3	4.9	0.12	0.009
	KXTT5	6.1	35.6	4.0	0.14	0.003
SWIW 2	KXTT1	5.5	40[1]	–	–	$2.5 \cdot 10^{-5}$
	KXTT2	5.0	166	2.0	$5.4 \cdot 10^{-2}$	0.0002
	KXTT3	4.6	12.6	4.5	0.12	0.007[2]
	KXTT5	6.1	25[1]	–	–	0.003

[1] Approximate peak arrival time – not obtained by modelling.

[2] Estimated from fitted curve – data missing.
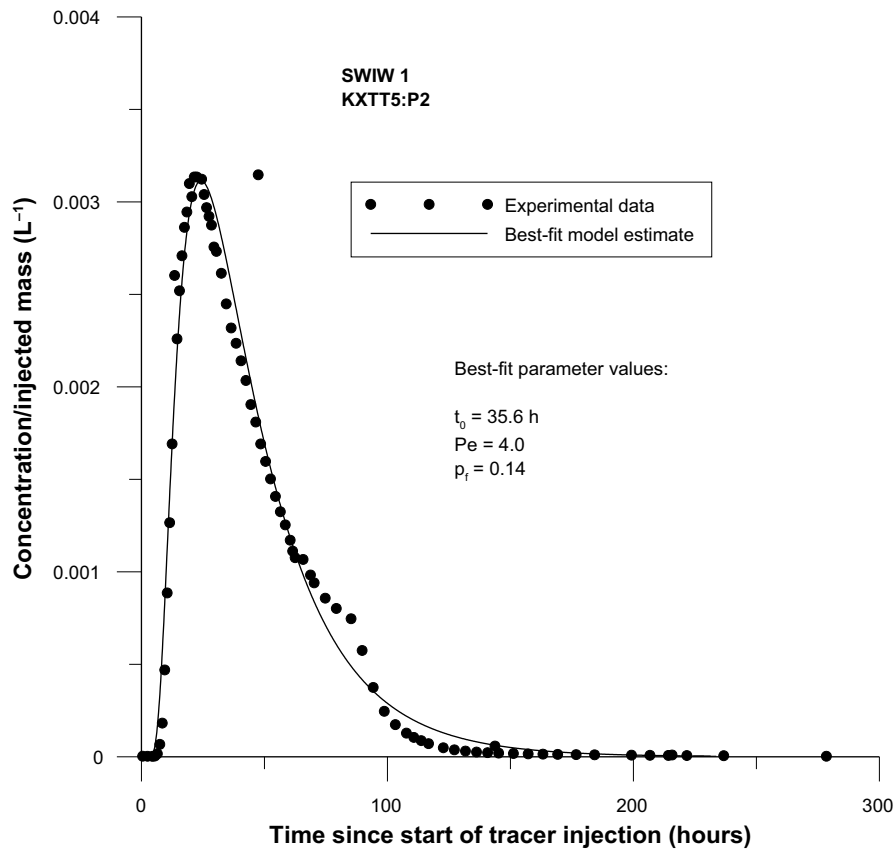
Figure 4-10. *Best-fit results for KXTT5 (SWIW test 1 only) breakthrough using a one-dimensional advection-dispersion model.*

The results indicate that tracer transport varies considerably among the observation borehole sections distributed across the plane of Feature A. In two of the boreholes, KXTT3 and KXTT5, transport is relatively fast and with moderate amounts of dispersion. The proportionality factor, *pf*, is a fitting parameter that is used to adjust the magnitude of the simulated breakthrough curve. In a radially converging tracer test, this parameter normally accounts for dilution in the sampling borehole. In this case, there should theoretically be no dilution due to pumping, all of the concentration decrease between the SWIW section in KXTT4 and other boreholes should be caused by dispersion and and/or other transport processes. One may calculate what *pf* should be from experimental injection data. In this case, *pf* should roughly be about 0.1 for both SWIW tests 1 and 2. From the values of *pf* in Table 4-3 above, it appears clear that transport towards KXTT3 and KXTT5 occurs without any "extra" dilution than what is caused by simple one-dimensional advection and dispersion. For the other boreholes with longer transport times, additional dilution is required to fit the breakthrough curve and it is possible that more complex mixing and/or diffusive processes are significant in those cases.

4.2   CEC

4.2.1   CEC pre-tests

As described in Section 3.3.2 several pre-tests were performed prior to the main CEC test. In Figure 4-11, Figure 4-12 and Figure 4-13 the tracer breakthrough curves in KXTT3:S3 are shown as well as the measured concentration in KXTT4:T3 during the three tracer pre-tests.
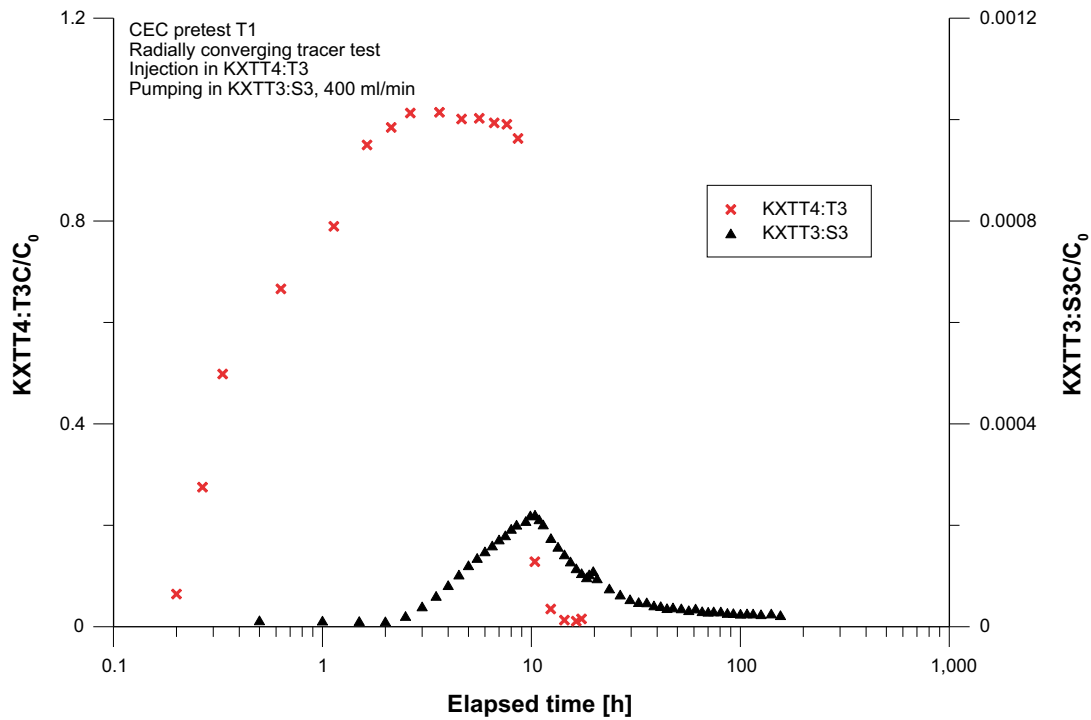
Figure 4-11. *Tracer breakthrough in KXTT3:S3 (black triangles) and tracer concentration in KXTT4:T3 (red crosses) during CEC pre-test T1.*
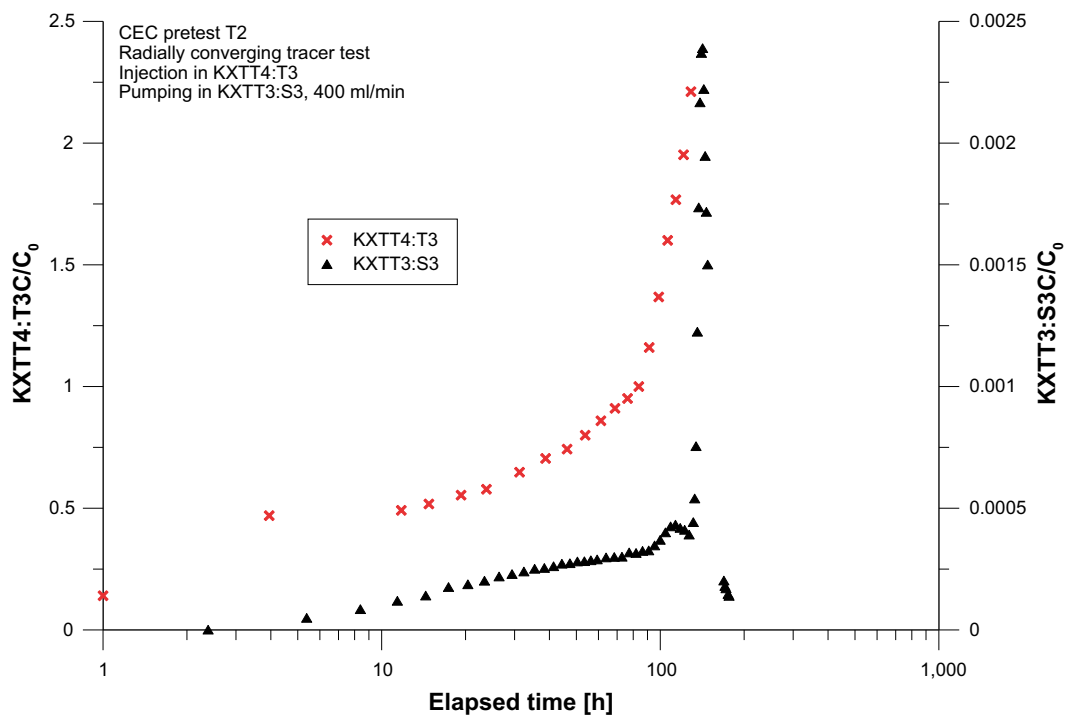
Figure 4-12. *Tracer breakthrough in KXTT3:S3 (black triangles) and tracer concentration in KXTT4:T3 (red crosses) during CEC pre-test T2.*
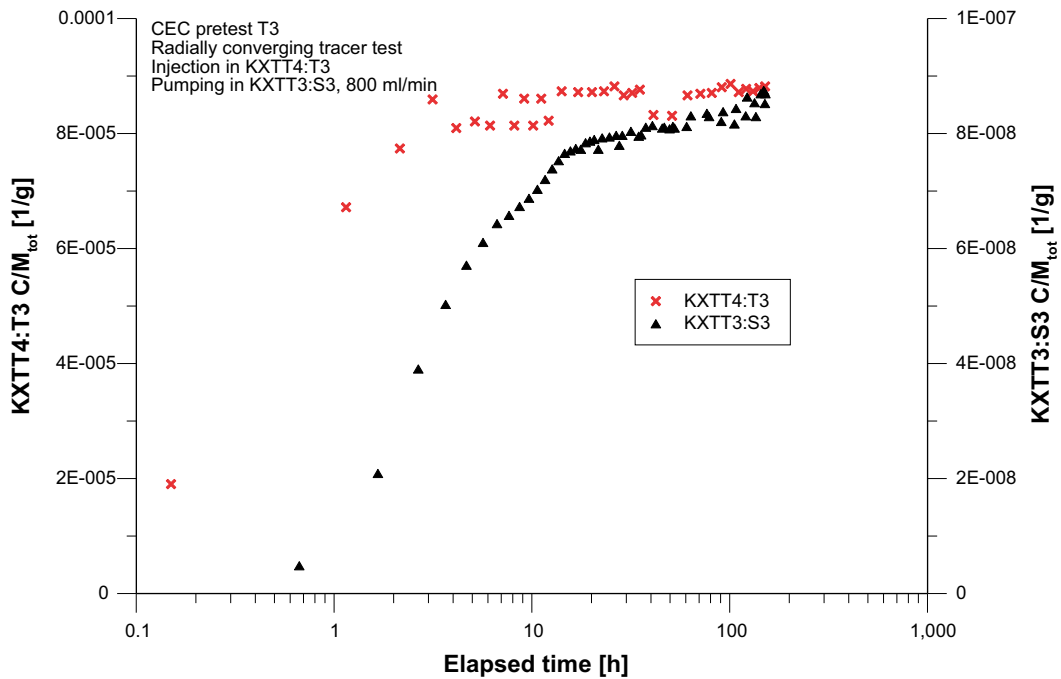
Figure 4-13. *Tracer breakthrough in KXTT3:S3 (black triangles) and tracer concentration in KXTT4:T3 (red crosses) during CEC pre-test T3.*

The objective of the CEC pre-test T1 was to make sure the tracer recovery in KXTT3:S3 was high enough to perform the main CEC test. The test was performed as a pulse injection; with an exchange injection, i.e. the section water was exchanged with water including tracer. After c 9 hours the water with tracer in the section was withdrawn from the borehole and replaced with water without tracer. The resulting tracer concentration in the injection section was close to a step function as seen in Figure 4-11. The mass recovery of the tracer in the pumping section was only c 50% at the end of the test. As seen in Figure 4-11, the concentration in the pumping section was still above the background at the end of the test, i.e. a prolongation of the test would result in a higher recovery. Still, the recovery in pre-test T1 was considered to be non-quantitative (a prerequisite to perform the main CEC test), and it was decided to perform an additional pre-test.

CEC pre-test T2 was carried out with a step injection in order to reach the appropriate concentration fast and a continuous injection to maintain the concentration. However, a stable concentration in the injection section was not achieved within reasonable time, cf. Figure 4-12. The tracer recovery for the test was estimated to 74%. However, this estimation is very uncertain due to the problems with gas injection during the test and the uncertainty in injection flow rate etc., see Section 3.3.2.

In order to investigate the poor results of pre-tests T1 and T2, it was decided to perform a dilution test to investigate if the flow condition in KXTT4:T3 while pumping in KXTT3:S3 remained unaltered since previous tests. Dilution tests D1 and D2 were performed while pumping with 400 ml/min in KXTT3:S3. The result of dilution test D1 and D2 was a much lower flow rate in KXTT4:T3 than during the previously performed COM test. From this observation, it was suspected that the low recovery in the T1 test might have been a result of changed flow conditions in the fracture, i.e., a lower conductivity between the two borehole sections used in the experiment.

Based on the results obtained, it was indicated that the pumping rate of 400 ml/h, previously used in the radioactive STT tracer experiment, was not enough to obtain a good tracer recovery. It was clear that one had to abandon the aim of performing a CEC test using the same flow conditions as in the TRUE STT experiments; instead the flow rate had to be increased. A third dilution test, D3, was therefore carried out in three steps with increasing flow rate in KXTT3:S3 from 400 ml/min to 600 ml/min and finally to 800 ml/min. The results of the dilution tests are presented in Appendix 5 as well as in Section 4.4.

The decision after the dilution tests was to perform a new CEC pre-test, T3, but with a higher pumping flow rate, 800 ml/min, to, hopefully, facilitate a higher tracer recovery. The performance of pre-test T3 was successful with a good balance between the concentration and flow rates in the step injection and continuous injection as well as the flow rate and section volume in KXTT4:T3. As seen in Figure 4-12 the concentration in KXTT4:T3 quickly became stable. The tracer recovery based on the flow rates and concentration at the end of the test was estimated to 93%. However, the concentration in KXTT3:S3 was still increasing somewhat at the time, so an even higher recovery was to be expected, if the test had been prolonged.

The flow rate in KXTT4:T3 during the pre-test T3 could be estimated with the continuous injection method to 49 ml/h.

4.2.2 CEC main test – overview of results

The main CEC test was performed with the same methodology and pumping flow rate as the CEC pre-.test T3, i.e. 800 ml/min and a combination of step injection and continuous injection. The injection concentration was increased in a step-wise manner with the intention of maintaining a constant injection concentration during each step. Three steps were employed and the injection concentration was increased with about a factor three for each new step. Figure 4-14 shows the tracer concentration of Uranine and Cs^+ in KXTT4:T3 and KXTT3:S3. Two injection failures are clearly visible in Figure 4-14 as a decrease of the concentration at c 90 h and 260 h, respectively. However, these interruptions are not considered to affect the possibility to evaluate the CEC test in any significant way.

The injected mass of Cs^+ was chosen according to the scoping calculations in Section 3.1.3 with the intention that Cs^+ would occupy all available sorption sites within the flow path and also reach the same constant relative concentration level in KXTT3:S3 as Uranine in Figure 4-14. As seen in Figure 4-14 the latter did not happen during the experimental time.

A visual inspection of the curves indicates a short tracer residence time for the conservative tracer Uranine, which also was expected. In order to illustrate this, a more detailed plot of the early times for the first injection step is shown in Figure 4-15.
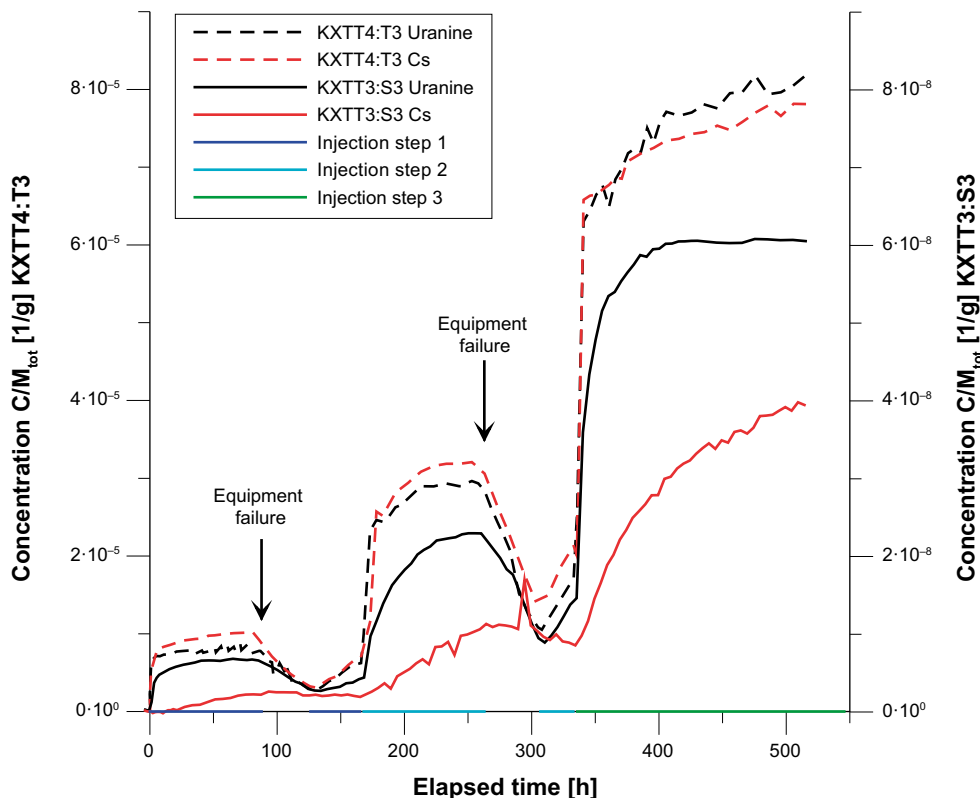
Figure 4-14. *Experimental tracer injection (KXTT4) and breakthrough data (KXTT3) for the CEC main tracer experiment. Tracer concentrations are normalized to total injected mass.*
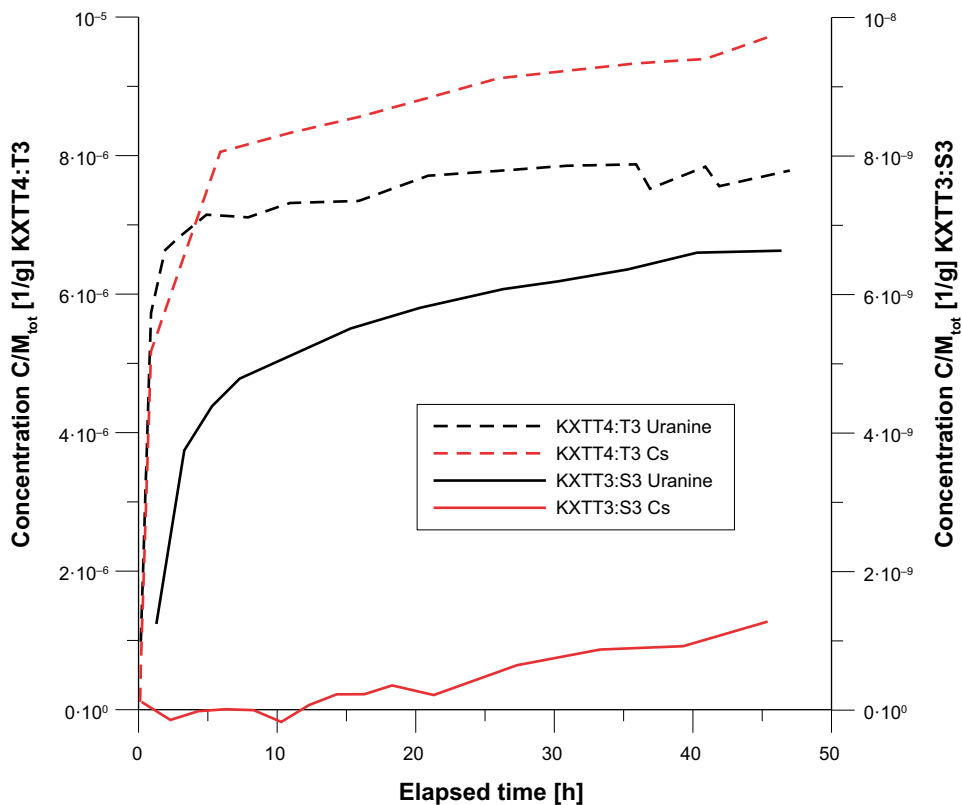
Figure 4-15. *Detailed view of the first injection step in Figure 4-14 above.*

The injection and sampling in KXTT4 continued until 545 h after the injection started. However, the last three analysed samples of Uranine from KXTT3 deviated considerably from the previous ones. No reasonable explanation was found for this, so it was decided that the CEC-test only should be evaluated based on samples until 516 h.

No sampling was carried out in the two borehole sections after the completion of the injection, even though the pumping of KXTT3:S3 continued for a while. Hence, a calculation of the tracer recovery in the usual way was not considered relevant. Instead, the Uranine recovery for each step was estimated from the flow rates and stable concentrations to be 90–100% in the CEC main test. The flow rate in KXTT4:T3 was estimated with the continuous injection method to be 36–45 ml/h during the CEC main test.

The breakthrough curve for Cs indicates substantial retardation compared with Uranine, which is not unexpected. However, there is no clear indication of decreasing sorption with increasing concentration, in accordance with the prior hypothesis about limitation of sorption sites with increasing concentration (see scoping calculations in Section 3.1.3).

Desorption of Cs-137 remaining from the STT1 experiment

The breakthrough curve concerning the desorbed Cs-137 tracer (remaining in the fracture system from the STT-1 injection in June 1997 (Andersson et al. 1998)) is shown in Figure 4-16. A slight increase in the concentration is indicated; from <1 Bq/kg at the start of the experiment going up to almost 2 Bq/kg at the end of the third injection. The increase is indicated to somewhat qualitatively follow the trend of the increase of non-radioactive Cs concentration in the fracture water during the experiment (given as a comparison in Figure 4-16). However, no quantitative correlation of the Cs-137 increase (< a factor 2) to the non-radioactive Cs concentration (a factor of ~10) can be observed. One should also be aware of that even the first injection involves an increase from the natural concentration of Cs from $4 \cdot 10^{-8}$ M (5 ppb, natural concentration) to $1 \cdot 10^{-3}$ M, i.e. >4 orders of magnitude. There is altogether a very limited response of increase in the Cs concentration which therefore somewhat contradicts a sorption model of being fully reversibly sorption of Cs to fracture walls in full contact with the flowing groundwater.
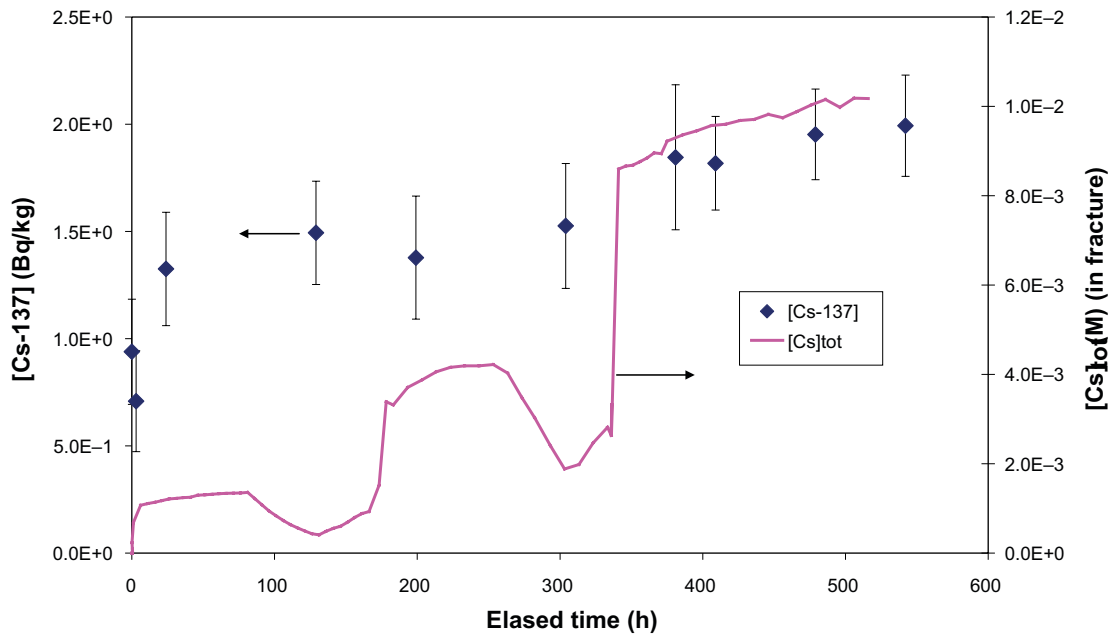
Figure 4-16. *Breakthrough curve of the Cs-137 tracer (injected during the STT-1 tracer experiment in June 1997), projected on the left Y-axis. As a comparison, the concentration of non-radioactive Cs at inlet of injection water in KXTT4:S3 borehole section is given and is projected to the right Y-axis.*

Based on a mass balance calculation of water taken out of the fracture system in the earlier performed tracer experiments (Winberg et al. 2000) (and its measured Cs-137 concentration) a total remaining Cs-137 activity of 4.4 MBq at the start of the CEC was estimated. By using this amount as a total mass, the measured concentration of Cs-137 in the range of 1–2 Bq/kg yields a C/M_{tot} (concentration in the water pumped in relation to the total activity remaining in the fracture) of $< 1 \cdot 10^{-9}$ g^{-1} for the "old" tracer. This is much lower than the measured values for the "new" Cs-131 tracer and therefore shows that the old Cs tracer is not fully available for cation exchange in the CEC experiment. The reason for this could be that the Cs sorption includes mechanisms that are not fully reversible and/or that the flow field in the CEC experiment was different than in the STT-1 tracer experiment. It can also be speculated that diffusion of the old Cs in to the rock matrix has occurred which makes it more difficult to reach for cation exchange de-sorption.

4.2.3   CEC main test – basic evaluation

The injected mass, M_{tot}, and the mass arriving at the pumping section, M_{pump}, for both Uranine and Cs are shown in Table 4-5. The injected mass was calculated from analysed concentrations of the injection solutions and the flow rates for the different injection periods. The mass arriving at the pumping section was estimated by integration of the breakthrough curves. The adsorbed mass of Cesium was calculated according to Equation 3-38 from the values given in Table 4-5 to $4.7 \cdot 10^{-2}$ moles. However, since it was indicated that full saturation of the sorption sites of the fracture was not obtained, the absorbed mass only corresponds to a minimum value of the cation exchange capacity. By assuming that the available sorption area, A_{sorb}, along the flow path is 0.5–3.0 m^2, according to the rough estimates in section 3.4.4, the CEC may be estimated to $> 2 \cdot 10^{-2}$ moles/m^2 (i.e. > 2 µmoles/cm^2).

Table 4-5. Calculated masses injected in KXTT4:T3 and arriving at KXTT3:S3 during the CEC main test.

	M_{tot}	M_{pump}
Uranine [g]	7.0	4.8
Cesium [moles]	1.4E–01	4.8E–02

4.2.4 CEC main test – modelling

1-D AD-model

As a first step, a simple one-dimensional advection-dispersion model (single pathway) without matrix diffusion was applied using an analytical solution (see section 3.4.2). The tracer injection function was approximated from the measured injection time series. The model was fitted to the experimental data using non-linear regression.

Uranine data

Initially, only the Uranine data were used in order to examine how well a one-dimensional advection-dispersion model describes the transport for a non-sorbing tracer. The fitted parameters were t_0 (residence time), Pe (Peclet number) and pf (proportionality factor). The latter parameter, assuming no other losses of tracer, accounts for the dilution in the pumped borehole.

The model best-fit to Uranine data is shown in Figure 4-17. Overall, this simple model explains Uranine data well. Some discrepancies occur during injection steps 2 and 3. During the second step, the simulated breakthrough curve is somewhat higher than the experimental one during a large portion of the ascending part. Towards the end of the third step, the simulated curve continues to increase somewhat, because it uses the experimental injection curve as input. However, this increase during the injection is not reflected in the Uranine breakthrough curve, which flattens out to a constant level.

The fit in Figure 4-17 was obtained with the following parameter values, with the coefficient of variation (parameter standard error as a fraction of the estimated value) in parentheses:

$t_0 = 1.9 \text{ h} \pm 0.9 \ (0.48)$,

$Pe = 0.77 \pm 1.00 \ (1.3)$,

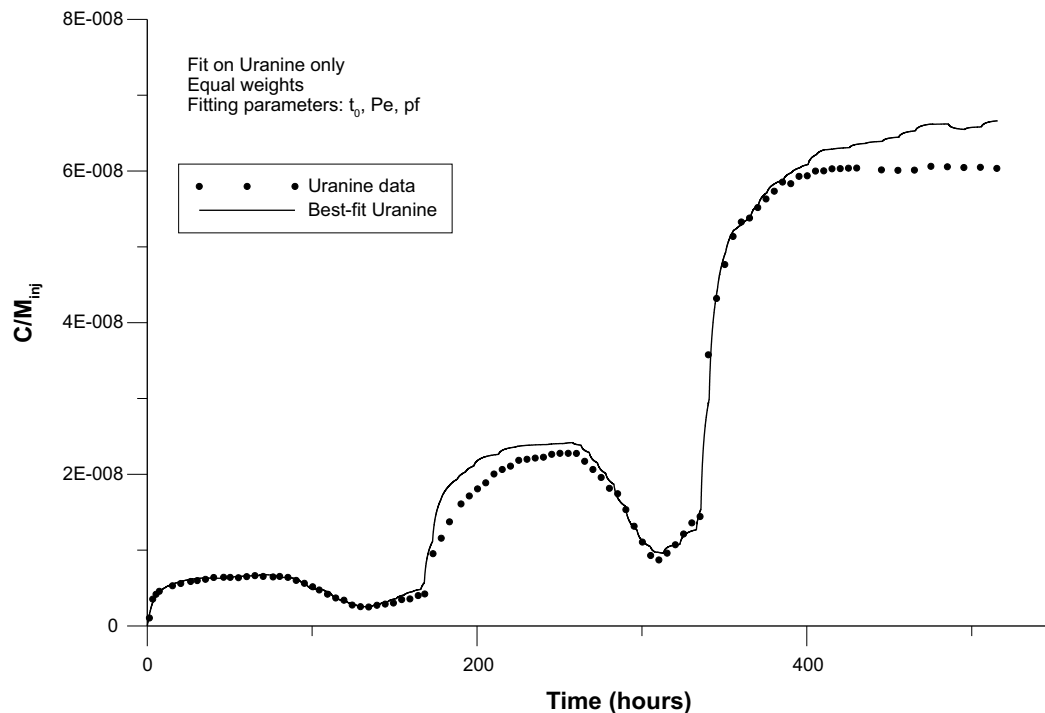$pf = (7.9 \pm 0.08) \cdot 10^{-4} \ (0.01)$.

Figure 4-17. *Model fit to Uranine data using a one-dimensional advection-dispersion model.*

As expected, the estimated residence time is relatively short. The estimated Peclet number is low, which means that an unusual amount of dispersion is required to fit the AD model to the Uranine data. For example, if one assumes that the transport distance is 4.6 m (see Figure 1-2), the longitudinal dispersivity would be about 6.0 m, i.e. larger than the transport distance. Such a large value of dispersivity is not consistent with the usual assumption that dispersivity should represent spreading on a relatively small scale and be considerably smaller than the transport scale. Very large dispersivity values may indicate, for example, multiple transport paths and/or other transport processes. However, although the overall model fit appears to be relatively good, as supported by a regression correlation coefficient of over 0.99, regression statistics indicate that estimation uncertainty is high for t_0 and very high for Pe. This is to a large extent due to high parameter correlation between these two parameters (more than 0.99). This means that these two parameters may be varied significantly without aggravating the model fit and it is therefore difficult to obtain good estimates of these parameters simultaneously.

Because of the high parameter correlation and large standard error for Pe, it is reasonable to question whether the Uranine curve can be fitted equally well with a more "reasonable" value of Pe. In order to illustrate this, an alternative case with a fixed value of $Pe = 5$ was run. The result of this is shown in Figure 4-18.

The regression result from the case with a fixed value of Pe and fitting on only Uranine is as follows:

$t_0 = 2.9$ h ± 0.2 (0.07),

$pf = (7.9 \pm 0.05) \cdot 10^{-4}$ (0.006).

The example with a fixed Pe shows that it is possible to fit the Uranine curve fairly well also with a more "reasonable" value of Pe, which is not surprising based on the regression statistics from the preceding case.

Despite the ambiguous results regarding estimation of the advective parameters based on the Uranine curve, a reasonable conclusion nevertheless is that a simple advection-dispersion model with one pathway explains the Uranine breakthrough curve fairly well.
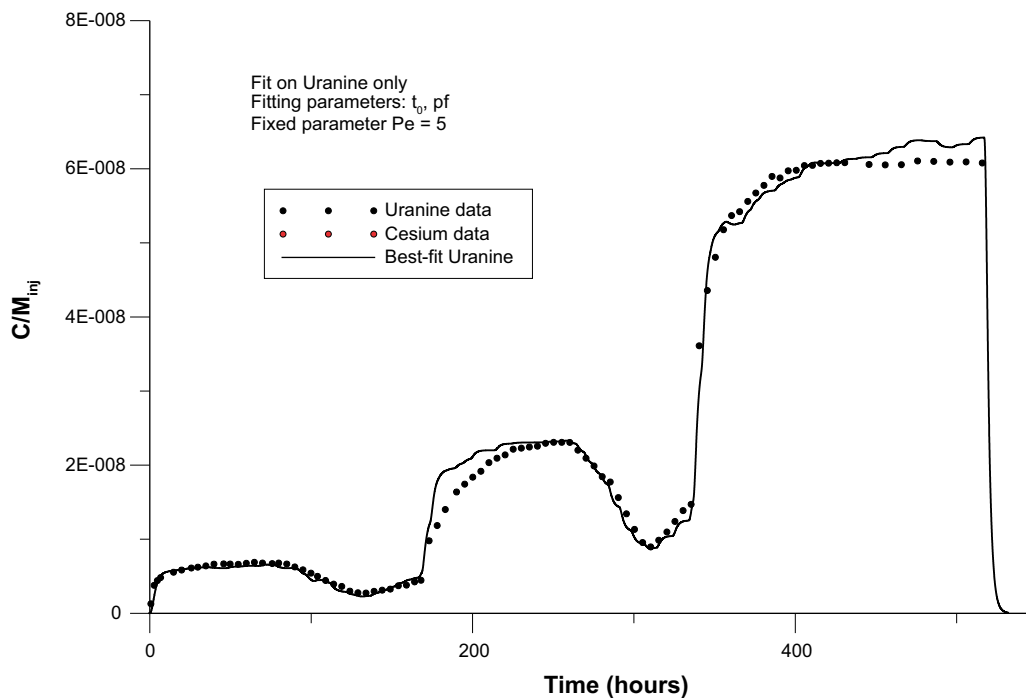
Figure 4-18. *Model fit to Uranine data using a one-dimensional advection-dispersion model. The value of Pe is fixed.*

The value of *pf* indicates an effective injection flow rate of about 38 ml/h, i.e. the flow of tracer-labelled water that leaves the injection section during the CEC test. The flow through the injection section, estimated from dilution measurements, varied between 36–45 ml/h during the CEC experiment. Thus, the estimated value of *pf* is consistent with experimental flow rates and this may be taken as an indication that the estimated flow rate in the injection borehole section indeed is representative for the flow rate through the actual tracer transport path.

Uranine and Cesium

Because of the good agreement between the AD-model and Uranine, a next step was to include the sorbing tracer, Cesium, to the analysis. As a first approach, the "standard" sorption model with equilibrium linear sorption was attempted. This is a reasonable first step because possible non-linear sorption effects or site-limitation are not obvious from only visual inspection of the breakthrough curves.

The Cs breakthrough curve was fit simultaneously with the Uranine curve. There are a number of ways that this can be done regarding choice of estimation parameters and weights on observations, etc. The first example entails estimation of four parameters: t_0, Pe, pf and the linear retardation factor, R, for the sorbing tracer. Observations are in this case given equal regression weights, i.e. no special emphasis on portions of the data in the regression. The resulting best-fit is show in Figure 4-19 below.

The fit in Figure 4-19 shows that an approximate fit to the sorbing tracer breakthrough curve can be obtained with a single retardation factor. The estimated parameter values are in this case:

$t_0 = 1.1 \pm 0.3$ h (0.27),

$Pe = 0.28 \pm 0.10$ (0.34),

$pf = (8.2 \pm 0.02) \cdot 10^{-4}$ (0.02),
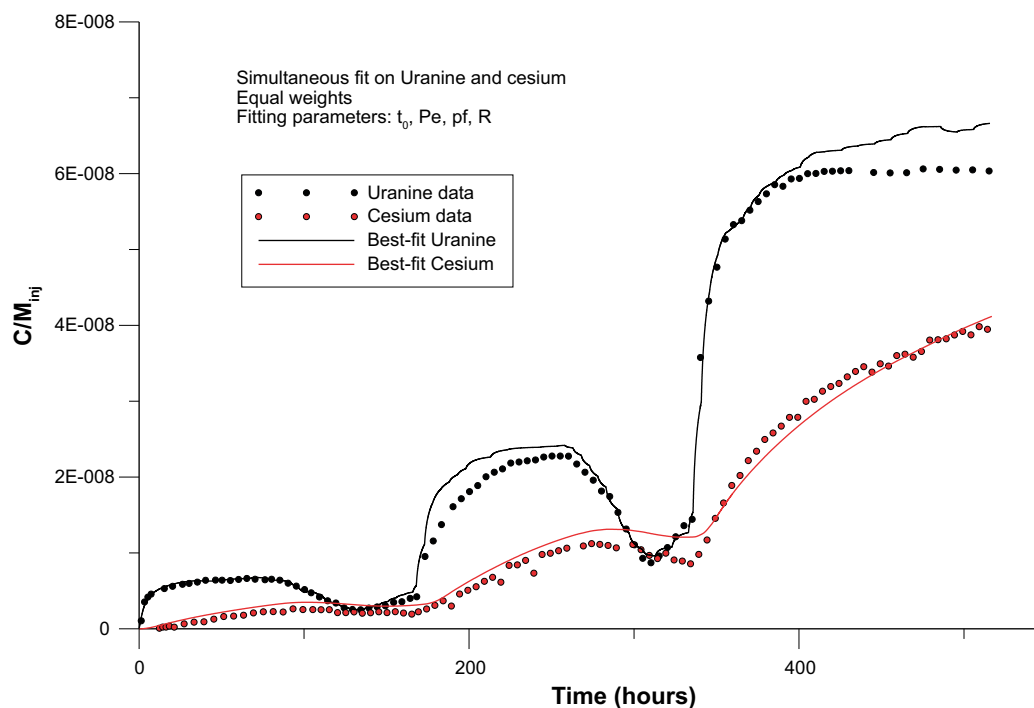
$R = 51 \pm 12$ (0.24).

Figure 4-19. *Model fit to Uranine and Cesium with a one-dimensional advection-dispersion model.*

The reason why estimation uncertainties for the residence time and the Peclet number are smaller in this case is that more data with high sensitivity to the estimated parameters are used in the regression analysis. This result is expected and typical for simultaneous fitting of non-sorbing and sorbing tracers. Another effect is that the parameter correlation between the residence time and the Peclet number is decreased. Again, however, the resulting Peclet number is very small

Although the linear sorption model appears to fit Cesium data fairly well in Figure 4-19 there are small but clear deviations during the two first injection steps. The model curves are slightly higher than the observed data, which may indicate that the sorption effect is underestimated for lower concentrations, i.e., a conclusion which would be consistent with e.g. a non-linear sorption caused by partial saturation as in the cation exchange model, cf. Section 3.1.3. In order to more clearly see this, an alternative fit is shown in Figure 4-20 in which only the first injection step is fitted for the sorbing tracer.

A basic hypothesis prior to the test is that sorption effects should decrease with increasing concentration. Therefore, the first injection step should be the one that can best be simulated by a linear sorption isotherm. The results from this regression run are shown in Figure 4-20 below.

The resulting parameter values are in this case:

$t_0 = 0.94 \pm 0.18$ h (0.19),

$Pe = 0.26 \pm 0.11$ (0.42),

$pf = (7.9 \pm 0.005) \cdot 10^{-4}$ (0.006),

$R = 101 \pm 13$ (0.13).

The bottom part of Figure 4-20 shows that the tracer breakthrough curves for both of the tracers fit the 1-D AD model very well during the first injection step and it appears that a simple transport model with linear equilibrium sorption is sufficient to explain the first injection step. The overall fit to the entire breakthrough curve with all three injection steps shows that the fit to Cs becomes worse with increasing concentration. More specifically, the 1-D AD model overestimates the sorption for the latter two injection steps. This is, at least qualitatively, consistent with the prior hypothesis about site-limited sorption, although the effect is much less obvious than in the scoping calculation example in section 3.1.3.

Again, the resulting Peclet number is very low, indicating very large effects of dispersion. This is a clearly unsatisfactory result and it is reasonable to ask whether it is possible to explain experimental data reasonably well also with more "normal" values of Pe, as was found to be the case when fitting only Uranine. Best-fit results for simultaneous fit of Uranine and the first injection step for Cs, using a fixed value of Pe = 5.0 and with t0, pf and R as fitting parameters, are shown in Figure 4-21. The figure clearly shows that it is not possible to simulate Cs breakthrough using "normal" Pe values and the standard advection-dispersion model with a linear retardation factor. In order to do this, it is necessary to allow the value of Pe to be very low, as in the preceding case above.

The results from the various regression runs with the standard advection-dispersion model with linear retardation are summarized in Table 4-6 below.

Table 4-6. Best-fit results from regression with one-dimensional transport model with linear equilibrium sorption. Values within brackets show parameter standard error as a fraction of the estimated value (i.e. coefficient of variation).

Case	t0 (h)	Pe	pf	R
Ur only	1.9 (0.48)	0.77 (1.3)	$7.9 \cdot 10^{-4}$ (0.01)	–
Ur only (fixed Pe = 5.0)	2.9 (0.07)	–	$7.9 \cdot 10^{-4}$ (0.01)	–
Ur+Cs; equal weights	1.1 (0.27)	0.28 (0.34)	$8.2 \cdot 10^{-4}$ (0.02)	51.2 (0.24)
Ur+Cs; weights=0 for Cs steps 2 and 3	0.94 (0.19)	0.26 (0.42)	$7.9 \cdot 10^{-4}$ (0.006)	101 (0.13)
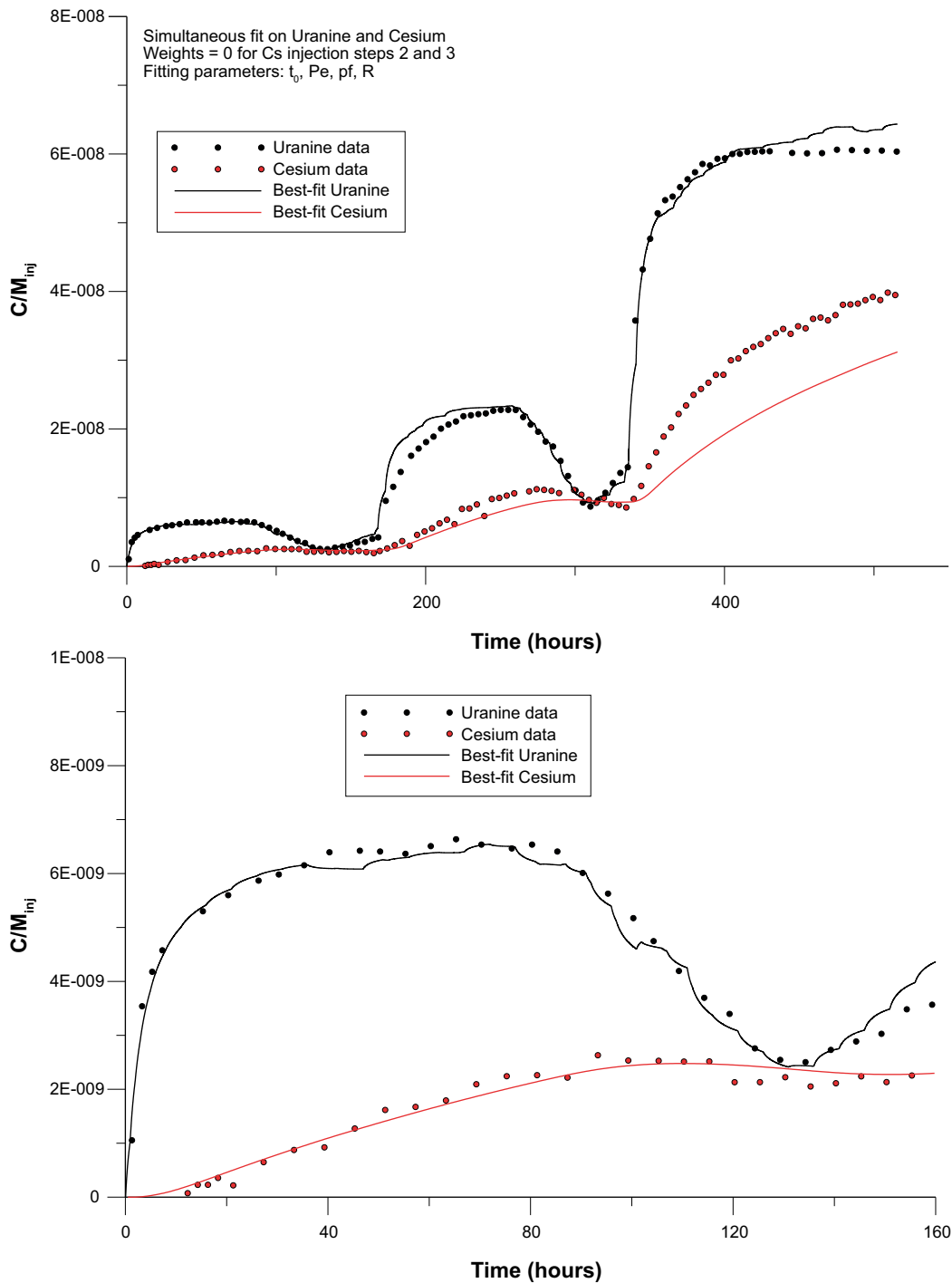
Figure 4-20. *Simultaneous model fit (top) of Uranine and Cesium with one-dimensional advection-dispersion model with linear sorption. Cesium data for injection steps 2 and 3 are not included in the fitting. The fit for the portion of the data corresponding to the first injection step is shown in more detail (bottom).*

Despite that low Peclet numbers are necessary to explain the retardation of Cs using a one-dimensional advection-dispersion model, the simulations with the simple advection-dispersion model with linear sorption indicate that this model may be sufficient to approximately explain experimental data during all three injection steps. However, there are indications of decreasing sorption with increasing solute concentrations, which may be interpreted as limitation of sorption sites. Because of this, attempts were made to fit the experimental results to a Langmuir sorption isotherm, which was used in the scoping calculations described above.
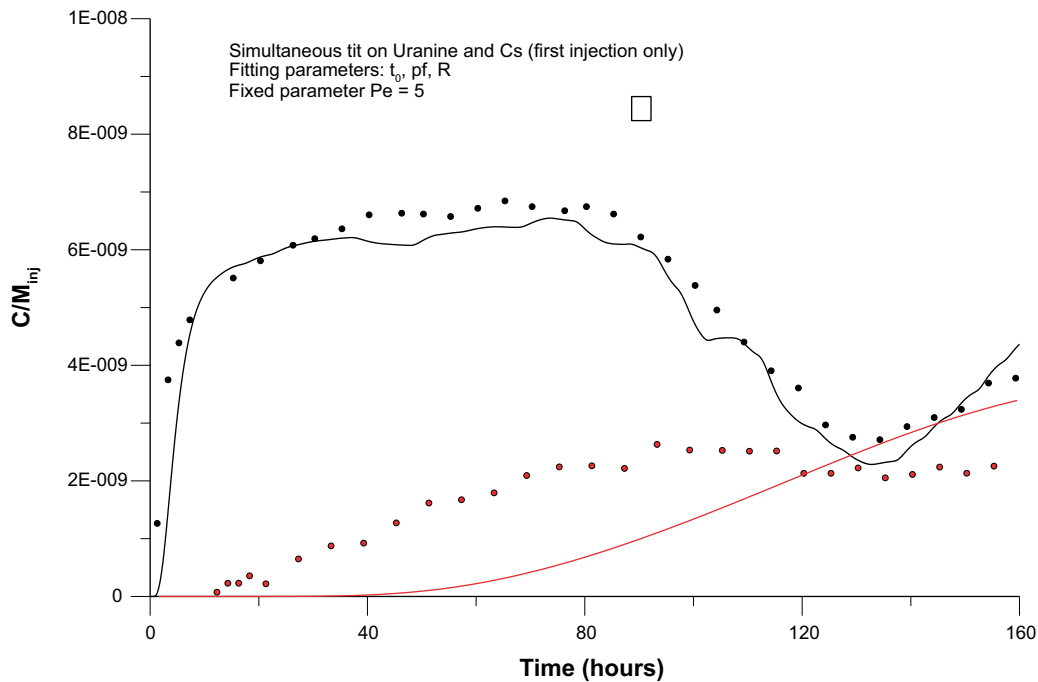
Figure 4-21. *Simultaneous fit of Uranine and Cs (first injection step) assuming a fixed value of Pe.*

Non-linear sorption

The evaluation above with a linear equilibrium sorption isotherm gave fairly clear indications that the relative sorption might decrease with increasing concentration, which also was the intended accomplishment with the step-wise injection procedure used. A natural further evaluation step was therefore to apply a non-linear sorption isotherm with site-limited sorption, i.e., the cation exchange capacity (CEC) model. As shown in Section 3.1.3, the cation exchange model can be approximated with a Langmuir isotherm, which also was used for the scoping calculations. As in the scopings, the SUTRA code was used for the Langmuir sorption simulations, this time in a parameter estimation mode. The basic transport model includes boundary conditions equivalent with the analytical model above used for linear sorption simulations. Further, the same tracer injection functions were used. The only fundamental difference from the analysis above is, thus, that a Langmuir isotherm is used instead of a linear isotherm.

One case with fitting of Uranine and Cesium data employing a Langmuir sorption isotherm is presented here. In this modelling, it was assumed that linear sorption was obtained during the first injection step with the lowest concentration (as modelled with the numerical parameter results given in the fourth row of Table 4-6). Consequently, it is assumed that influence of site limitation according to the Langmuir model was only obtained for the second and third injection step. This means that the fit for Uranine and the first injection step for Cs are identical to Figure 4-20 and that all general transport parameters obtained in that modelling (i.e., t_0, Pe, and pf) can directly be transferred to Langmuir modelling as fixed parameters. With the assumption that concentration-independent sorption is obtained in the first injection step, the evaluated R in the fourth row of Table 4-6 is as described by Equation 3-7 as identical to $(1+Ab_1N_{max})$. The lumped parameter of Ab_1N_{max} can thus be calculated from $(R-1)$, which then can be inserted in the modelling as a fixed parameter. Hence, the only estimation parameter employed is the second Langmuir parameter, b_1. The resulting fit is shown in Figure 4-22, which corresponds to a b_1 parameter with a numerical value of 0.14 m^3/moles. Combining this with the fixed parameter of Ab_1N_{max} =100 obtained from the attempt to model the first part of the breakthrough curve using a linear model, one can calculate the combined parameter of AN_{max} of 710 moles/m^3. These two combined parameters can not be identified individually and the basic outcome of this is that one has to know the fracture aperture ($2/A$, as described by Equation 3-5) in order to determine the surface related sorption site concentration N_{max} (moles/m^2) for the fracture.

The fit in Figure 4-22 may be argued to be the best one among the cases presented here if one considers the overall fit to during all three injection steps. However, although the Langmuir model is closer to Cs data for injection steps 2 and 3, respectively, the shape of the simulated Cs curve does not entirely conform to the experimental curve. In particular, the experimental curve at the end of injection 3 appears to level out to a larger extent than the simulated curve.

In the case of linear equilibrium sorption, the effective sorption parameter that may be uniquely estimated from a breakthrough curve is the retardation factor, R). This parameter consists of the combined product of the two Langmuir parameters (b1 and Nmax) and the fracture aperture and, consequently, no determination of the individual values of these parameters is possible. In the case of non-linear sorption according to the Langmuir model, R, furthermore, varies with the total concentration of tracer added to the system.

The Langmuir coefficients give a retardation factor (Equation 3-6) at low concentrations of about 100, which is to be expected because this example builds on one of the cases with only linear sorption. At higher Cesium concentrations (e.g., at the output concentration at the end of the third injection step) R would be approximately 27. The decreasing retardation with increasing Cs concentration is consistent with the hypothesis of site-limitation effects on Cesium sorption and the fact that this model gives somewhat better fit to the experimental curve compared to the pure linear model in Figure 4-20 is an indication that there is a site limitation effect in the experiment. However, it is obvious that the site limitation effect is much lower than what was predicted from the results from laboratory experiments and earlier in situ experiments; this particularly since saturation is not obtained.

In order to calculate values of the Langmuir coefficient N_{max} (i.e., the corresponding to the surface related CEC, cf. Figure 3-9), assumed values of the surface/volume ratio (i.e., A) in the flowing fracture (see Section 3.1.3) are required. Thus, the magnitudes of the estimated value of this coefficient depend on the conceptualization of the transport path. This is analogous to the more commonly applied linear isotherm ("K_d-sorption"), for which K_d only can be estimated if independent values of the surface/volume ratio (or density/porosity in a porous media approach) are available.
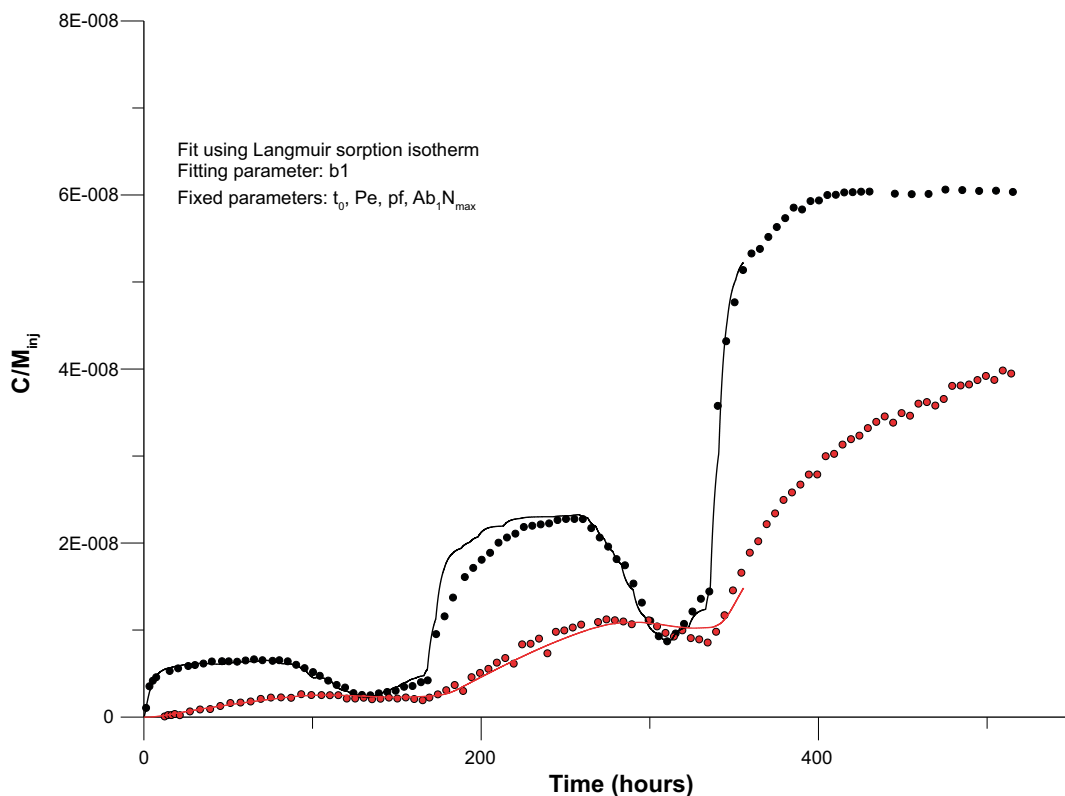
Figure 4-22. *Fit of Cesium data to a one-dimensional advection-dispersion model with Langmuir sorption. The modelling is based on the numerical values of the parameters obtained from the linear modelling of the results of the first injection (cf. Figure 4-20) and the only fitting parameter added to that modelling is the Langmuir b_1 parameter.*

Using the same assumptions as for the scoping calculations (cf. Chapter 3.1.3) the transport would take place in a plane-parallel fracture with an aperture of $1.5 \cdot 10^{-3}$ m (i.e. a surface/volume ratio, A, of $1.3 \cdot 10^3$ m^{-1}) the estimated value of the N_{max} would be 0.5 moles/m^2. This estimate also requires an assumption about the dilution in the pumping borehole section, because the coefficients are related to the actual concentration values in the transport path. In this case the estimated dilution factor, pf, was used.

Using the Langmuir parameters obtained from the breakthrough curve fitting , one could back-calculate these values to corresponding CEC parameters (i.e., the inverse process as described in Section 3.1.3). This, cf. Figure 4-23, would yield a CEC of 0.5 moles/m^2 and a selectivity coefficient (K_c) of 27 M$^{-1/2}$. A comparison with the values for these parameters obtained from laboratory experiments which were used in the scoping calculation of this experiment (CEC = 0.003 moles/m^2 and K_c = 720 M$^{-1/2}$) gives differences in the sorption site concentration by 2 orders of magnitudes and differences in the selectivity of Cs versus competing cations (e.g., Ca^{2+}) by a factor of 30. The high value for CEC indicate that matrix diffusion may be an important factor. However, matrix diffusion is not enough to explain the difference considering the estimates of additional CEC given in Table 3-2. One interpretation of this finding could be that a more CEC-rich solid phase than mylonite (e.g., fault gouge material) is in contact with the flowing water in the flow path. It is also indicated that this solid phase is not as selective to Cs as the material used in the laboratory experiment.

The comparatively low selectivity indicates that the highest used Cs-concentration ($\sim$10 mM in the injected water) is not sufficient to saturate cation exchange sites. Using the CEC constants calculated above, one will obtain that a maximum of 55% of the total number of the cation exchange sites can be occupied using a 10 mM Cs concentration. In order to obtain close to full occupation of the cation exchange sites (e.g., 96%) one would have had to increase the aqueous Cs concentration up to 0.2 M.

In order to illustrate a theoretical breakthrough curve for Cs that reaches the injection concentration, the fitted Langmuir coefficients were used to extend the simulated curve. This is shown in Figure 4-24. The extension is based on hypothetical extension of the injection functions for Uranine and Cesium, respectively, and therefore not included in Figure 4-22.

Integration of the difference between the Uranine and the Cs breakthrough curve using the extended breakthrough curves of the Langmuir model in Figure 4-24 yields that 0.057 moles can at most adsorb during the third injection step with 10 mM Cs concentration, cf. Figure 4-25. Combining this with the calculation that this concentration can at most occupy 55% of the total CEC, one can calculate the total amount of cation exchange sites available in the flow path as 0.057/0.55 = 0.10 moles.
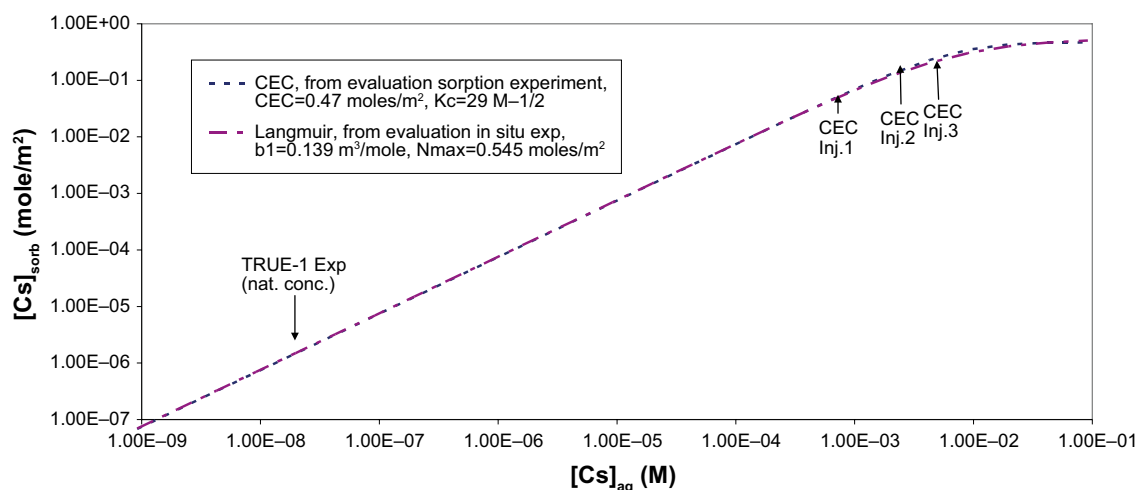
***Figure 4-23.** Langmuir sorption model obtained from the evaluation of the* in situ *CEC experiment, given in comparison to the CEC sorption model, fitted to the Langmuir model. The surface to volume relation applied in this calculation is the same as was used in the scoping calculation, cf. Figure 3-9. The Cs concentrations used in the CEC experiments are marked in the figure, together with the concentration used in the TRUE-1 tracer experiment, i.e., the natural background concentration.*
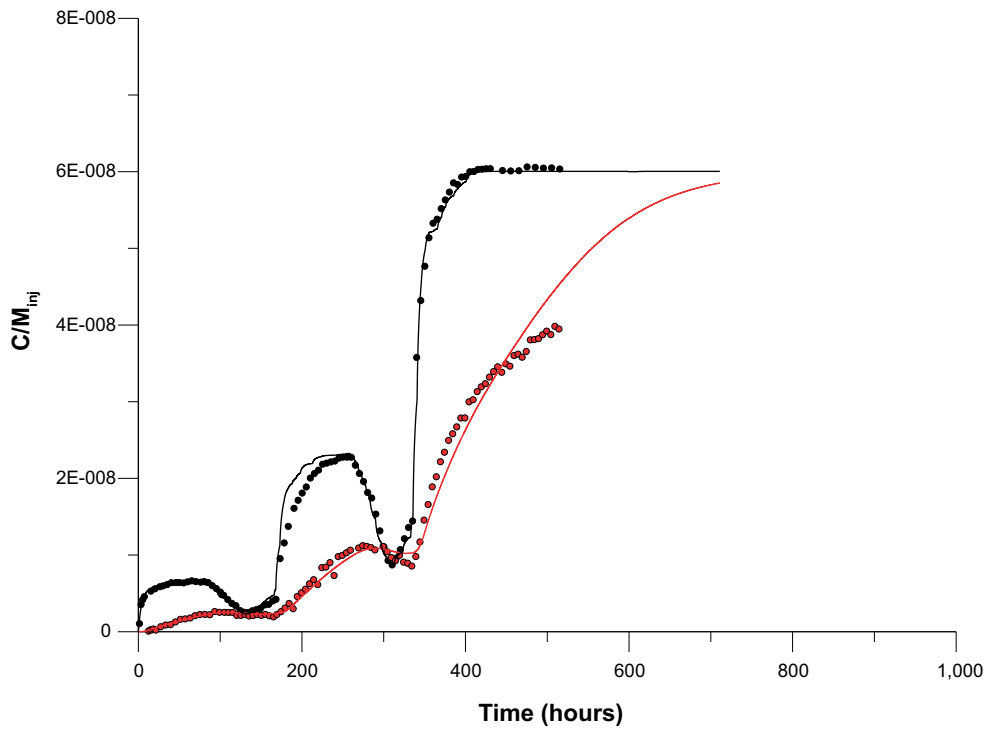
Figure 4-24. *Extension of fit in Figure 4-22 based on hypothetical extension of injection functions for Uranine and Cesium.*
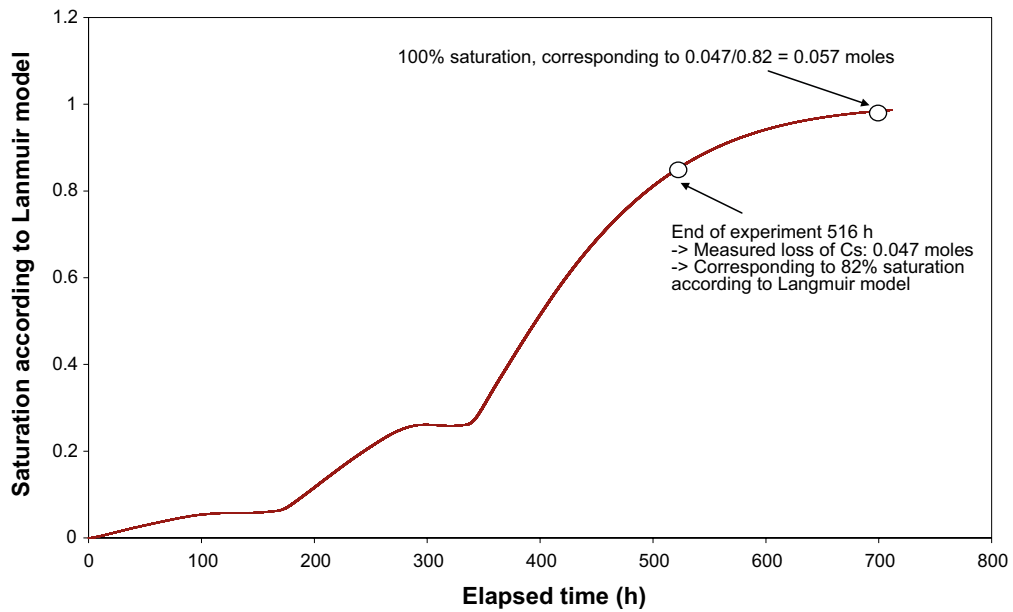
Figure 4-25. *Accumulated occupation of the cation exchange sites during the CEC test. The level of 1 ("saturation") refers to the saturation that, according to the Langmuir model, maximally can be obtained by using the Cs concentration in the third injection step, i.e., ~10 mM and does not coincide with saturation of all cation exchange sites.*

Alternatively, the combination of the retardation coefficient and the estimated value of b_1 may be used to calculate the maximum sorption capacity per volume transport path. This is made using the assumption that linear adsorption is obtained during the injection of the lowest concentration. Thereby Equation 3-7 can be applied and transformed in order to calculate the estimated value of the combined parameter of AN_{max} which then will represent the maximum sorption capacity per volume flow path (e.g. moles/m^3) according to:

$$AN_{max} = \frac{R_{LM} - 1}{b_1}$$
Equation 4-1

Although the fit to Cesium for the third injection step is not satisfactory, one may nevertheless calculate, by integration of the curves, the amount of sorbed Cesium in the transport path, as was done above in Section 4.2.3. In this case the sorbed mass is about 0.057 moles or about 7.5 g. According to Equation 3-6 and the fitted Langmuir coefficients, the retardation factor for a Cs concentration equal to the injection concentration is 17.8, which indicates that significant sorption capacity is still available in the transport path. In order to obtain close to saturation of sorption sites (i.e. when R approaches 1), the fitted Langmuir coefficients indicate that a concentration about one magnitude higher would be required.

4.3 COM

The results from the COM tests are in this section presented by each parameter as defined in Section 3.4.5 (s_p/Q_{pump}, t_R/r^2, Q_{flow}/Q_{theory} and T_{Th}/T_M). For each parameter a response matrix is presented with colour coding according to the index defined. Pair-wise figures are also presented for each parameter in order to visualize the directional results where the colours of the arrows indicate the strength in the response. The arrows origins at the observation hole and points to the pumping hole (i.e. indicates the flow direction). The first of each pair of figures show the responses for all tests except for the tests where higher flow rates were used in KXTT3 and KXTT4. The second show responses while pumping in KXTT3 and KXTT4 with lower and higher flow rates, respectively. If the response differs between high and low pumping rate the arrows are split in two. The response at high pumping rate is shown in the upper half of the arrow and consequently the response at low pumping rate is shown in the lower half.

The results from the COM tests could be compared to similar tests previously performed at the site (Winberg et al. 2000, Andersson et al. 2002a).
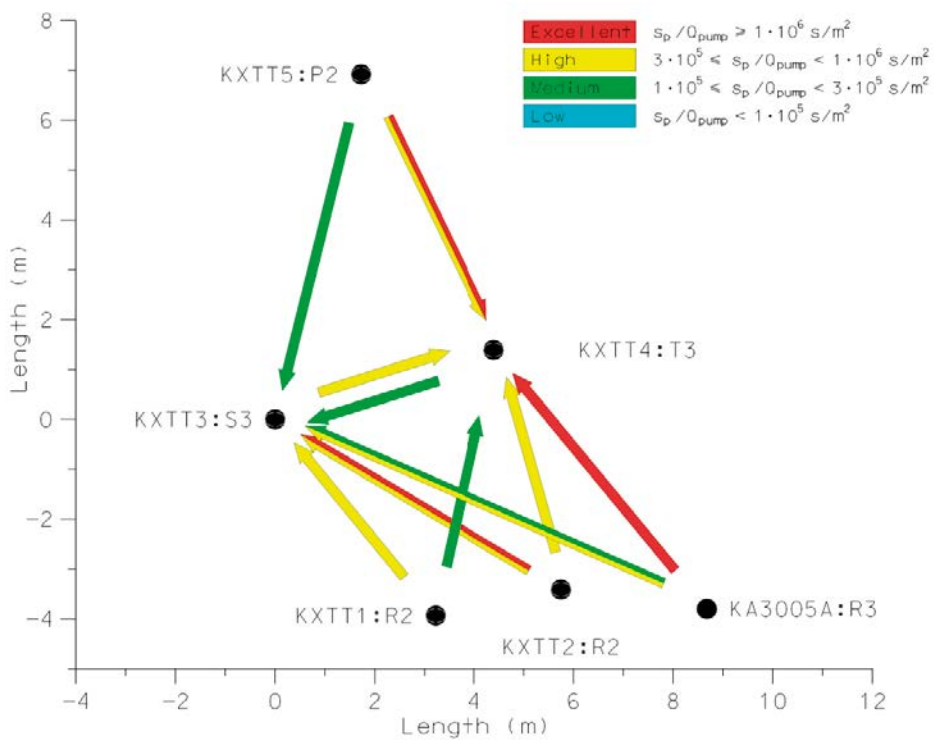
4.3.1 Drawdown response, s_p/Q_{pump}

The drawdown responses, as measured by s_p/Q_{pump}, are shown in Table 4-7, Figure 4-26 and Figure 4-27 and display a range of about one order of magnitude. Despite the large variation in values of s_p/Q_{pump} it is difficult to draw any firm conclusions from the parameter due to the fact that s_p/Q_{pump} does not incorporate any distance relationship as it could be expected that the drawdown should be larger closer to the pumping hole. However, it is clear that s_p/Q_{pump} between the boreholes KA3005A, KXTT4 and KXTT5 is relatively high indicating a good connectivity between the boreholes which can not be explained by a short distance between the boreholes. The values of s_p/Q_{pump} are also relatively high between KXTT2 and KXTT3, as well as between KXTT2 and KA3005A. However, the distance between the latter two sections is short which may explain the relatively high value.

Figure 4-27 has different colours on three of the arrows that may be interpreted as change in s_p/Q_{pump} depending on the flow rate. However, a closer look in Table 4-7 reveals that the changes actually are quite small.
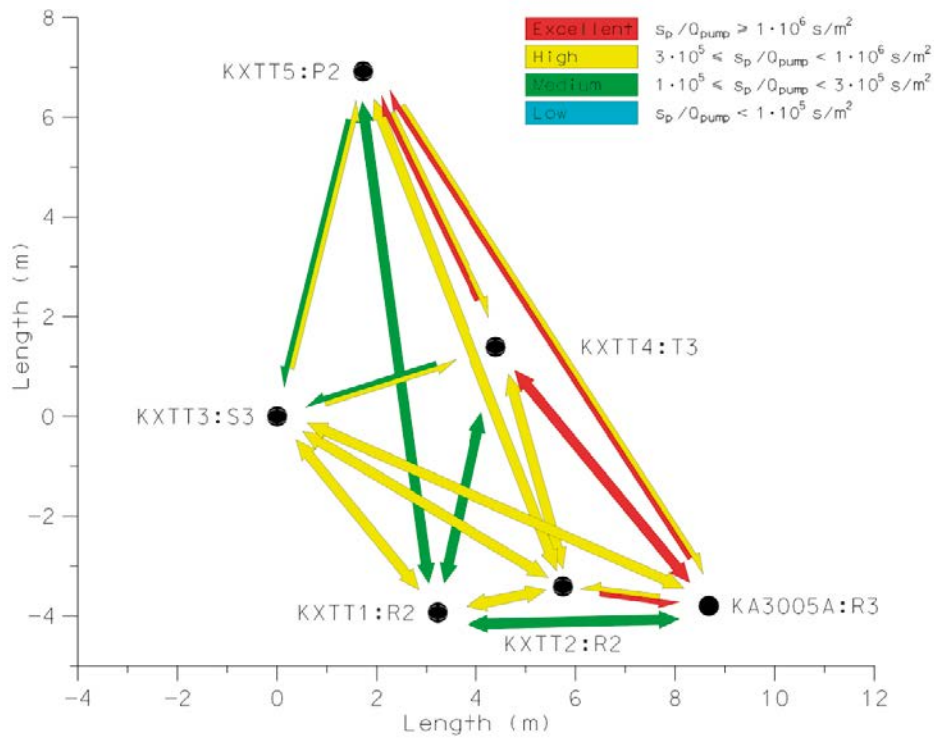
Figure 4-26. *Visualization of drawdown responses between boreholes for TRUE-1 Complementary multi-hole reciprocal cross flow tests.*

Figure 4-27. *Visualization of drawdown responses for pumping rate 385 ml/min resp. 2,800 ml/min in KXTT3 and pumping rate 200 ml/min resp. 600 ml/min in KXTT4.*

Table 4-7. Drawdown response matrix (s_p/Q_{pump}) for TRUE-1 Complementary multi-hole reciprocal cross flow tests.

		Observation hole					
	Q_{pump} [ml/min]	KXTT1	KXTT2	KXTT3	KXTT4	KXTT5	KA3005A
KXTT1	350		4.76E+05	4.67E+05	1.93E+05	1.96E+05	1.89E+05
KXTT2	190	3.77E+05		7.42E+05	4.08E+05	3.55E+05	8.01E+05
KXTT3	385	4.53E+05	9.79E+05		2.96E+05	2.69E+05	3.08E+05
KXTT3	2,800	5.37E+05	2.13E+06		2.92E+05	2.58E+05	2.83E+05
KXTT4	200	2.51E+05	4.70E+05	3.43E+05		8.93E+05	1.01E+06
KXTT4	600	2.09E+05	4.76E+05	3.18E+05		1.10E+06	1.05E+06
KXTT5	1,540	2.20E+05	5.12E+05	3.35E+05	1.52E+06		1.39E+06
KA3005A	870	2.06E+05	1.14E+06	3.11E+05	1.10E+06	9.35E+05	

(Left label: Pumping hole)

$s_p/Q_{pump} \geq 1 \cdot 10^6$ s/m^2	Excellent
$3 \cdot 10^5 \leq s_p/Q_{pump} < 1 \cdot 10^6$ s/m^2	High
$1 \cdot 10^5 \leq s_p/Q_{pump} < 3 \cdot 10^5$ s/m^2	Medium
$s_p/Q_{pump} < 1 \cdot 10^5$ s/m^2	Low

4.3.2 Temporal response, t_R/r^2

The time responses, t_R/r^2, from the COM-tests are shown in Table 4-8, Figure 4-28 and Figure 4-29. The scanning time in the pressure monitoring system was two seconds, setting the lower limit and resolution of the time response. However, no time responses estimated to two seconds in the evaluation resulted in the classes medium (green) or bad (blue) making the lower measurement limit of time response sufficient for the evaluation made here.
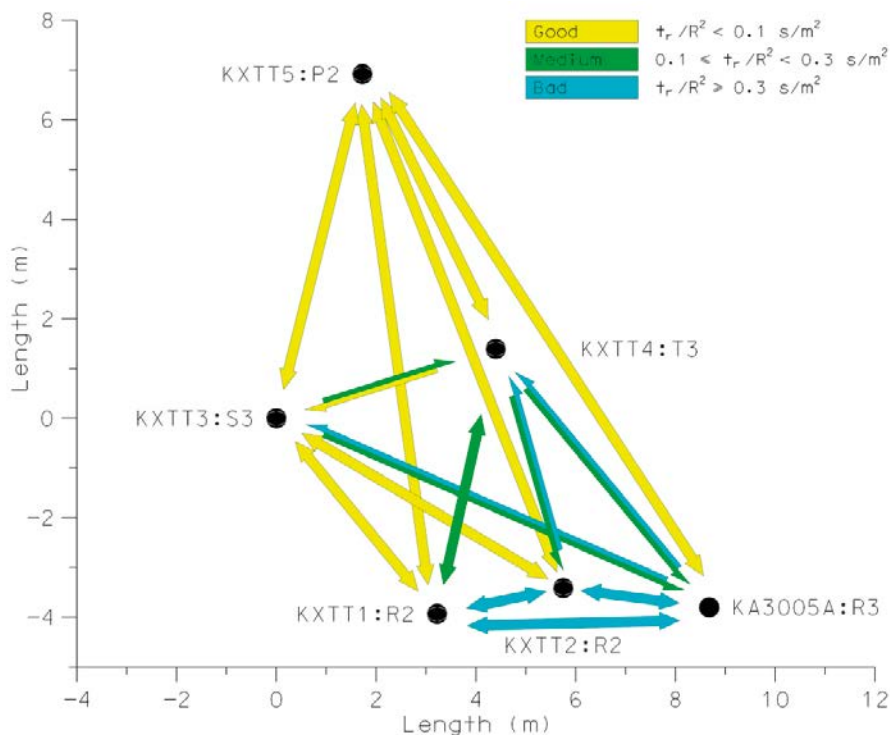
Figure 4-28. *Visualization of temporal responses between boreholes for TRUE-1 Complementary multi-hole reciprocal cross flow tests.*
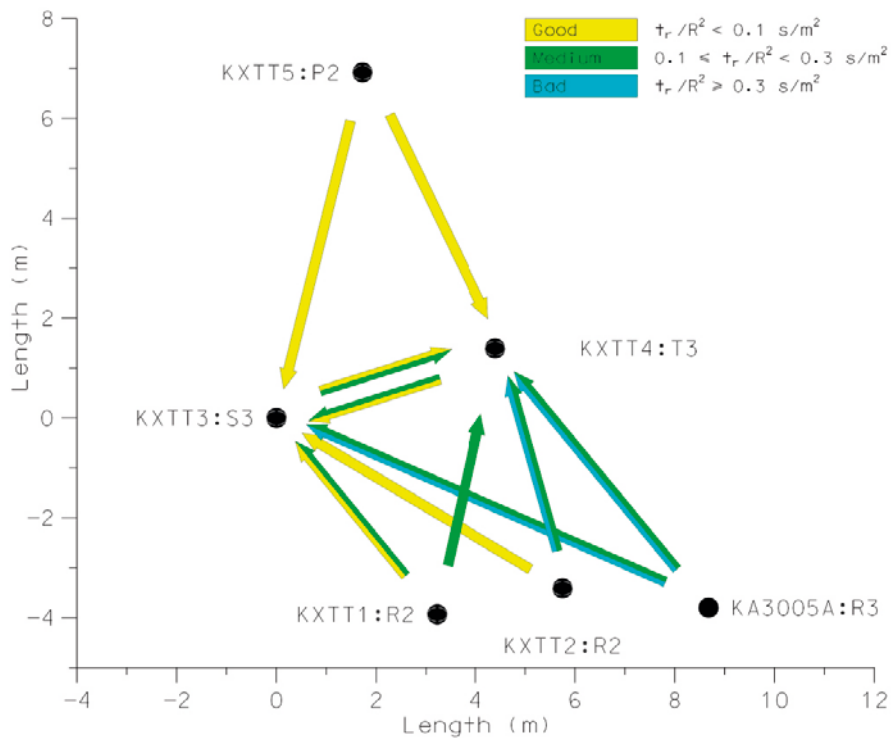
Figure 4-29. Visualization of temporal responses for pumping rate 385 ml/min resp. 2,800 ml/min in KXTT3 and pumping rate 200 ml/min resp. 600 ml/min in KXTT4.

Table 4-8. Temporal response (t_R/r^2) matrix for TRUE-1 Complementary multi-hole reciprocal cross flow tests.

| | | Q_{pump} [ml/min] | Observation hole | | | | | |
			KXTT1	KXTT2	KXTT3	KXTT4	KXTT5	KA3005A
	KXTT1	350		0.60	0.08	0.13	0.03	2.62
	KXTT2	190	0.90		0.09	0.24	0.07	1.15
Pumping hole	KXTT3	385	0.08	0.09		0.09	0.04	0.65
	KXTT3	2,800	0.15	0.09		0.19	0.08	0.16
	KXTT4	200	0.20	0.40	0.19		0.05	0.31
	KXTT4	600	0.13	0.24	0.09		0.05	0.13
	KXTT5	1,540	0.03	0.05	0.04	0.05		0.04
	KA3005A	870	0.54	0.69	0.11	0.13	0.01	

$t_R/r^2 < 0.1$ s/m^2	Good
$0.1 \leq t_R/r^2 < 0.3$ s/m^2	Medium
$t_R/r^2 \geq 0.3$ s/m^2	Poor

Some patterns may be observed, especially when looking at Figure 4-28. The responses between KXTT1, KXTT2 and KA3005 were all poor. Also the responses between these boreholes and KXTT3 and KXTT4 are in some cases poor or medium. All responses to or from KXTT5 are considered as good. The general pattern of the time responses may be summarised as good in the upper and left part and not as good in the lower part of Feature A as displayed in Figure 4-28.

When comparing the different pumping rates in KXTT3 and KXTT4, as shown in Figure 4-29, a decreasing or stable t_R/r^2 is expected for higher pumping flow rates. This is also found for most

boreholes. Unexpectedly, some values of t_R/r^2 increase with higher flow rate. However, in these boreholes the time responses are very short (2–4 seconds). Hence, the observations may be an effect of the relatively low time resolution (two seconds) and not a true characteristic of Feature A.

4.3.3   Drawdown (s_p/Q) and temporal response (t_R/r^2)

The drawdown and temporal responses from several tests may be plotted together in a time-response plot as for example Andersson et al. (2002a) have done in earlier studies. In Figure 4-30 and Figure 4-31 are pressure responses and response times are plotted together. In Figure 4-30 the colours indicate the pumping section while the symbols inside the circles indicate the observation sections. In Figure 4-31 it is vice versa, i.e. the colours indicate the pumping section while the symbols inside the circles indicate the pumping section. Flow paths with good connectivity, i.e. a large drawdown and fast response, are found in the upper left corner of the figures while the flow paths with poor connectivity are found in the lower right corner.

Figure 4-30 and Figure 4-31 confirms the conclusions in previous sections to a large degree. Combinations of KXTT4, KXTT5 and KA3005A are generally found close to the upper left corner, indicating good connectivity. Also the flow paths between KXTT3 and KXTT2 suggest good connectivity. Combinations of KA3005A and KXTT2 on the other hand are situated more to the upper right corner suggesting a large but slow pressure response. KXTT5 is generally found in the left part of both figures indicating that the pressure response is rather fast when KXTT5 is involved but the magnitude of the pressure response varies. Another observation from Figure 4-30 and Figure 4-31 is that KXTT1 generally is found in the lower half of the diagrams indicating that the borehole does not facilitate larger pressure depressions. However, as stated above, the index s_p/Q_{pump} is not distance dependent and therefore conclusions may be uncertain.

### 4.3.4   Flow rate, Q_{flow}/Q_{theory}

The flow rate in the observation holes, calculated as the Q_{flow}/Q_{theory} ratio is presented in Table 4-9, Figure 4-32 and Figure 4-33. The evaluation of the dilution tests is presented in Appendix 2. The uncertainties due to the unknown flow direction as presented in Section 3.4.5 are given within brackets in Table 4-9. In general, these uncertainties do not change much except for the flow responses in KXTT3 where the uncertainties are relatively large.

The relatively large uncertainties regarding KXTT3 are due to a relatively high natural flow rate in KXTT3. However, based on Figure 1-4 it is reasonable to assume that the direction of the natural flow in KXTT3 is not towards the other boreholes in Feature A, possibly with the exception of KXTT5. Hence, it is likely that the flow rate ratios are even higher in KXTT3 than indicated in Table 4-9.

For the evaluation of flow rate with the dilution method, the background concentration of the tracer is subtracted from the measured concentration. However, for the analysis of the samples from the dilution measurements, some indications were found suggesting a variable background concentration during the tests. This uncertainty in background concentration makes the evaluation, especially for periods with a low concentration, more uncertain than normally found for dilution tests. The specific evaluations that were considered as clearly affected by this uncertainty or by scattered data in general, are those for KXTT3 when pumping in KXTT2 and KXTT4 with 600 ml/min, and for KA3005A while pumping in KXTT3 and KXTT4.

Despite the uncertainties discussed above some interesting observation are made. In most cases, the Q_{flow}/Q_{theory} ratio is well below 1 which would indicate rather poor flow responses in the observation holes. The flow responses in KXTT3 are in most cases excellent when pumping the other boreholes which are seen as red arrows pointing from KXTT3 in Figure 4-32. On the other hand, when pumping in KXTT3 the flow responses of the other boreholes are generally low or medium. This characteristic of the flow responses where KXTT3 is involved suggests that the majority of the water flowing into KXTT3 during pumping originates from a rock volume not covered by the other measured boreholes since the flow responses in these boreholes are low to medium. Also, the relatively high flow rate in KXTT3 while pumping the other boreholes indicates that a relatively large portion of the water is flowing through KXTT3 towards the other boreholes. The same characteristics are also found for KXTT5 but to a lesser extent since the response in KXTT5 generally is medium while the responses in the other boreholes generally are low while pumping in KXTT5.
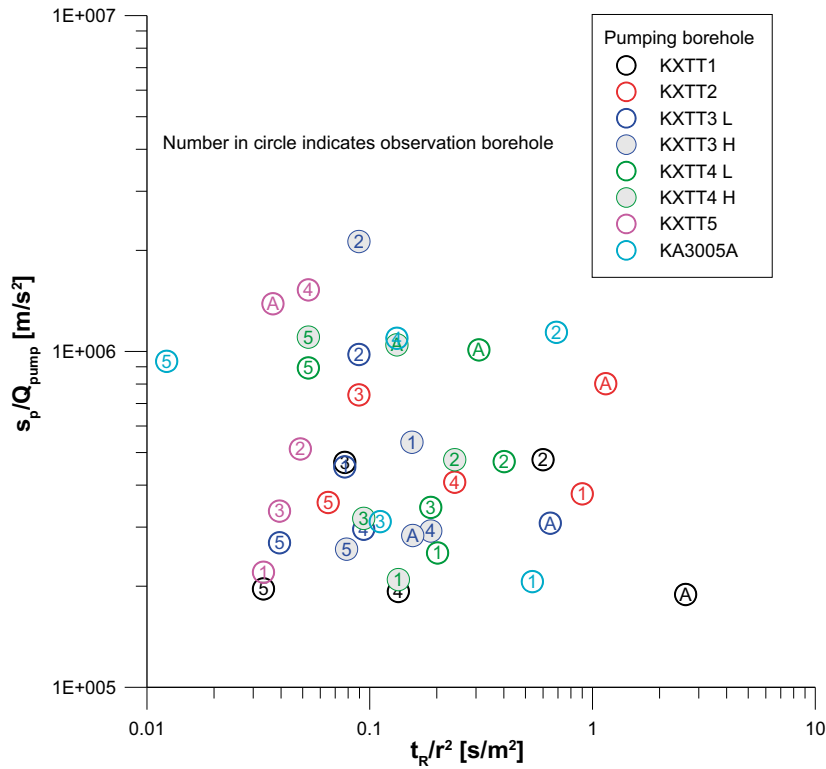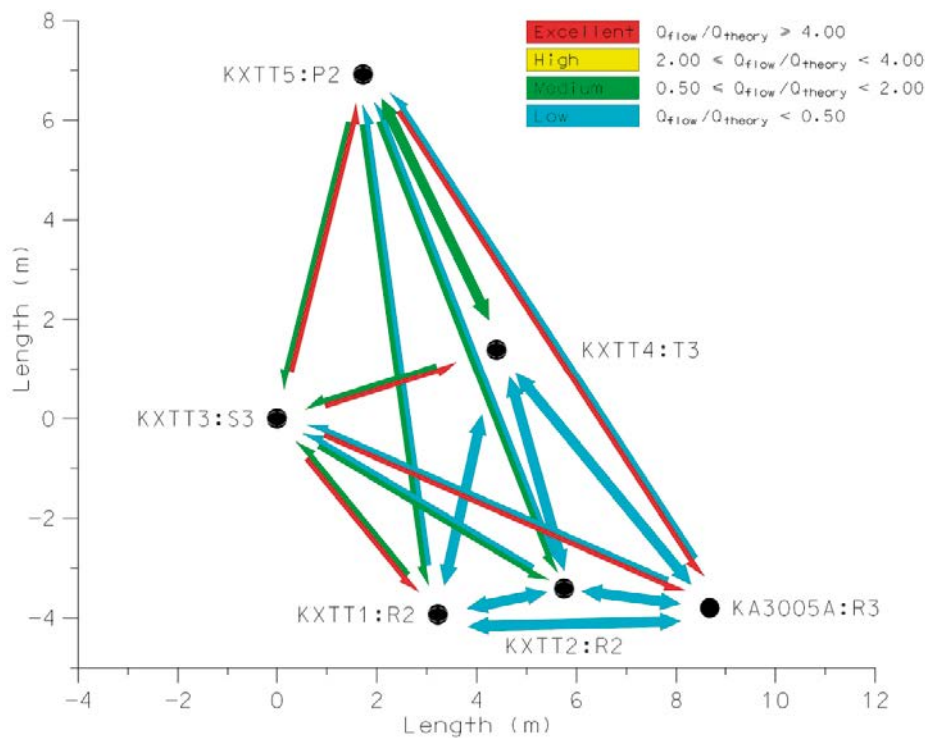
Figure 4-30. *Diagnostic plot of pressure responses. The colour represents the pumping borehole according to the legend while the numbers indicate the observation borehole.*
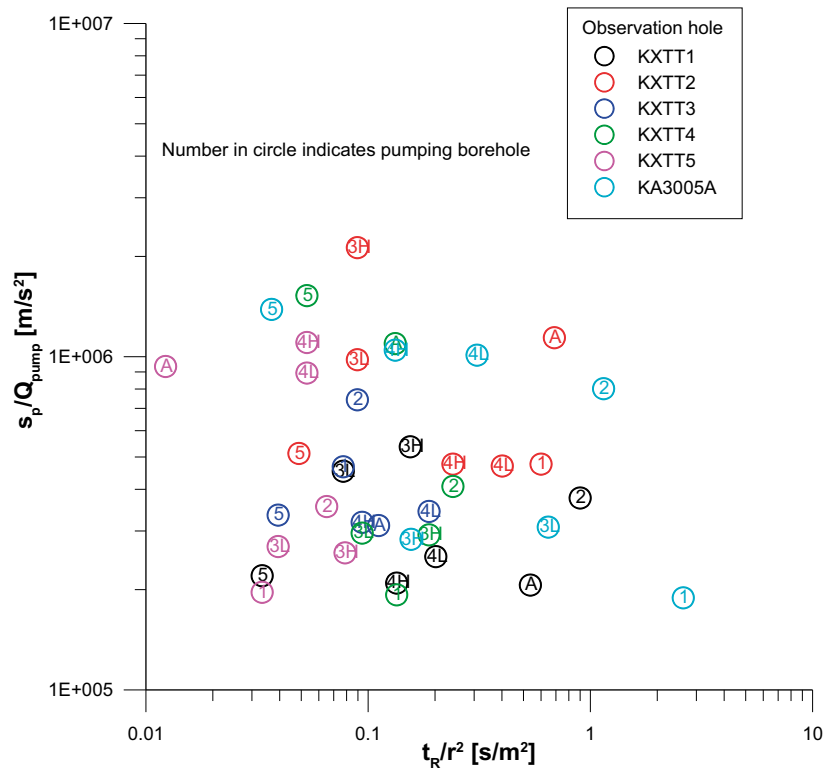
Figure 4-31. *Diagnostic plot of pressure responses. The colour represents the observation borehole according to the legend while the numbers indicate the pumping borehole.*

Figure 4-32. *Flow rate ratio between boreholes for TRUE-1 Complementary multi-hole reciprocal cross flow tests.*
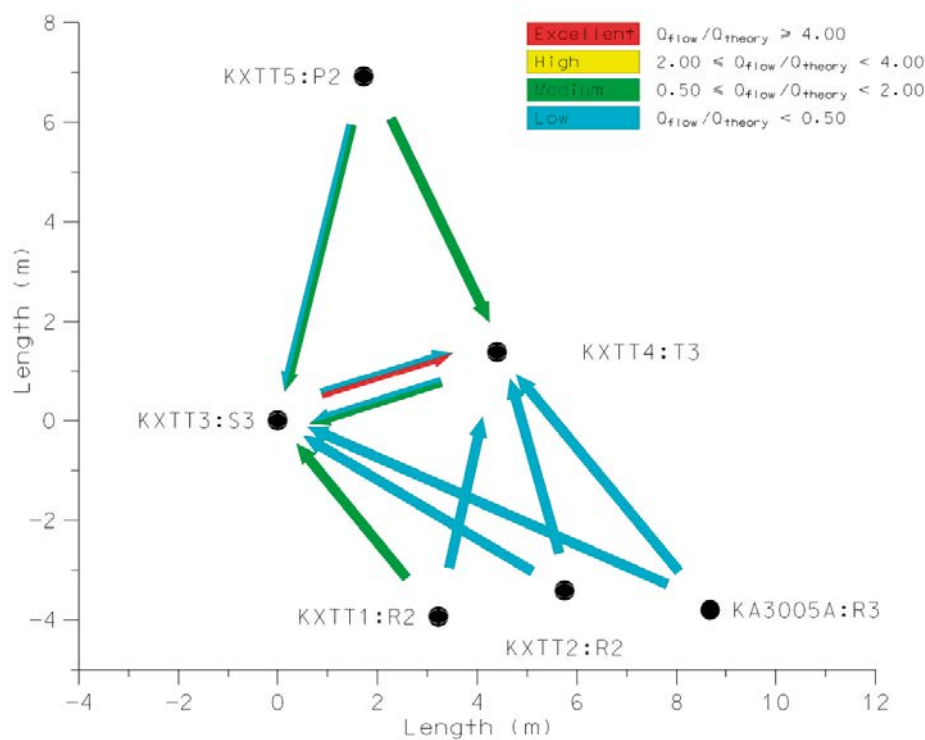
Figure 4-33. *Flow rate ratio for pumping rate 385 ml/min resp. 2,800 ml/min in KXTT3 and pumping rate 200 ml/min resp. 600 ml/min in KXTT4.*

Another interesting observation is that the flow responses between KXTT1, KXTT2, KXTT4 and KA3005A are all low, indicating an area of rather low connectivity or long flow paths.

When comparing the flow responses during lower and higher flow rates in KXTT3 and KXTT4, there is a tendency that the flow rate ratio, with a few exceptions, decrease with a higher pumping rate. This may be due to boundary conditions or may indicate some kind of restriction in the majority of the flow paths.

Table 4-9. Flow rate ratio (Q_{flow}/Q_{theory}) matrix for TRUE-1 Complementary multi-hole reciprocal cross flow tests.

		Q_{pump} [ml/ min]	Observation hole					
			KXTT1	KXTT2	KXTT3	KXTT4	KXTT5	KA3005A
Pumping hole	KXTT1	350		0.02 (±0.03)	6.52 (±2.74)	0.10 (±0.01)	1.19 (±0.50)	−0.02 (±0.01)
	KXTT2	190	0.25 (±0.08)		1.57 (±6.65)	0.19 (±0.01)	1.61 (±0.93)	0.14 (±0.01)
	KXTT3	385	0.97 (±0.07)	0.27 (±0.07)		0.58 (±0.01)	1.19 (±0.29)	0.29 (±0.01)
	KXTT3	2,800	1.62 (±0.01)	0.06 (±0.01)		0.34 (±0.00)	0.46 (±0.04)	0.04 (±0.00)
	KXTT4	200	0.13 (±0.15)	0.22 (±0.11)	4.82 (±4.36)		1.34 (±0.49)	−0.21 (±0.02)
	KXTT4	600	0.11 (±0.05)	0.07 (±0.04)	0.05 (±1.45)		1.29 (±0.16)	−0.01 (±0.01)
	KXTT5	1,540	0.22 (±0.03)	0.08 (±0.02)	4.40 (±0.64)	0.58 (±0.00)		−0.03 (±0.00)
	KA3005A	870	0.11 (±0.04)	0.21 (±0.01)	8.17 (±2.06)	0.45 (±0.00)	5.62 (±0.23)	

$Q_{flow}/Q_{theory} \geq 4.0$	Excellent
$2.0 \leq Q_{flow}/Q_{theory} < 4.0$	High
$0.5 \leq Q_{flow}/Q_{theory} < 2.0$	Medium
$Q_{flow}/Q_{theory} < 0.5$	Low

4.3.5 Transmissivity, T_{Th}/T_M

Evaluated transmissivity values, T_M and T_{Th}, are shown in Table 4-10 and Figure 4-34. Generally, the values of T_{Th} are slightly higher than the corresponding values of T_M which results in a transmissivity ratio, T_{Th}/T_M, as shown in Table 4-11 and Figure 4-35, slightly higher than unity. A change of flow rate does not seem to change this relationship, see Figure 4-36.

By only considering the transmissivity ratio, T_{Th}/T_M, it may be concluded that Feature A is rather homogenous regarding transmissivity. However, the transmissivity values, as presented in Table 4-10 and Figure 4-34, do not support such a conclusion. For a specific flow path it seems like the transmissivity in one direction often is significantly different from the transmissivity in the opposite direction. This could be interpreted as a real difference in the transmissivity depending of the flow direction, which would imply activation of different flow paths depending of flow direction. However, it seems unlikely that this effect would play such a major role for almost all of the tested flow paths. A perhaps more likely explanation of this result may be that T_{Th} mostly depends on the hydraulic properties close to the pumping hole and not so much of the characteristics close to observation hole. Hence, T_{Th} is strongly correlated to T_M.

Some interesting results may still be observed. When pumping in KXTT3, the T_{Th}/T_M ratio for KXTT2 is excellent. This may be interpreted as a very good hydraulic connection between the two holes. However, if this was the case, it is expected that T_{Th}/T_M for KXTT3 while pumping in KXTT2 would be at least as high while it in fact is classified as medium. This difference in T_{Th}/T_M for the two flow paths may instead be caused by a negative hydraulic boundary on the right side of KXTT2 in Figure 4-35. Another interesting observation is that T_{Th}/T_M is high for all observation holes while pumping in KXTT5 but that this effect is not reciprocal.
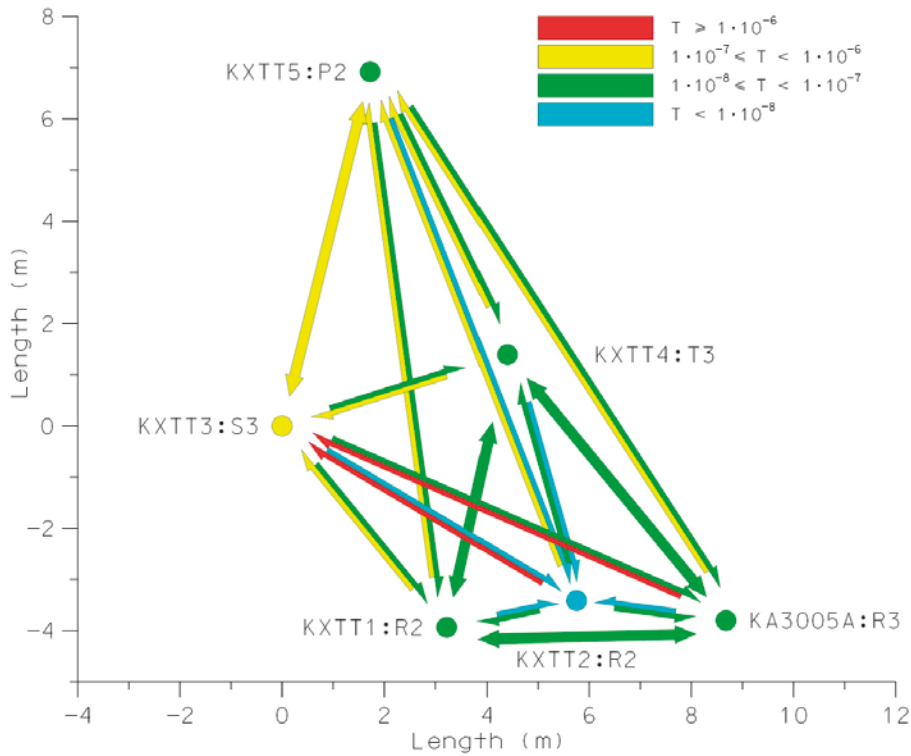
Figure 4-34. Transmissivity in each pumping hole (colour code one each dot) and from each observation hole while pumping (colour code one each arrow).
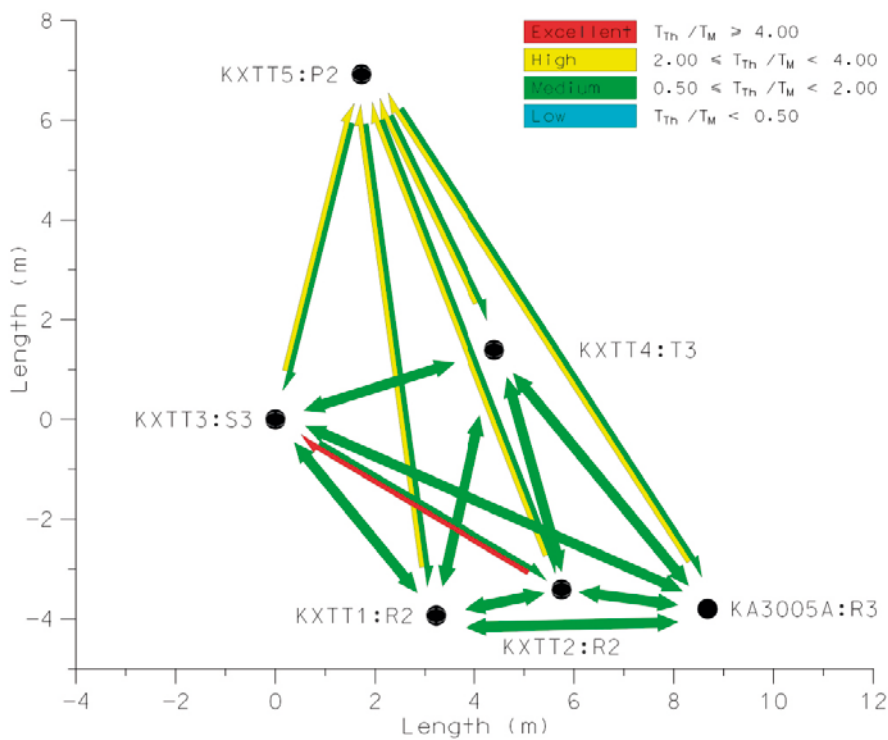
Figure 4-35. Transmissivity ratio between boreholes for TRUE-1 Complementary multi-hole reciprocal cross flow tests.
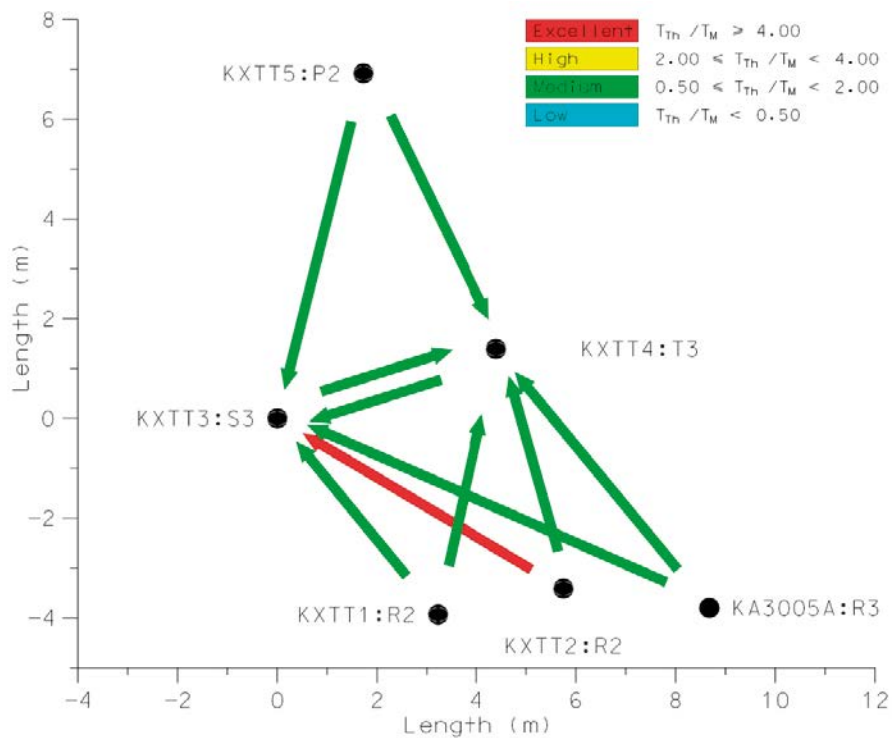
Figure 4-36. *Ratio for pumping rate 385 ml/min resp. 2,800 ml/min in KXTT3 and pumping rate 200 ml/min resp. 600 ml/min in KXTT4.*

When considering only values of T_M as indicated by coloured dots in Figure 4-34, it is obvious that KXTT3 has a higher transmissivity and KXTT2 has a lower transmissivity than the other boreholes. This fact is also consistent with the discussion above about a negative hydraulic boundary close to KXTT2.

Table 4-10. Transmissivity, T_M and T_{Th}, for TRUE-1 Complementary multi-hole reciprocal cross flow tests.

			T_{Th} [m²/s] Observation hole					
	Qpump [ml/min]	T_M [m²/s]	KXTT1	KXTT2	KXTT3	KXTT4	KXTT5	KA3005A
KXTT1	350	1.2E–08		1.4E–08	1.6E–08	1.6E–08	1.8E–08	1.6E–08
KXTT2	190	6.2E–09	7.2E–09		8.8E–09	8.3E–09	9.6E–09	7.5E–09
KXTT3	385	6.0E–07	9.0E–07	2.4E–06		8.9E–07	9.6E–07	1.0E–06
KXTT3	2,800	2.7E–07	3.7E–07	1.4E–06		3.3E–07	3.6E–07	3.8E–07
KXTT4	200	5.7E–08	6.5E–08	6.6E–08	6.5E–08		7.3E–08	7.5E–08
KXTT4	600	2.4E–08	2.8E–08	2.8E–08	2.7E–08		2.9E–08	3.0E–08
KXTT5	1,540	5.3E–08	1.6E–07	1.7E–07	1.5E–07	1.8E–07		2.0E–07
KA3005A	870	3.7E–08	3.9E–08	3.6E–08	4.3E–08	4.2E–08	4.7E–08	

Pumping hole (row label group)

Table 4-11. Transmissivity ratio (T_{Th}/T_M) matrix for TRUE-1 Complementary multi-hole reciprocal cross flow tests.

		Q_{pump} [ml/min]	Observation hole					
			KXTT1	KXTT2	KXTT3	KXTT4	KXTT5	KA3005A
Pumping hole	KXTT1	350		1.18	1.36	1.37	1.55	1.37
	KXTT2	190	1.17		1.42	1.34	1.55	1.21
	KXTT3	385	1.51	4.00		1.49	1.61	1.74
	KXTT3	2,800	1.40	5.39		1.25	1.34	1.43
	KXTT4	200	1.15	1.15	1.14		1.27	1.31
	KXTT4	600	1.16	1.15	1.13		1.22	1.25
	KXTT5	1,540	2.97	3.14	2.81	3.47		3.86
	KA3005A	870	1.05	0.97	1.17	1.14	1.26	

$T_{Th}/T_M \geq 4$	Excellent
$2.00 \leq T_{Th}/T_M < 4.00$	High
$0.50 \leq T_{Th}/T_M < 2.00$	Medium
$T_{Th}/T_M < 0.50$	Low

4.4 Flow rate in KXTT4:T3 during pumping in KXTT3:S3

During the course of the three experiments, the flow rate in KXTT4:T3 during pumping in KXTT3:S3 was evaluated a number of times, both by dilution tests and by continuous injection. As shown in Table 4-12, the flow rate in April 2006 was 52 ml/h while pumping with c 385 ml/h. This was slightly higher than during previous experiments at the TRUE-1 site with similar conditions, see Table 4-12. However, in June the same year the flow rate had decrease to only 13 ml/h. After that, the flow rate slowly increased again but not to the level that existed in April. Possible causes for observed changes are discussed in Section 5.4.

In order to secure good recovery during the CEC test it was decided to increase the pumping flow rate to 800 ml/min. From August to December 2006 the flow rate in KXTT4:T3 was rather stable around between 36 and 49 ml/h, with a pumping flow rate of 800 ml/min in KXTT3:S3.

Table 4-12. Groundwater flow through KXTT4:T3 under natural conditions and during pumping in KXTT3:S3. Volume in KXTT4:T3 is assumed to be 1,590 ml.

Test	Date	Q_{pump} KXTT3:S3 [ml/min]	Q_{flow} KXTT4:T3 [ml/h]
RC-1 (Andersson 1996)	960223–960228	400[1]	18[1]
PDT-3 (Andersson and Wass 1998)	970612–970703	400[1]	32[1]
STT-1 (Andersson et al. 1998)	970715–971002	400[1]	31–43[1]
Dilution test (COM)	060427	385	52
Dilution test (COM)	060428	2800	220
Dilution test D1	060608–060613	400	13
Dilution test D2	060614–060616	400	18
Dilution test D3, step 1		400	24
Dilution test D3, step 2	060815–060822	600	32
Dilution test D3, step 3		800	40–46
Cont. Inj. Pre test CEC, T3	060822–060830	800	49
Cont. Inj. Main test CEC, step 1	061118	800	45
Cont. Inj. Main test CEC, step 2	061126	800	38
Cont. Inj. Main test CEC, step 3	061206	800	36

[1] Test performed with pumping in KXTT3:R2 and dilution measurement in KXTT4:R3, see Appendix 1.

5 Discussion and conclusions

5.1 SWIW

It may be more appropriate to regard the SWIW experiment as a combination of a SWIW test and a radially diverging tracer test because the observations of tracer response in the four surrounding borehole sections are at least as interesting as the recovery in the SWIW section itself. Observations in other borehole sections have not been possible for the SWIW tests carried out within the site investigation programs, and the TRUE SWIW test results are therefore somewhat unique in this respect and provide firm evidence of tracer mobility and spread during a SWIW test.

Perhaps the most unexpected result is the low tracer recovery in the SWIW section. In fact, this was the reason why two SWIW tests were carried out. The first SWIW test gave a tracer recovery of only about two percent. However, tracer breakthrough were observed in all of the four observation boreholes and one interpretation after the first test was that most of the tracer may had been lost to fractures or zones with high hydraulic gradients due to the vicinity of the tunnel. A follow-up test was therefore carried out with the only main difference being a substantial decrease in the total injected water volume. The design of the second SWIW test was based on visual inspection of the various breakthrough curves from the first test and it was surprising that the tracer recovery in the second test did not increase more than to about 11 percent.

Irrespective of the low recovery in the SWIW section, the results from the observation sections clearly demonstrate the heterogeneous nature of the radial solute spreading during the water injection phase. Although the distances between the SWIW section and the observation sections are fairly similar, tracer residence times as well as peak tracer concentrations vary over about one magnitude. One-dimensional transport modelling indicated that only one of the observation sections (KXTT3:S3) gave consistent results for both of the SWIW experiments. In addition, the results from this borehole section are the ones most easily interpreted as typical breakthrough from a radially diverging experiment. In other sections, interpretation is more ambiguous especially when considering the combined results from both of the tests.

5.2 CEC

The cation exchange capacity (CEC) experiment was performed with the intention to saturate the fracture of the Feature A flow path between KXTT4 and KXTT3 with a strongly sorbing tracer (i.e., Cs+) in relatively high concentrations to investigate the sorption capacity of the flow path.

Estimates of the surface cation exchange capacity based on measured mylonite sampled in the Feature A gave a CEC of $3.4 \cdot 10^{-3}$ mole/m^2. Estimates of a total rock surface of the flow path are in the range of 0.5–3 m^2, if disregarding surface roughness and internals mineral surfaces in the rock matrix. One could thus predict a total amount of cation exchange sites of $(1.7–10) \cdot 10^{-3}$ moles in the flow path.

However, simply by measuring the experimental loss of Cs, it was found that > 0.047 moles of Cs was lost because of adsorption. Due to the underestimation of the sorption capacity in the scoping calculations for the experiment (based on the mylonite CEC), too low concentrations of Cs were used in the experiment which entailed that saturation was never achieved in the experiment.

There are a number of possible explanations for this:

• It is possible that there is interaction in the flow path with a rock material with higher CEC than the mylonite. For example, fault gouge material has been reported (Byegård et al. 2010) to have a CEC in the range of 0.14 moles/kg. The observation of a total loss of > 0.047 moles at the end of the CEC experiment would thus imply that > 0.3 kg of fault gouge material would be present in the actual flow path. Using the evaluated total capacity of 0.10 moles for the transport path, one would end up with an estimation of 0.6 kg fault gouge material.

During earlier investigations no evidence of fault gouge material was found in core samples from Feature A, possibly due to flushing during the drilling. However, clay minerals found in Feature A may indicate presence of fault gouge material (Winberg et al. 2000).

- Matrix diffusion will cause inner surfaces (e.g., surfaces of microfractures and/or grain boundary porosity) to interact with the injected Cs, however, no observation has been made of quantities enough to explain the observed Cs retardation. Based on the experimentally based estimation of a CEC of 0.005 moles/kg of mylonite (cf. Section 4.2) this would imply that > 10 kg of mylonite would have been saturated with Cs by cation exchange. Assuming a total fracture surface in the transport path of 3 m^2 (cf. Section 3.4.4) together with a rock density of 2,700 kgm^{-3}, this would correspond to 10 kg/2,700 kgm^{-3} / 3 m^2 = 1.2 mm average penetration depth in the rock matrix. Since the experimental duration time is ~ 500 h, this would correspond to an apparent diffusivity rate of 8·10^{-13} m^2/s, which is somewhat high, but still realistic.

Furthermore, there is a systematic deviation of the experimental breakthrough curve in relation to the model assuming reversible sorption, indicating that there would be non- or slowly reversibility in the Cs interaction with the rock material. This indication is to some degree also supported by the observation of no, or at least very little, de-sorption of the STT-1 injected Cs-137 taking place in the CEC experiment. However, since the modelling in this work was restricted to surface sorption interaction, it can not be excluded that these two observations could be explained by a matrix diffusion process.

5.3   COM

There are several ways to interpret the results from the COM-tests. First of all, one might discuss if the interpretation should be made in two or three dimensions. In earlier investigations at the TRUE-1 site, Feature A was interpreted as a single fracture plane with a few sub parallel fractures, or possibly splay fractures (Winberg et al. 2000). The)interpretation made by Winberg et al. (2000) is also supported by Andersson et al. (2002a). In the present investigation, nothing contrary to this conceptualisation was found. Therefore, the interpretation of the results from the COM-tests are made assuming a two dimensional character of Feature A.

Previous analyses of flow dimensions from hydraulic tests generally result in flow dimensions higher than two (Winberg et al. 2000). This could be interpreted as a system dominated by interconnecting fractures at the site, which would contradict the concept of planar two-dimensional flow in the tested region. However, the first period of a hydraulic test, which is assumed to reflect conditions close to the test section, is often so affected by borehole storage effects and/or unstable pumping rates or injection pressure that it is impossible to use for transient evaluation of flow dimensions. Hence, without any detailed study of the foundation for the flow dimensions higher than two, it is reasonable to conclude that these higher flow dimensions reflect conditions farther away from the borehole sections than what was studied in the COM tests. The interpretation is presented graphically in Figure 5-1, where red indicates areas with high conductivity, white medium conductivity and blue low conductivity. The basis for the interpretation was that the conductivity of Feature A was classified as medium (white) except for:

- High conductivity at KXTT3 and low at KXTT2 (supported by TM).

- Low conductivity between KXTT1, KXTT2, KXTT4 and KA3005A (supported by tR/r^2 and Qflow/Qtheory) except for medium conductivity between KXTT3 and KXTT2 (supported by TTh/TM).

- High conductivity to the left of KXTT3 and KXTT5 (supported by high Qflow/Qtheory in KXTT3 and to some degree in KXTT5 while pumping the other boreholes but not the other way around).

Observe that this interpretation is one of many possible and it is not unambiguous. No attempts to validate this interpretation by using a numerical hydrological model were made within the present study. Instead, the interpretation may be considered as a suggestion for a first setup for a model of Feature A.
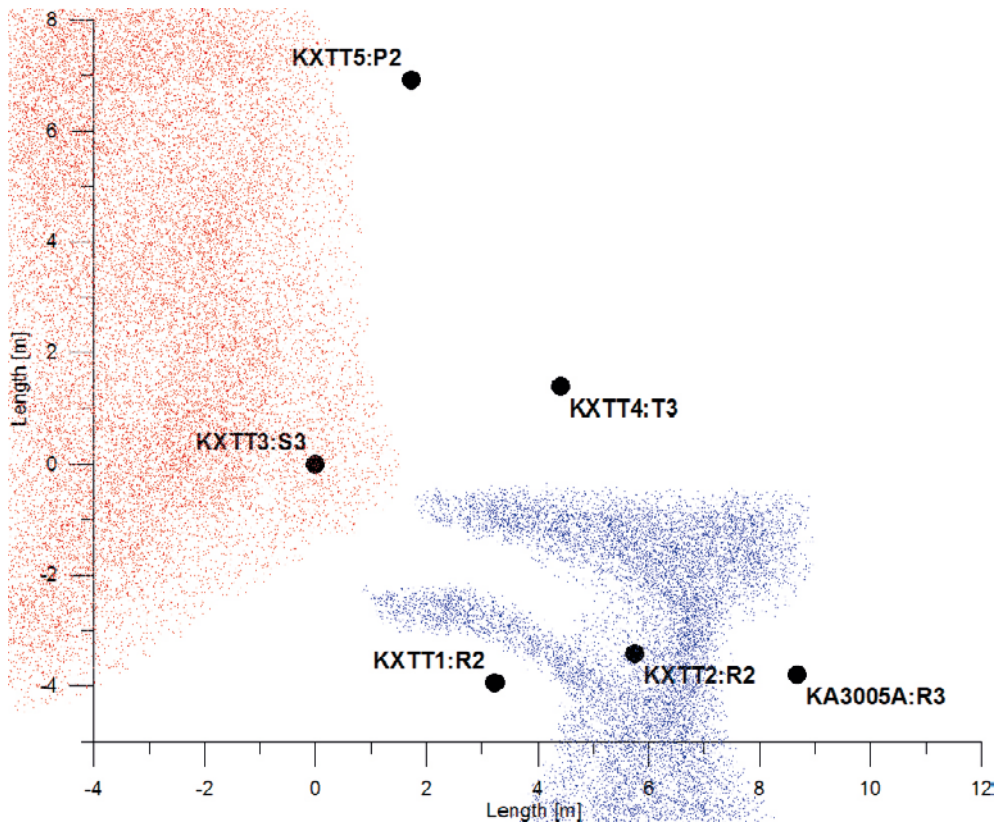
Figure 5-1. Interpretation of the conductivity distribution of Feature A based on the COM-test results. Red colour indicates high conductivity, white medium and blue low conductivity.

Results from previous tracer dilution tests at the TRUE-1 site while pumping in Feature A in KXTT4 (Test CX1) and KXTT3 (Test CX3) (Andersson et al. 2002a) are not presented in the same way as the COM tests. Still, an overview of these earlier tests reveals similar results as the COM tests with a relatively large flow response in KXTT3 and KXTT5 while pumping in KXTT4 and a large response in KXXT1 and KXTT5 while pumping in KXTT3.

Since earlier hydraulic interference tests (Winberg et al. 2000, Andersson et al. 2002a) primarily focused on distinction between features, such as Feature A and B, a different setup of intervals for s_p/Q_{pump} and t_R/r^2 were used than for the evaluation of the COM tests. Consequently, the results are not directly comparable.

A hydraulic test made with low or medium conductivity close to the borehole and higher conductivity some distance away may be expected to display a flow dimension higher than two. The interpretation of a high conductivity area to the left of KXTT3 and KXTT5 in Figure 5-1 may therefore be consistent with the earlier interpretation of flow dimensions from hydraulic tests in Feature A (Winberg et al. 2000). This area of higher conductivity may in fact be a structure denoted NW-2' in Winberg et al. (2000).

It is clear that the COM tests reveal variations in the conductivity field in the studied part of Feature A. Channelling effects may play a role in these variations. For example, the low conductivity area indicated in Figure 5-1 is intercepted by a higher conductivity field between KXTT3 and KXTT2 which may be interpreted as a channel in Feature A. However, it is not possible to firmly establish whether channels exist or not in this part of Feature A based solely on the results from the COM tests.

The interpretation of the results from the COM tests shows that a systematic alteration of pumping borehole in combination with registration of pressure and flow responses may give a good foundation for a detailed modelling of a feature or site.

Many cross hole tracer tests have previously been made in Feature A (Winberg et al. 2000, Andersson et al. 2002a). It is most likely that an incorporation of these kinds of results would improve and facilitate the interpretation of Feature A further. Also a transient evaluation of the pressure responses could prove helpful since information of storativity, flow regimes and outer boundaries could be obtained and included in the interpretation.

5.4   Flow rate in KXTT4:T3 during pumping in KXTT3:S3

As shown in Table 4-12 above, there are changes of the flow rate in KXTT4:T3 while pumping in KXTT3:S3 during both 1996–1997 and during 2006. The flow rate may be influenced by a number of factors such as displacement of fracture material (fault gouge), minor changes in the outer boundary conditions (near tunnel desaturation/dewatering), seasonal effects, chemical precipitation or possibly microbial activity (bio film).

Effects on hydraulic systems due to extraordinary events such as blasting have been noted earlier, for example by Rhén and Forsmark (2001). However, no such activities are reported for this period in the vicinity of the TRUE-1 site (Nyberg et al. 2007).

A significant decrease of the flow rate in KXTT4:T3 while pumping in KXTT3:S3 was observed between the end of April (dilution test COM) and the beginning of June 2006 (dilution test D1). From June to August 2006 (dilution tests D2 and D3), the flow rate increased but not to the same level as in April the same year.

As mentioned in Section 3.3.2, gas was accidentally injected in KXTT4:T3 during tracer test T1, in between dilution test COM and D1. KXXT4:T3 was then drained in order to remove the injected nitrogen gas. It is unfortunately not possible to establish whether all injected nitrogen was drained from KXTT4:T3. Possible remaining nitrogen may have been trapped in fracture pockets thereby affecting the flow situation in KXTT4:T3. Assuming that the groundwater was not saturated, the trapped nitrogen gas would eventually dissolve into the groundwater. An increase of the flow rate, as observed during the summer of 2006, would then be a likely response. Accordingly, it is not unlikely that the flow rate changes observed during 2006 were caused by the accidental gas injection.

References

SKB's (Svensk Kärnbränslehantering AB) publications can be found at www.skb.com/publications.

Andersson P, 1996. Äspö Hard Rock Laboratory. TRUE 1st stage tracer test program. Experimental data and preliminary evaluation of the TRUE-1 radially converging tracer test (RC-1). SKB PR HRL-96-24, Svensk Kärnbränslehantering AB.

Andersson P, Wass E, 1998. Äspö Hard Rock Laboratory. TRUE 1st stage tracer test program. Preliminary design tests for tests with radioactive sorbing tracers (PDT-1, PDT-2, PDT-3). Experimental description and preliminary evaluation. SKB PR HRL-98-13, Svensk Kärnbränslehantering AB.

Andersson P, Johansson H, Nordqvist R, Skarnemark G, Skålberg M, Wass E, 1998. Äspö Hard Rock Laboratory. TRUE 1st stage tracer test programme. Tracer tests with sorbing tracers, STT-1. Experimental description and preliminary evaluation. SKB Technical note TN-98-10t, Svensk Kärnbränslehantering AB.

Andersson P, Wass E, Byegård J, Johansson H, Skarnemark G, 1999. Äspö Hard Rock Laboratory. TRUE 1st stage tracer test programme. Tracer tests with sorbing tracers, STT-2. Experimental description and preliminary evaluation. SKB IPR-99-15, Svensk Kärnbränslehantering AB.

Andersson P, Wass E, Gröhn S, Holmqvist M, 2002a. Äspö Hard Rock Laboratory. TRUE-1 continuation project. Complementary investigations at the TRUE-1 site – Crosshole interference, dilution and tracer tests, CX-1 – CX-5. SKB IPR-02-47, Svensk Kärnbränslehantering AB.

Andersson P, Byegård J, Dershowitz B, Doe T, Hermanson J, Meier P, Tullborg E-L, Winberg A (ed.), 2002b. Final report of the TRUE Block Scale project 1. Characterisation and model development. SKB TR-02-13 Svensk Kärnbränslehantering AB.

Andersson P, Byegård J, Winberg A, 2002c. Final report of the TRUE Block Scale project. 2. Tracer tests in the block smale. SKB TR-02-14, Svensk Kärnbränslehantering AB.

Andersson P, Byegård J, Billaux D, Cvetkovic V, Dershowitz W, Doe T, Hermanson J, Poteri A, Tullborg E-L, Winberg A (ed), 2007. TRUE Block Scale Continuation project. Final report. SKB TR-06-42, Svensk Kärnbränslehantering AB.

Byegård J, Skarnemark G, Skålberg M, 1995. The use of some ion-exchange sorbing tracer cations in in-situ experiments in high saline groundwaters. In: Murakami T, Ewing R C (eds). Scientific basis for nuclear waste management XVIII: symposium held in Kyoto, Japan, 23–27 October 1994. Pittsburgh, PA: Materials Research Society. (Materials Research Society Symposium Proceedings 353), 1077–1084.

Byegård J, Johansson H, Skålberg M, Tullborg E-L, 1998. The interaction of sorbing and non-sorbing tracers with different Äspö rock types. Sorption and diffusion experiments in the laboratory scale. SKB TR-98-18, Svensk Kärnbränslehantering AB.

Byegård J, Widestrand H, Nilsson K, Gustafsson E, Kronberg M, 2010. Long-term Sorption Diffusion Experiment (LTDE-SD). Performance of main in-situ experiment and results from water phase measurements. SKB IPR-10-10, Svensk Kärnbränslehantering AB.

Cooley R L, 1979. A method of estimating parameters and assessing reliability for models of steady ground water flow. 2. Application of statistical analyses. Water Resources Research, 15, 603–617.

Fetter C W, 1999. Contaminant hydrogeology. 2nd ed. Upper Saddle River, NJ: Prentice Hall.

Gaines G L, Thomas H C, 1953. Adsorption studies on clay minerals. II. A formulation of the thermodynamics of exchange adsorption. Journal of Chemical Physics 21, 714–718.

Halevy E, Moser H, Zellhofer O, Zuber A, 1967. Borehole dilution techniques – a critical review. In Isotopes in hydrology: proceedings of the symposium on isotopes in hydrology held by the International Atomic Energy Agency in co-operation with the International Union of Geodesy and Geophysics in Vienna 14–18 November 1966. Vienna: International Atomic Energy Agency, 530–564.

Javandel I, Doughty C, Tsang C-F, 1984. Groundwater transport: handbook of mathematical models. Washington, DC: American Geophysical Union.

Lee T-C, 1999. Applied mathematics in hydrogeology. Boca Raton, FL: Lewis Publishers.

Levenberg K, 1944. A method for the solution of certain non-linear problems in least squares. Quarterly of Applied Mathematics 2, 164–168.

Marquardt D, 1963. An Algorithm for Least-Squares Estimation of Nonlinear Parameters. Journal of the Society for Industrial and Applied Mathematics. Vol 11, No 2, 431–441.

Nordqvist R, 1994. Documentation of some analytical flow and transport models implemented for use with PAREST – User manual. Geosigma GRAP 94 006, Uppsala.

Nordqvist R, 2008. Evaluation and modelling of SWIW tests performed within the SKB site characterisation programme. SKB R-08-104, Svensk Kärnbränslehantering AB.

Nyberg G, Jönsson S, Wass E, 2007. Äspö Hard Rock Laboratory. Hydro monitoring program. Report for 2006. SKB IPR-07-10, Svensk Kärnbränslehantering AB.

Poteri A, Billaux D, Dershowitz W, Gómez-Hernández J, Cvetkovic V, Hautojärvi A, Holton D, Medina A, Winberg A (ed), 2002. Final report of the TRUE Block Scale project. 3. Modelling of flow and transport. SKB TR-02-15, Svensk Kärnbränslehantering AB.

Rhén I, Forsmark T, 2001. Äspö Hard Rock Laboratory. Prototype repository. Hydrogeology. Summary report of investigations before the operation phase. SKB IPR-01-65, Svensk Kärnbränslehantering AB.

Sigurdsson O, Hjerne C, 2014. Overcoring of resin impregnated boreholes KXTT3 and KXTT4 at the TRUE-1 site. TRUE-1 completion. SKB P-11-21, Svensk Kärnbränslehantering AB.

Voss C I, 1984. SUTRA – A finite-element simulation model for saturated-unsaturated, fluid-density-dependent ground-water flow with energy transport or chemically-reactive single-species solute transport: Water-Resources Investigations Report 84-4369, U.S. Geological Survey, Denver, Colorado.

Widestrand H, Andersson P, Byegård J, Skarnemark G, Skålberg M, Wass E, 2001. In situ migration experiments at Äspö Hard Rock Laboratory, Sweden: results of radioactive tracer migration studies in a single fracture. Journal of Radioanalytical and Nuclear Chemistry 250, 501–517.

Widestrand H, Byegård J, Börjesson S, Berglin A, Wass E, 2006. Äspö Hard Rock Laboratory. LTDE Long-term diffusion Experiment. Functionality tests with short-lived radionuclides 2005. SKB IPR-06-05, Svensk Kärnbränslehantering AB.

Widestrand H, Byegård J, Selnert A, Skålberg M, Höglund S, Gustafsson E, 2010. Long-term Sorption Diffusion Experiment (LTDE-SD). Supporting laboratory program – Sorption diffusion experiments and rock material characterisation, with supplement of adsorption studies on intact rock samples for the Forsmark and Laxemar site investigations. SKB IPR-10-11, Svensk Kärnbränslehantering AB.

Winberg A, Andersson P, Hermanson J, Byegård J, Cvetkovic V, Birgersson L, 2000. Äspö Hard Rock Laboratory. Final report of the first stage of the tracer retention understanding experiments. SKB TR-00-07, Svensk Kärnbränslehantering AB.

Winberg A, Andersson P, Byegård J, Poteri A, Cvetkovic V, Dershowitz W, Doe T, Hermanson J, Gómez-Hernández J, Hautojärvi A, Billaux D, Tullborg E-L, Holton D, Meier P, Medina A, 2003. Final report of the TRUE Block Scale project. 4. Synthesis of flow, transport and retention in the block scale. SKB TR-02-16, Svensk Kärnbränslehantering AB.

Borehole instrumentation

Table A1-1 and A1-2 shows the instrumentation of the boreholes at the TRUE-1 site from the drilling of the boreholes until present. The data presented in the tables are compiled from Sicada, HMS-manual (Winberg et al. 2000, Andersson et al. 2002a). None of the references were complete in the aspect of borehole instrumentation. Some data were also different in the references. In these cases, a judgement based on experience and knowledge of the site, was made between the different data. The differences are given in the notations of each table.

Table A1-1. Instrumentation of boreholes KXTT1, KXTT2 and KXTT3 at the TRUE-1 site.

Borehole	Sec	Secup [m]	Seclow [m]	Date YYMMDD Start	Stop	Sec	Secup [m]	Seclow [m]	Date YYMMDD Start	Stop	Sec	Secup [m]	Seclow [m]	Date YYMMDD Start	Stop
KXTT1	P1	17.00	28.76	950707	951211[1]	R1[2]	17.00	28.76	951211						
	P2	15.00	16.00	950707	951211[1]	R2[2]	15.00[3]	16.00	951211						
	P3	8.50	10.50	950707	951211[1]	R3[2]	7.50	11.50	951211						
	P4	3.00	7.50	950707	951211[1]	R4[2]	3.00	6.50	951211						
KXTT2	P1	14.30	18.30	950708	951206	R1	16.55	18.3	951206[4]						
	P2	11.30	13.30	950708	951206	R2	14.55	15.55	951206[4]						
	P3	8.80[5]	10.30	950708	951206	R3	11.55	13.55	951206[4]						
	P4	3.05	7.80	950708	951206	R4	7.55	10.55	951206[4]						
						R5	3.05	6.55	951206[4]						
KXTT3	P1	15.42	17.43	950708	951211[6]	R1[2]	15.42	17.43	951211	051025	S1	15.77	17.43	051026	070410
	P2	10.92[7]	14.42	950708	951211[6]	R2[2]	12.42	14.42	951211	051025	S2	14.97	15.52	051026	070410
	P3	8.92	9.92	950708	951211[6]	R3[2]	8.92	11.42	951211	051025	S3	12.67	14.72	051026	070410
	P4	3.17	7.92	950708	951211[6]	R4[2]	3.17	7.92	951211	051025	S4	8.92	11.67	051026	
											S5	3.17	7.92	051026	

[1] No stop date in Sicada.
[2] Installation missing in Sicada.
[3] 15.50 m according to Winberg et al. (2000).
[4] Other date in the HMS manual.
[5] 8.30 m according to Sicada.
[6] Other date according to Sicada.
[7] 10.93 m according to Winberg et al. (2000).
[8] 46.93 m according to Winberg et al. (2000).

Table A1-2. Instrumentation of boreholes KXTT4, KXTT5 and KA3005A at the TRUE-1 site.

Borehole	Sec	Secup [m]	Seclow [m]	Date YYMMDD Start	Stop	Sec	Secup [m]	Seclow [m]	Date YYMMDD Start	Stop	Sec	Secup [m]	Seclow [m]	Date YYMMDD Start	Stop	Sec	Secup [m]	Seclow [m]	Date YYMMDD Start	Stop
KXTT4	P1	24.42	49.31	950718	951211[6]	R1[2]	24.42	49.31	951211	991214	S1	14.92	49.31	991214[6]	051027	T1	15.77	49.31	051027	070410
	P2	14.92	23.42	950718	951211[6]	R2[2]	14.92	23.42	951211	991214	S2	12.92	13.92	991214[6]	051027	T2	13.93	15.52	051027	070410
	P3	11.42	13.92	950718	951211[6]	R3[2]	11.42	13.92	951211	991214	S3	11.92	12.42	991214[6]	051027	T3	11.67	13.68	051027	070410
	P4	8.42	10.42	950718	951211[6]	R4[2]	8.42	10.42	951211	991214	S4	8.42	10.92	991214[6]	051027	T4	8.42	10.67	051027	070410
	P5	3.17	7.42	950718	951211[6]	R5[2]	3.17	7.42	951211	991214						T5	3.17	7.42	051027	
KXTT5	P1	10.81	25.85	991214																
	P2	9.61	9.81	991214																
	P3	6.11	8.61	991214																
	P4	3.11	5.11	991214																
KA3005A	P1	46.43	58.11	950227	951101	1	0	58.11	951101	951207	R1	51.03	58.11	951207						
	P2	44.43	45.43	950227	951101						R2	46.78[8]	50.03	951207						
	P3	38.93	43.43	950227	951101						R3	44.78	45.78	951207						
	P4	36.93	37.93	950227	951101						R4	39.03	43.78	951207						
	P5	6.53	35.93	950227	951101						R5	6.53	38.03	951207						

[1] No stop date in Sicada.

[2] Installation missing in Sicada.

[3] 15.50 m according to Winberg et al. (2000).

[4] Other date in the HMS manual.

[5] 8.30 m according to Sicada.

[6] Other date according to Sicada.

[7] 10.93 m according to Winberg et al. (2000).

[8] 46.93 m according to Winberg et al. (2000).

Dilution tests during COM test

The results of the dilution test evaluations from the COM-test are presented below in Tables A2-1 to A2-6 and Figures A2-1 to A2-19. In Tables A2-1 to A2-6 some of the tests are marked with a note. Note *a* indicates an uncertain evaluation due to low concentration. Note *b* indicates an uncertain evaluation due to scattered data.

Table A2-1. Result of dilution test evaluation in observation section KXTT1:R2.

| | Fit | | | | | | |
Event	From [h]	To [h]	Slope	Data points	R^2	Q [ml/min]	Note
Pumping KXTT3:S3 400 ml/min	9.17	20.17	–5.36E–02	22	0.973	1.31	
Pumping KXTT3:S3 2,800 ml/min	21.67	29.67	–6.05E–01	16	0.995	15.95	
Undisturbed period 2	30.33	124.98	–1.15E–02	39	0.529	0.27	a
Pumping KXTT1:R2 350 ml/min	na	na	na	na	na	na	
Undisturbed period 3	na	na	na	na	na	na	
Pumping KXTT5:P2 1,540 ml/min	177.00	195.12	–3.03E–02	18	0.976	0.75	
Undisturbed period 4	195.12	270.02	–8.34E–03	24	0.998	0.15	
Pumping KXTT2:R2 190 ml/min	273.05	293.05	–1.69E–02	20	0.991	0.32	
Undisturbed period 5	294.05	322.05	–7.90E–03	27	0.988	0.08	
Pumping KXTT4:T3 200 ml/min	323.13	336.13	–7.91E–03	13	0.939	0.08	
Pumping KXTT4:T3 600 ml/min	337.13	360.13	–1.27E–02	23	0.992	0.21	
Undisturbed period 6	361.13	441.58	–6.54E–03	28	0.997	0.07	
Pumping KA3005A 870 ml/min	442.58	461.58	–1.65E–02	19	0.993	0.30	

Table A2-2. Result of dilution test evaluation in observation section KXTT2:R2.

| | Fit | | | | | | |
Event	From [h]	To [h]	Slope	Data points	R^2	Q [ml/min]	Note
Pumping KXTT3:S3 400 ml/min	9.17	20.17	–1.47E–02	22	0.752	0.27	
Pumping KXTT3:S3 2,800 ml/min	20.67	30.17	–2.04E–02	19	0.827	0.42	
Undisturbed period 2	31.38	123.88	–4.53E–03	37	0.994	0.09	
Pumping KXTT1:R2 350 ml/min	128.42	147.58	–4.77E–03	19	0.748	0.06	
Undisturbed period 3	148.58	174.58	–5.93E–03	25	0.936	0.09	
Pumping KXTT5:P2 1,540 ml/min	175.58	194.58	–1.25E–02	19	0.965	0.26	
Undisturbed period 4	198.08	270.08	–3.94E–03	24	0.986	0.07	
Pumping KXTT2:R2 190 ml/min	na	na	na	na	na	na	
Undisturbed period 5	na	na	na	na	na	na	
Pumping KXTT4:T3 200 ml/min	323.58	336.58	–9.22E–03	13	0.467	0.16	
Pumping KXTT4:T3 600 ml/min	337.58	360.59	–8.97E–03	23	0.793	0.15	
Undisturbed period 6	361.37	441.58	–4.01E–03	32	0.899	0.06	
Pumping KA3005A 870 ml/min	442.60	461.60	–4.50E–02	19	0.995	1.10	

Table A2-3. Result of dilution test evaluation in observation section KXTT3:S3.

Event	From [h]	To [h]	Fit Slope	Data points	R²	Q [ml/min]	Note
Pumping KXTT3:S3 400 ml/min	na	na	na	na	na	na	
Pumping KXTT3:S3 2,800 ml/min	na	na	na	na	na	na	
Undisturbed period 2	na	na	na	na	na	na	
Pumping KXTT1:R2 350 ml/min	129.42	145.42	−3.08E−01	16	0.998	8.00	
Undisturbed period 3	152.32	169.35	−1.31E−01	17	0.999	3.42	
Pumping KXTT5:P2 1,540 ml/min	176.47	181.47	−8.85E−01	5	1.000	22.98	
Undisturbed period 4	195.03	271.95	−3.63E−02	27	0.662	0.94	a
Pumping KXTT2:R2 190 ml/min	272.95	292.95	−3.06E−02	20	0.360	0.79	a
Undisturbed period 5	295.78	321.78	−1.35E−01	26	0.999	3.51	
Pumping KXTT4:T3 200 ml/min	322.78	335.78	−1.44E−01	13	0.959	3.73	
Pumping KXTT4:T3 600 ml/min	336.78	358.78	−4.72E−03	22	0.016	0.12	a
Undisturbed period 6	364.25	409.25	−1.22E−01	15	0.994	3.18	
Pumping KA3005A 870 ml/min	442.00	453.00	−5.15E−01	10	0.988	13.38	

Table A2-4. Result of dilution test evaluation in observation section KXTT4:T3.

Event	From [h]	To [h]	Fit Slope	Data points	R²	Q [ml/min]	Note
Pumping KXTT3:S3 400 ml/min	10.17	20.17	−3.88E−02	20	0.996	0.87	
Pumping KXTT3:S3 2,800 ml/min	21.17	30.33	−1.48E−01	18	0.997	3.67	
Undisturbed period 2	31.38	126.38	−8.49E−04	38	0.517	−0.04	
Pumping KXTT1:R2 350 ml/min	131.58	147.58	−7.38E−03	13	0.904	0.11	
Undisturbed period 3	148.58	174.58	−3.20E−03	24	0.716	0.00	
Pumping KXTT5:P2 1,540 ml/min	177.58	193.87	−1.46E−01	18	0.998	3.52	
Undisturbed period 4	195.07	272.00	−4.21E−03	28	0.914	0.06	
Pumping KXTT2:R2 190 ml/min	273.00	293.00	−8.34E−03	20	0.982	0.13	
Undisturbed period 5	295.00	320.87	−4.21E−03	26	0.984	0.02	
Pumping KXTT4:T3 200 ml/min	na	na	na	na	na	na	
Pumping KXTT4:T3 600 ml/min	na	na	na	na	na	na	
Undisturbed period 6	na	na	na	na	na	na	
Pumping KA3005A 870 ml/min	444.50	461.50	−4.39E−02	17	0.996	1.05	

Table A2-5. Result of dilution test evaluation in observation section KXTT5:P2.

Event	From [h]	To [h]	Fit Slope	Data points	R²	Q [ml/min]	Note
Pumping KXTT3:S3 400 ml/min	10.17	20.17	−1.11E−01	19	0.998	1.14	
Pumping KXTT3:S3 2,800 ml/min	20.67	27.67	−2.94E−01	14	0.998	3.19	
Undisturbed period 2	38.88	126.38	−3.98E−02	35	0.896	0.38	
Pumping KXTT1:R2 350 ml/min	131.83	146.83	−7.11E−02	15	0.998	0.68	
Undisturbed period 3	147.83	172.83	−7.26E−02	25	1.000	0.69	
Pumping KXTT5:P2 1,540 ml/min	na	na	na	na	na	na	
Undisturbed period 4	na	na	na	na	na	na	
Pumping KXTT2:R2 190 ml/min	277.22	293.23	−5.01E−02	9	0.959	0.49	
Undisturbed period 5	294.23	322.23	−1.20E−02	28	0.734	0.06	
Pumping KXTT4:T3 200 ml/min	323.23	336.23	−7.57E−02	13	0.968	0.78	
Pumping KXTT4:T3 600 ml/min	337.23	346.23	−2.07E−01	9	0.998	2.25	
Undisturbed period 6	361.23	440.42	−3.23E−03	28	0.707	−0.01	
Pumping KA3005A 870 ml/min	442.50	450.50	−6.14E−01	8	0.992	6.83	

**Table A2-6.** Result of dilution test evaluation in observation section KA3005A:R2.

Event	From [h]	To [h]	Fit Slope	Data points	R^2	Q [ml/min]	Note
Pumping KXTT3:S3 400 ml/min	11.97	19.97	–7.88E–03	16	0.376	0.21	b
Pumping KXTT3:S3 2,800 ml/min	20.47	29.97	–7.43E–03	19	0.203	0.20	b
Undisturbed period 2	33.50	126.50	–7.56E–04	31	0.433	0.01	
Pumping KXTT1:R2 350 ml/min	128.17	147.17	–1.65E–03	19	0.366	–0.03	
Undisturbed period 3	148.17	175.17	–1.95E–03	27	0.656	–0.01	
Pumping KXTT5:P2 1,540 ml/min	176.17	194.17	–3.85E–04	18	0.117	–0.07	
Undisturbed period 4	195.17	267.47	–1.28E–03	25	0.706	0.03	
Pumping KXTT2:R2 190 ml/min	272.82	292.82	–6.47E–03	20	0.859	0.17	
Undisturbed period 5	293.82	321.82	–1.12E–03	28	0.121	–0.04	b
Pumping KXTT4:T3 200 ml/min	322.82	335.82	6.78E–04	13	0.009	–0.11	b
Pumping KXTT4:T3 600 ml/min	336.82	360.82	–1.91E–03	24	0.343	–0.01	b
Undisturbed period 6	361.60	436.60	–2.99E–04	25	0.134	–0.03	b
Pumping KA3005A 870 ml/min	na	na	na	na	na	na	

Legend for figures in Appendix 2

+ Data
— Undisturbed periods
⟷ Pumping KXTT3 385 ml/min
⟷ Pumping KXTT3 2800 ml/min
⟷ Pumping KXTT1 350 ml/min
⟷ Pumping KXTT5 1540 ml/min
⟷ Pumping KXTT2 190 ml/min

— Fit: Pumping KXTT3 385 ml/min
— Fit: Pumping KXTT3 2800 ml/min
— Fit: Pumping KXTT1 350 ml/min
— Fit: Pumping KXTT5 1540 ml/min
⟷ Pumping KXTT4 200 ml/min
⟷ Pumping KXTT4 600 ml/min
⟷ Pumping KA3005A 870 ml/min

— Fit: Pumping KXTT2 190 ml/min
— Fit: Pumping KXTT4 200 ml/min
— Fit: Pumping KXTT4 600 ml/min
— Fit: Pumping KA3005A 870 ml/min
— Fit: Undisturbed periods 1

Figure A2-1. *Uranine concentration in KXTT1:R2 between 0 and 150 h. Fit to pumping periods in KXTT3 and undisturbed period #2.*
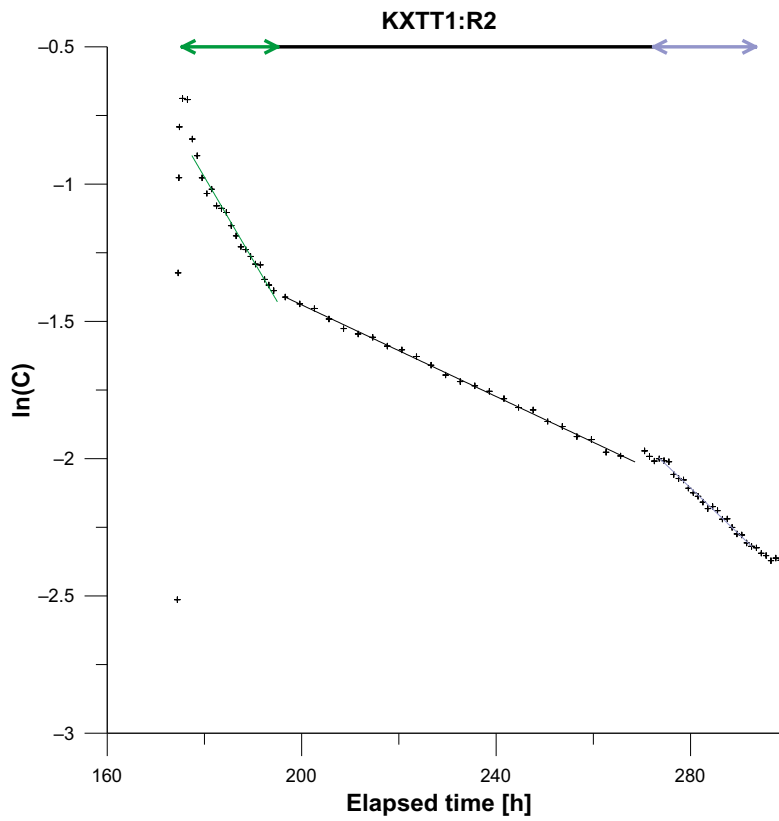
Figure A2-2. *Uranine concentration in KXTT1:R2 between 160 and 300 h. Fit to pumping periods in KXTT5 and KXTT2 and undisturbed period #4.*
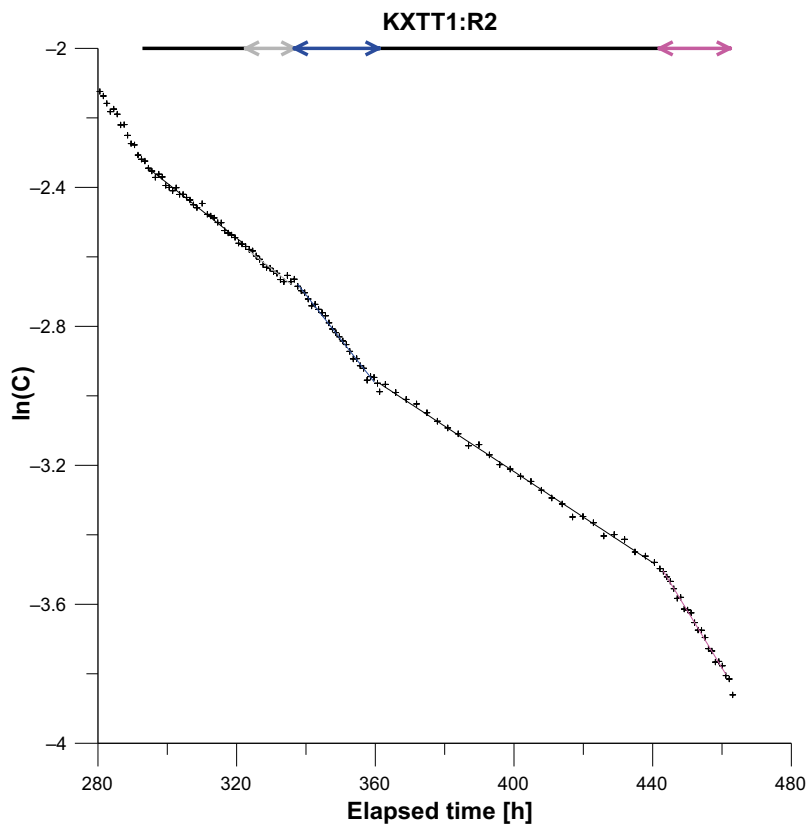
Figure A2-3. *Uranine concentration in KXTT1:R2 between 280 and 480 h. Fit to pumping periods in KXTT4 and KA3005A and undisturbed period #5 and #6.*
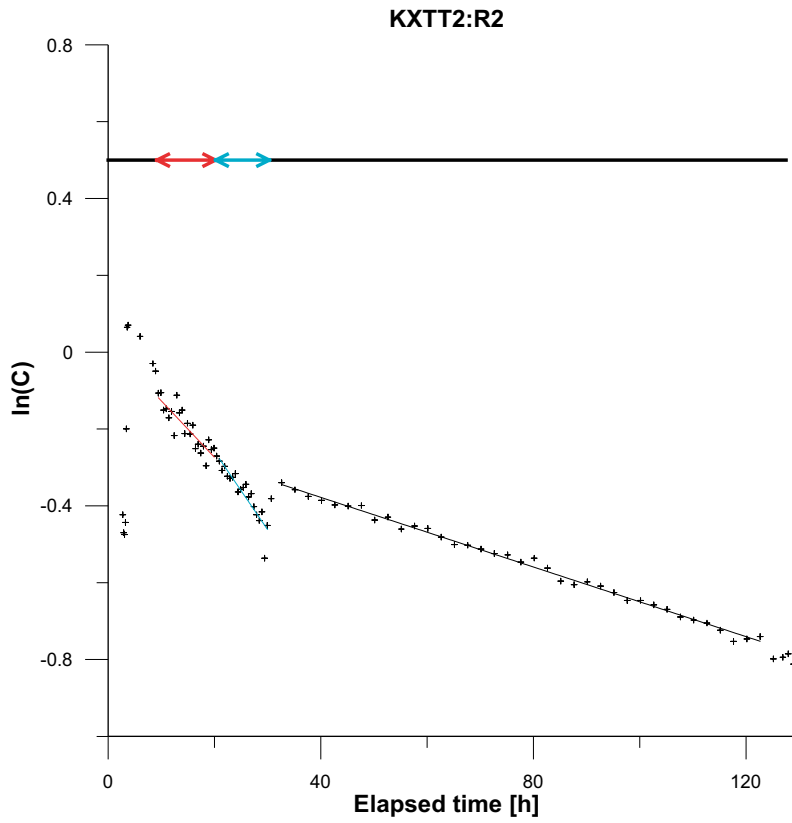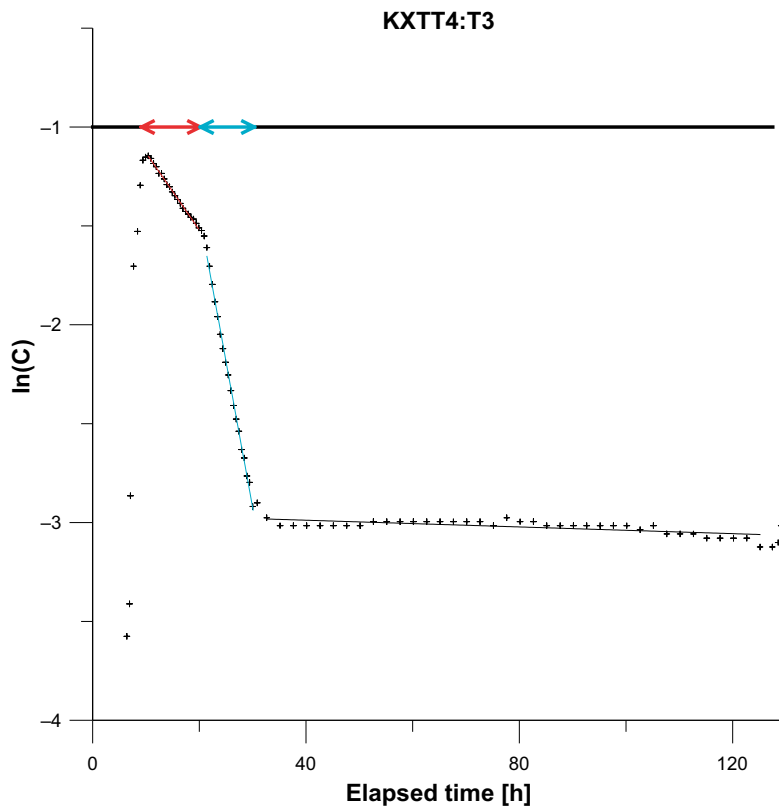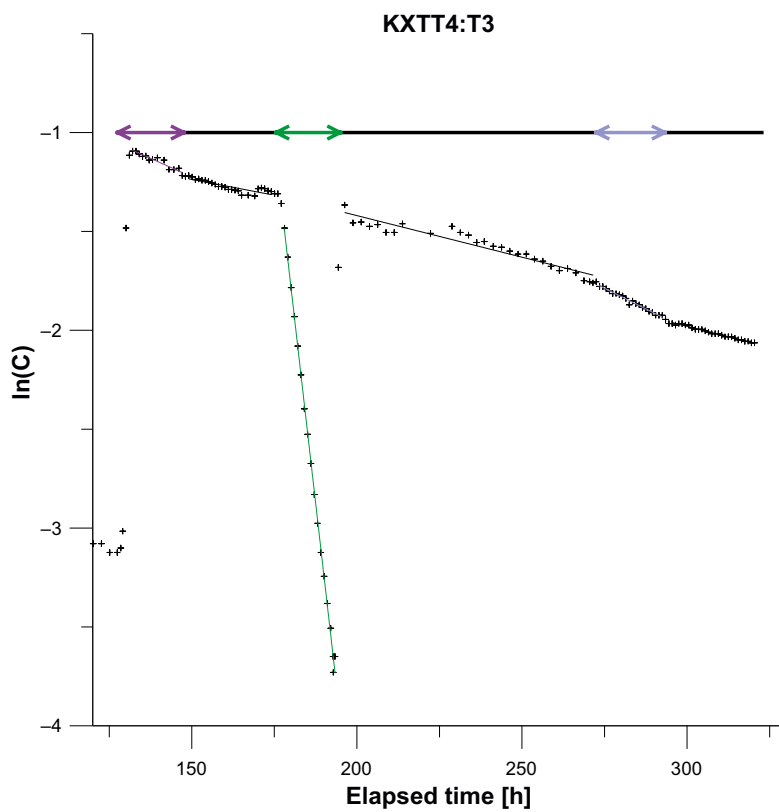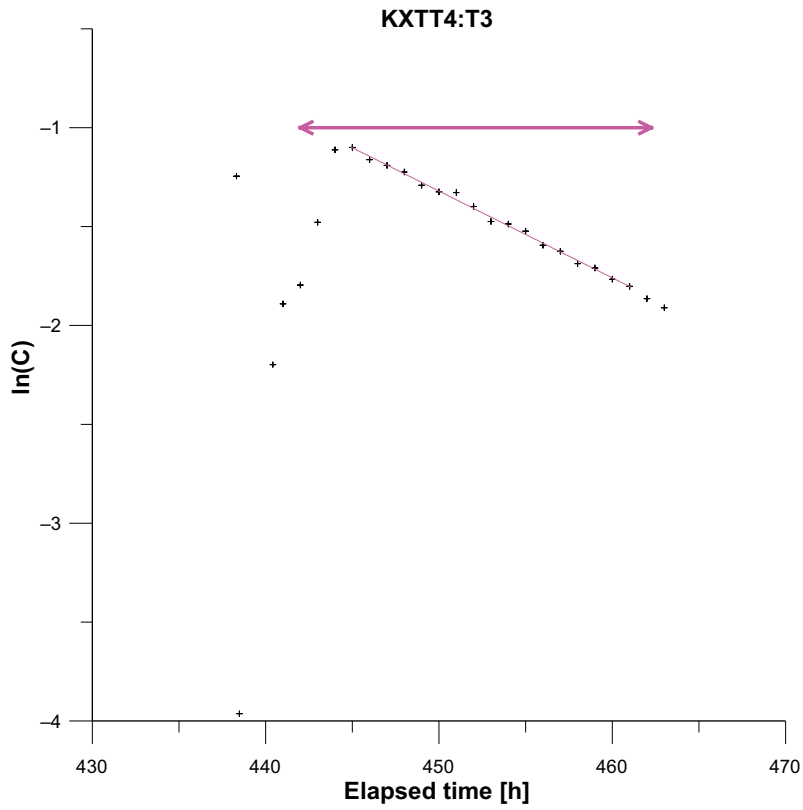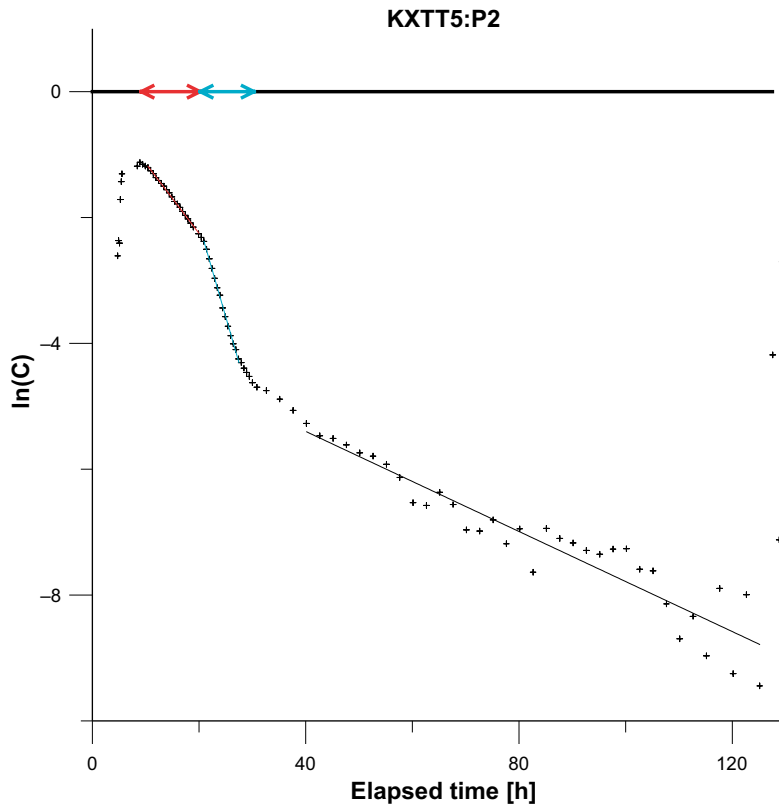
Figure A2-4. *Uranine concentration in KXTT2:R2 between 0 and 130 h. Fit to pumping periods in KXTT3 and undisturbed period #2.*
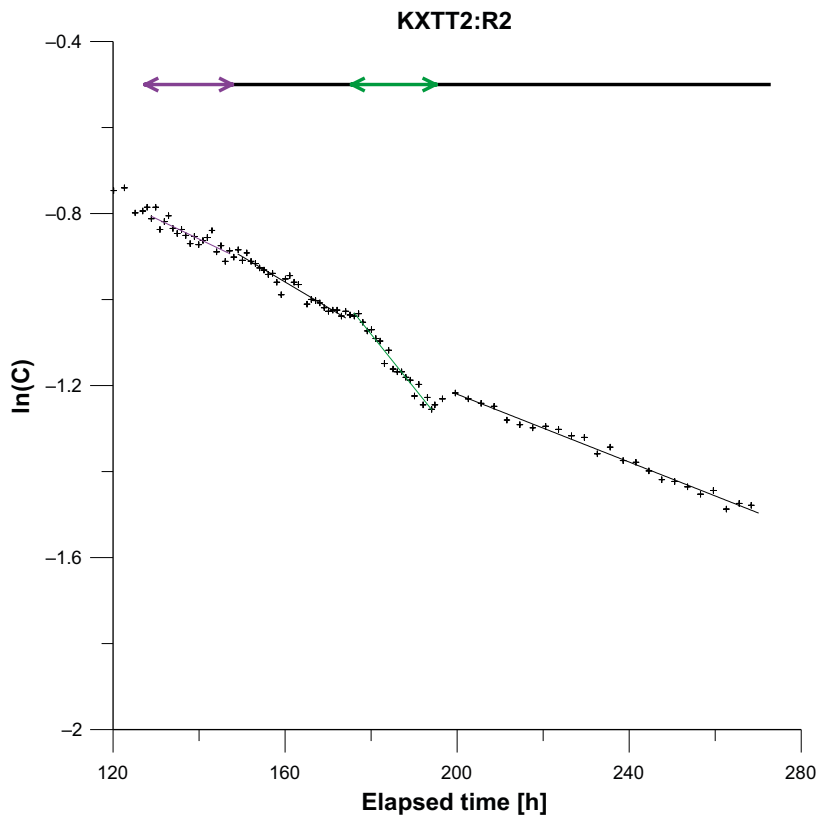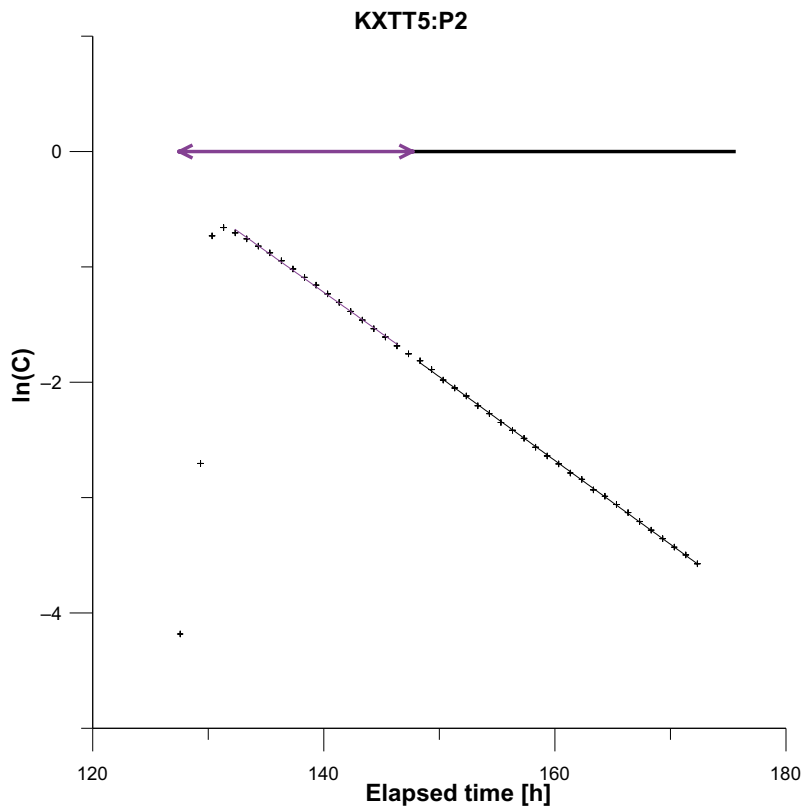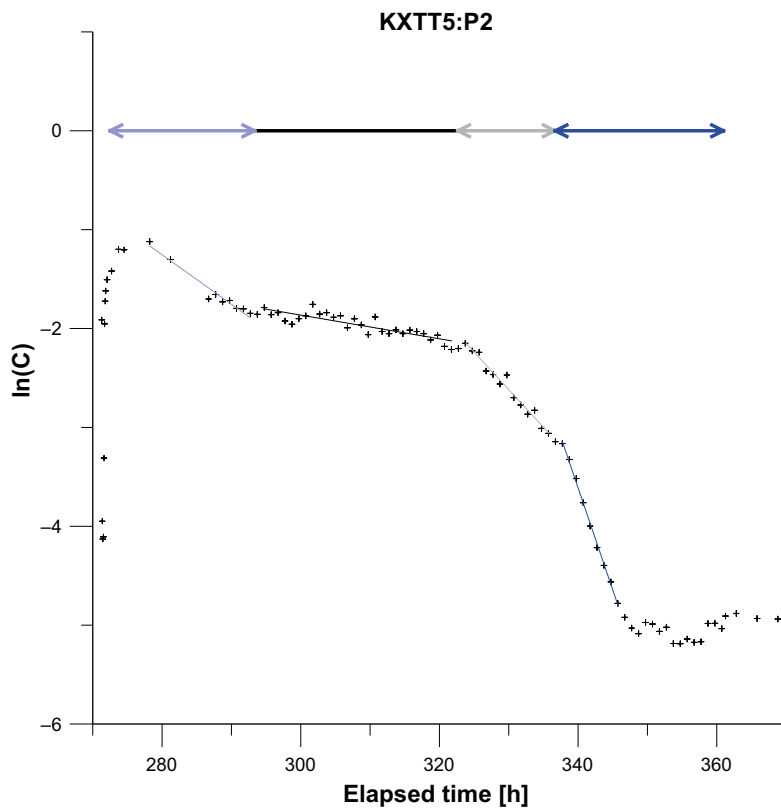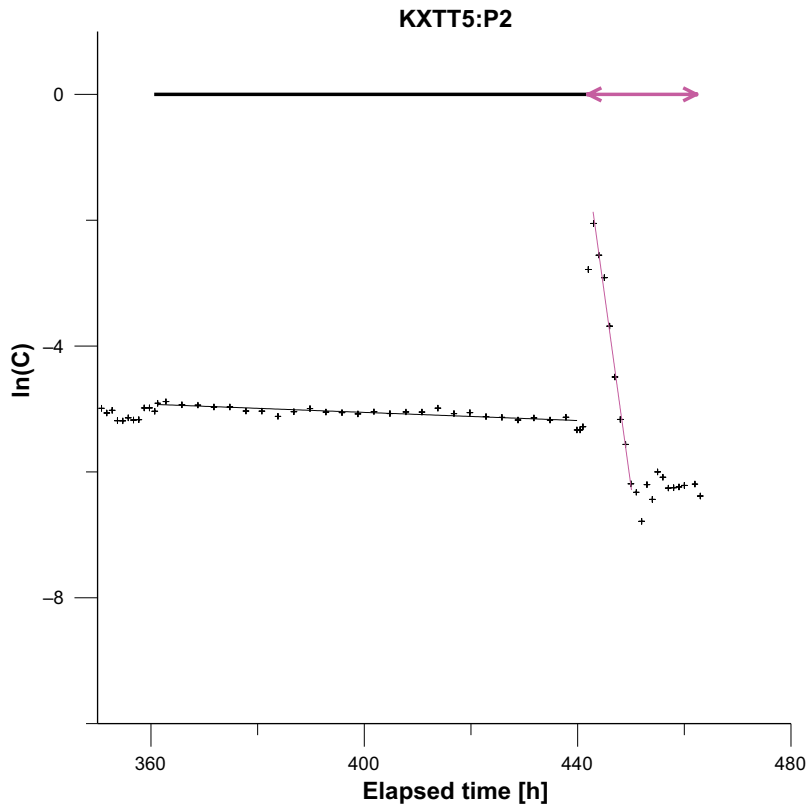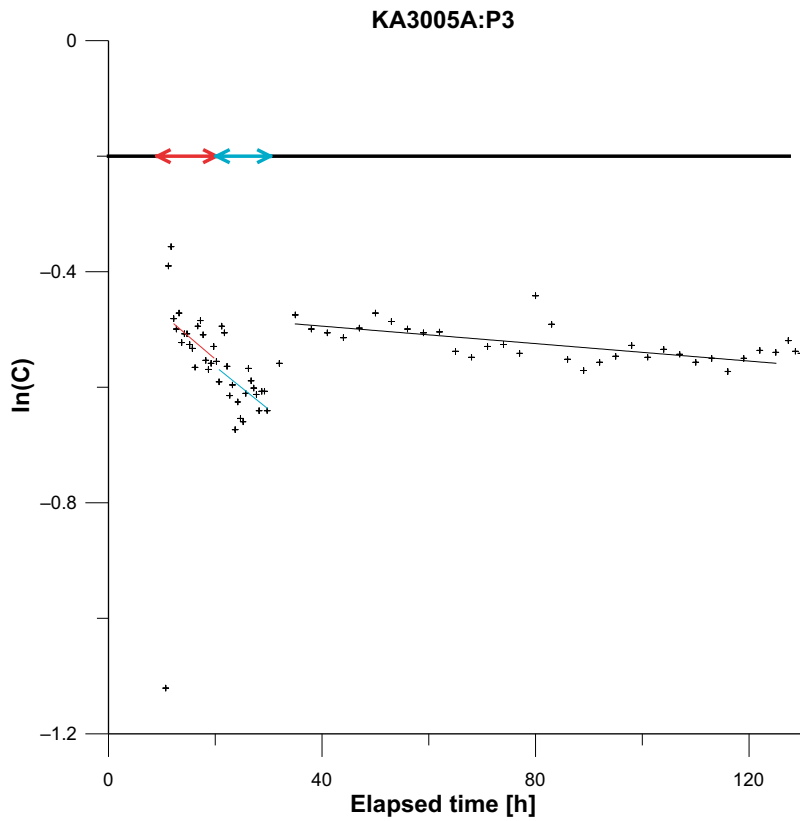

Figure A2-5. *Uranine concentration in KXTT2:R2 between 120 and 280 h. Fit to pumping periods in KXTT1 and KXTT5 and undisturbed period #3 and #4.*
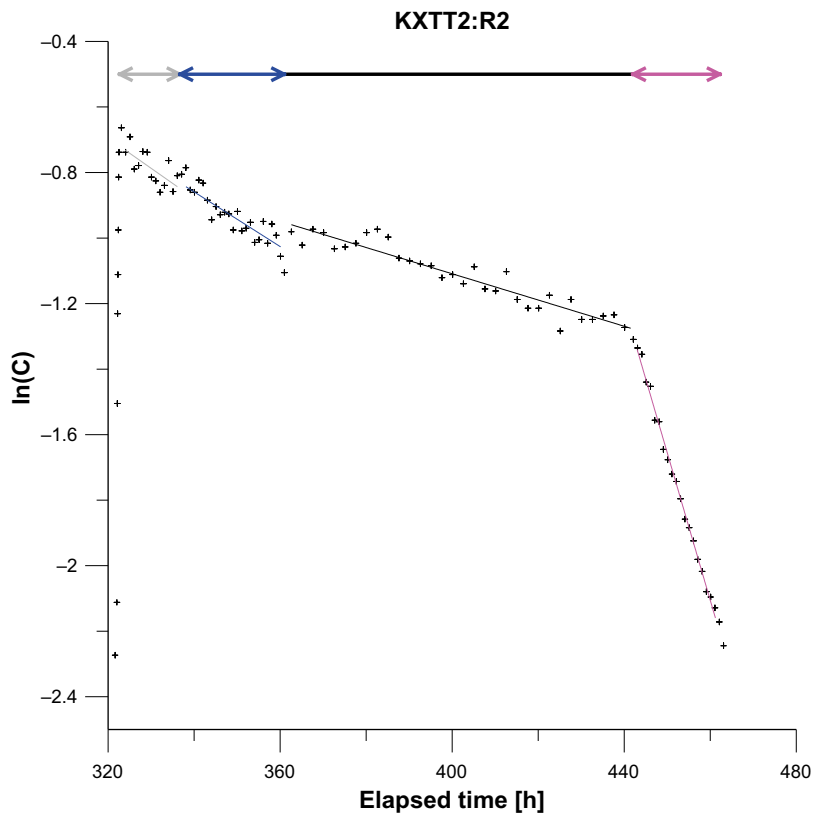
Figure A2-6. *Uranine concentration in KXTT2:R2 between 320 and 480 h. Fit to pumping periods in KXTT4 and KA3005A and undisturbed period #6.*
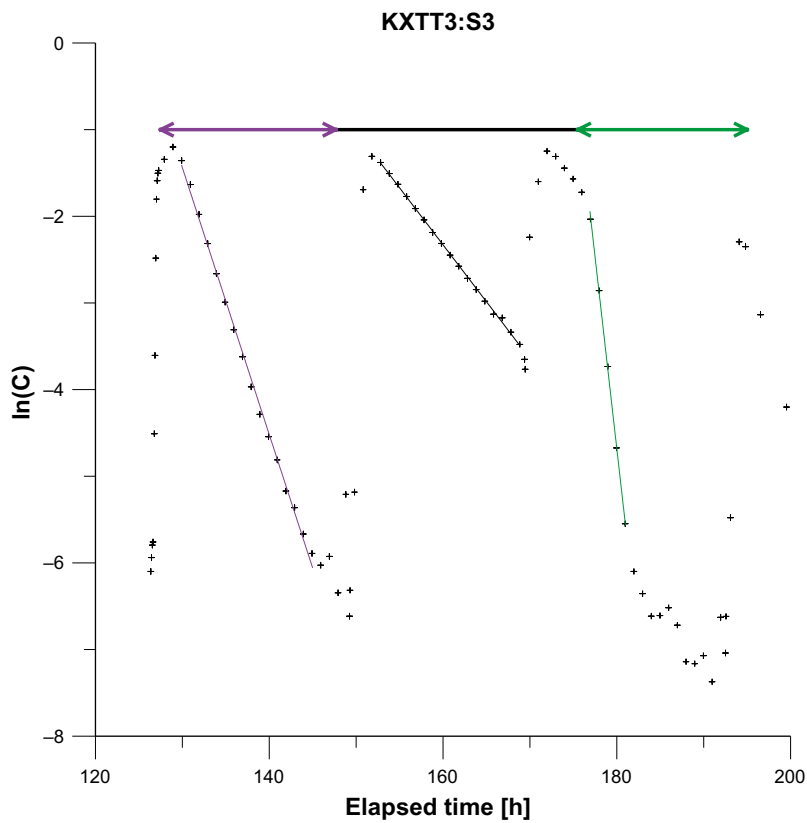
Figure A2-7. *Uranine concentration in KXTT3:S3 between 120 and 200 h. Fit to pumping periods in KXTT1 and KXTT5 and undisturbed period #3.*
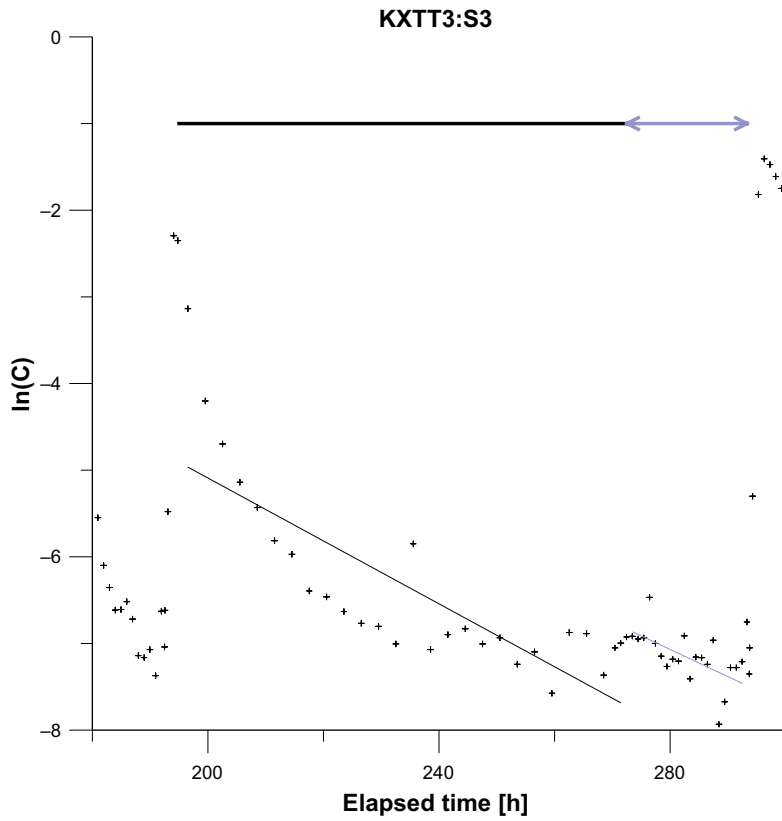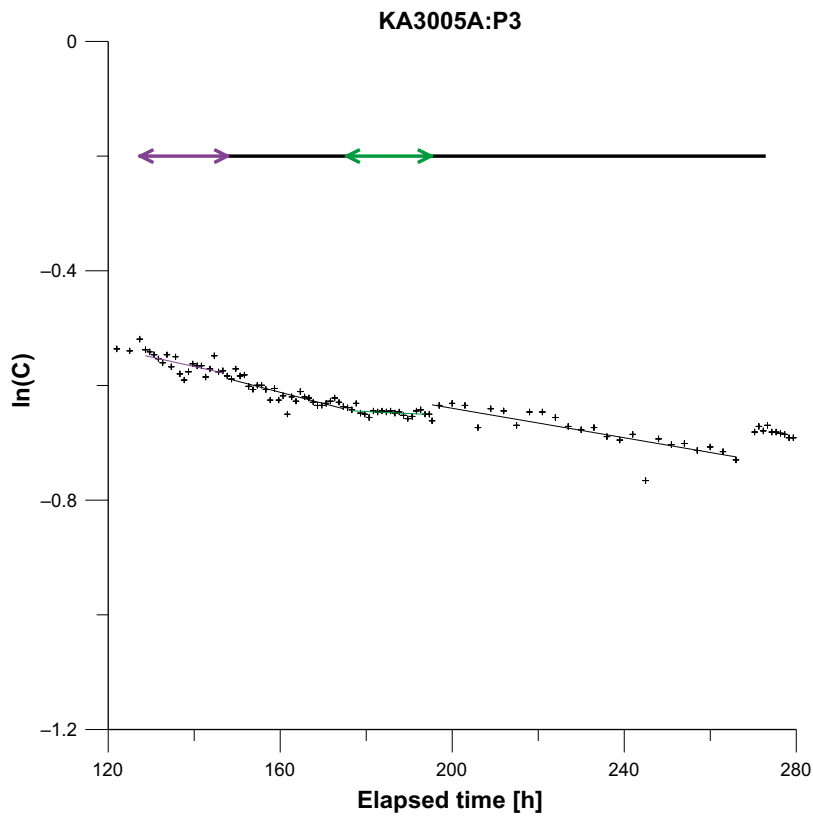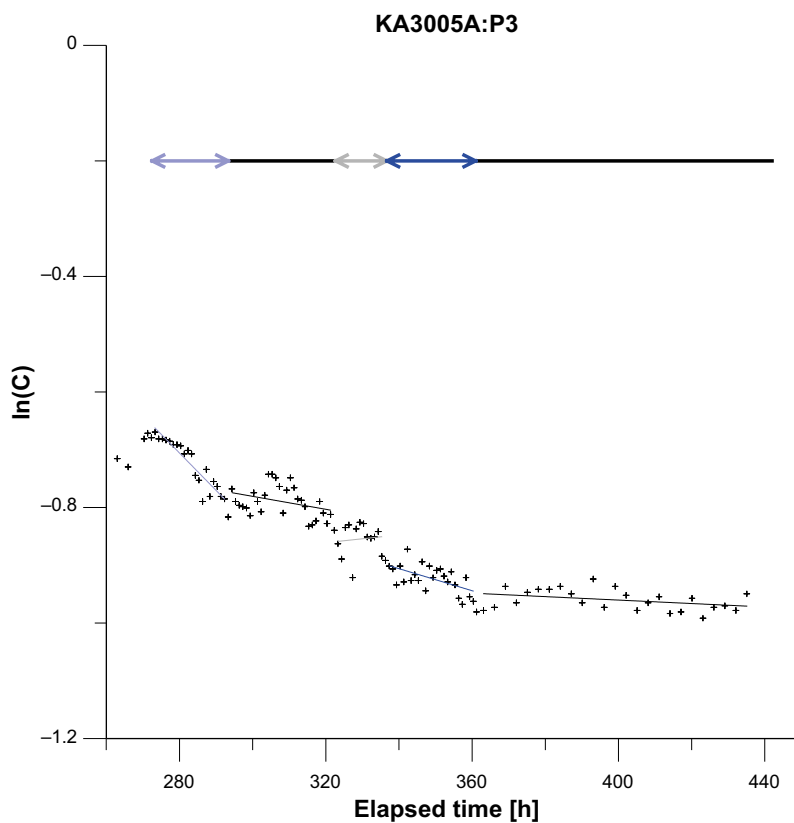
Figure A2-8. *Uranine concentration in KXTT3:S3 between 180 and 300 h. Fit to pumping period in KXTT2 and undisturbed period #4.*
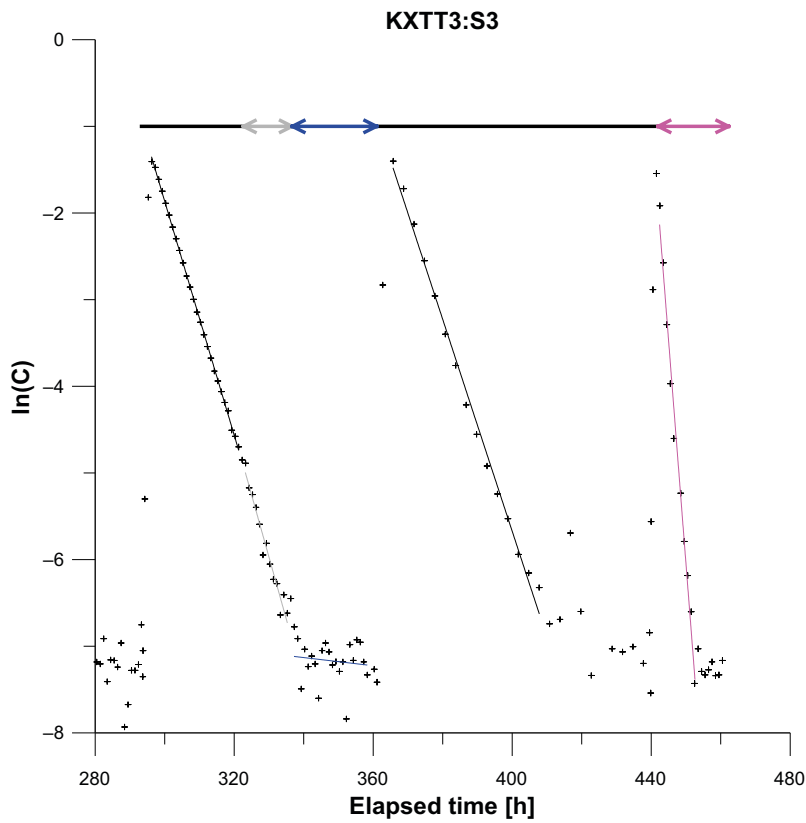
Figure A2-9. *Uranine concentration in KXTT3:S3 between 280 and 480 h. Fit to pumping periods in KXTT4 andKA3005A and undisturbed periods #5 and #6.*

Figure A2-10. *Uranine concentration in KXTT4:T3 between 0 and 130 h. Fit to pumping periods in KXTT3 and undisturbed period #2.*

Figure A2-11. *Uranine concentration in KXTT4:T3 between 120 and 330 h. Fit to pumping periods in KXTT1, KXTT5 and KXTT2 and undisturbed period #3, #4 and #5.*

Figure A2-12. *Uranine concentration in KXTT4:T3 between 430 and 470 h. Fit to pumping period in KA3005A.*

Figure A2-13. *Uranine concentration in KXTT5:P2 between 0 and 130 h. Fit to pumping periods in KXTT3 and undisturbed period #2.*

Figure A2-14. *Uranine concentration in KXTT5:P2 between 120 and 180 h. Fit to pumping period in KXTT1 and undisturbed period #3.*

Figure A2-15. *Uranine concentration in KXTT5:P2 between 270 and 370 h. Fit to pumping periods in KXTT2 and KXTT4 and undisturbed period #5.*

Figure A2-16. *Uranine concentration in KXTT5:P2 between 350 and 480 h. Fit to pumping period in KA3005A and undisturbed period #6.*

Figure A2-17. *Uranine concentration in KA3005A:P3 between 0 and 130 h. Fit to pumping periods in KXTT3 and undisturbed period #2.*

Figure A2-18. *Uranine concentration in KA3005A:P3 between 120 and 280 h. Fit to pumping periods in KXTT1 and KXTT5 and undisturbed periods #3 and #4.*

Figure A2-19. *Uranine concentration in KA3005A:P3 between 270 and 450 h. Fit to pumping periods in KXTT2 and KXTT4 and undisturbed period #5 and #6.*

Feature A

Table A3-1. Calculated intercepts of Feature A at the TRUE-1 site. The coordinates are given in the Äspö96 system.

Borehole	Borehole length [m]	Northing [m]	Easting [m]	Elevation [m]
KXTT1	15.79	7,435.26	2,323.26	–403.41
KXTT2	15.04	7,432.78	2,323.80	–402.96
KXTT3	14.10	7,438.01	2,321.43	–399.54
KXTT4	12.10	7,433.66	2,322.30	–398.28
KXTT5	9.71	7,435.83	2,320.55	–392.81
KA3005A	44.97	7,430.01	2,324.72	–403.39

Table A3-2. Calculated distances between intercepts of Feature A in boreholes at the TRUE-1 site.

Distance [m]	KXTT1	KXTT2	KXTT3	KXTT4	KXTT5	KA3005A
KXTT1		2.58	5.09	5.46	10.95	5.46
KXTT2	2.58		6.69	4.99	11.09	2.95
KXTT3	5.09	6.69		4.61	7.13	9.47
KXTT4	5.46	4.99	4.61		6.14	6.73
KXTT5	10.95	11.09	7.13	6.14		12.78
KA3005A	5.46	2.95	9.47	6.73	12.78	

Dilution tests during SWIW test 2
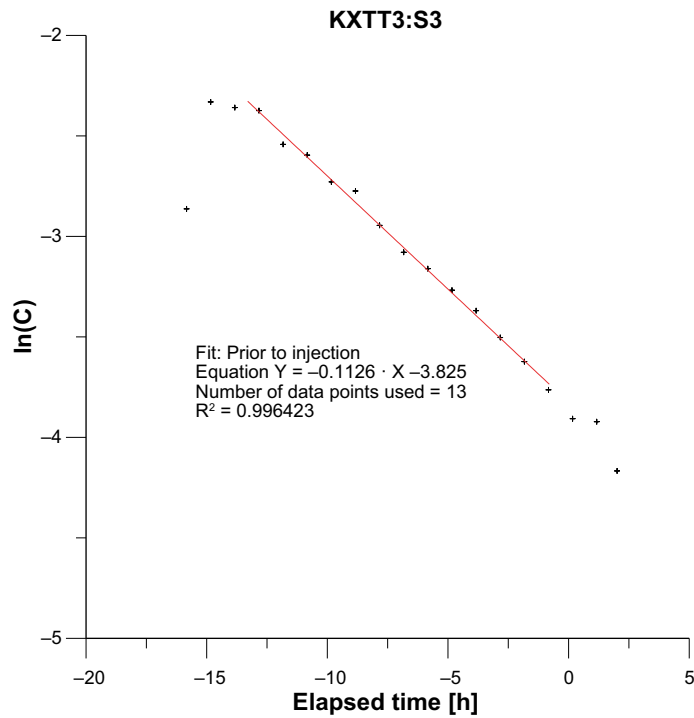
Figure A4-1. *Rhodamine WT concentration in KXTT3:S3 prior to injection in KXTT4:T3.*
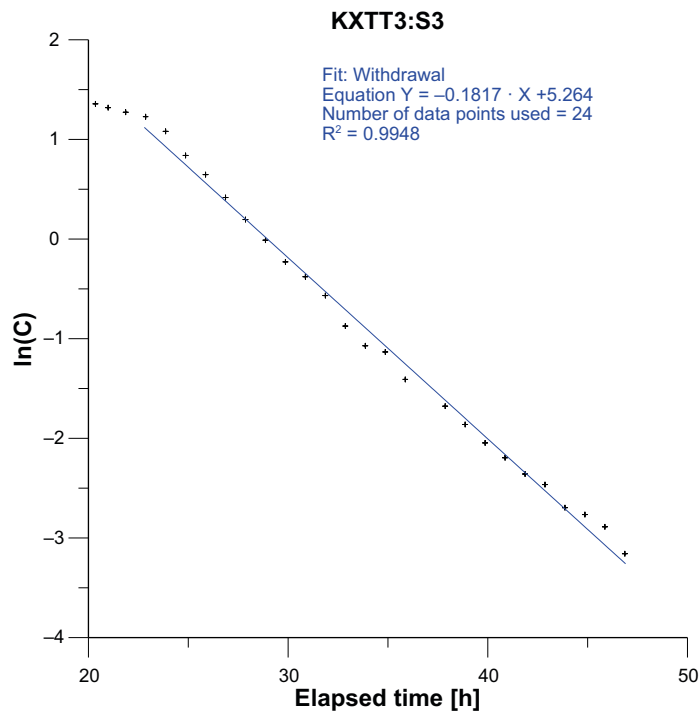

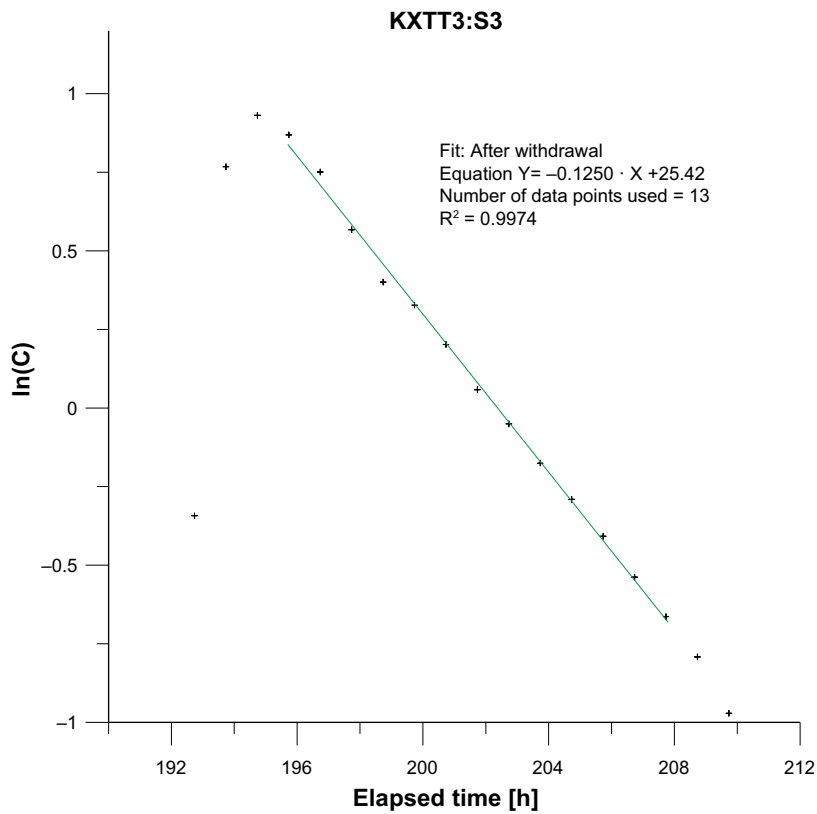*Figure A4-2.* *Rhodamine WT concentration in KXTT3:S3 during withdrawal in KXTT4:T3.*

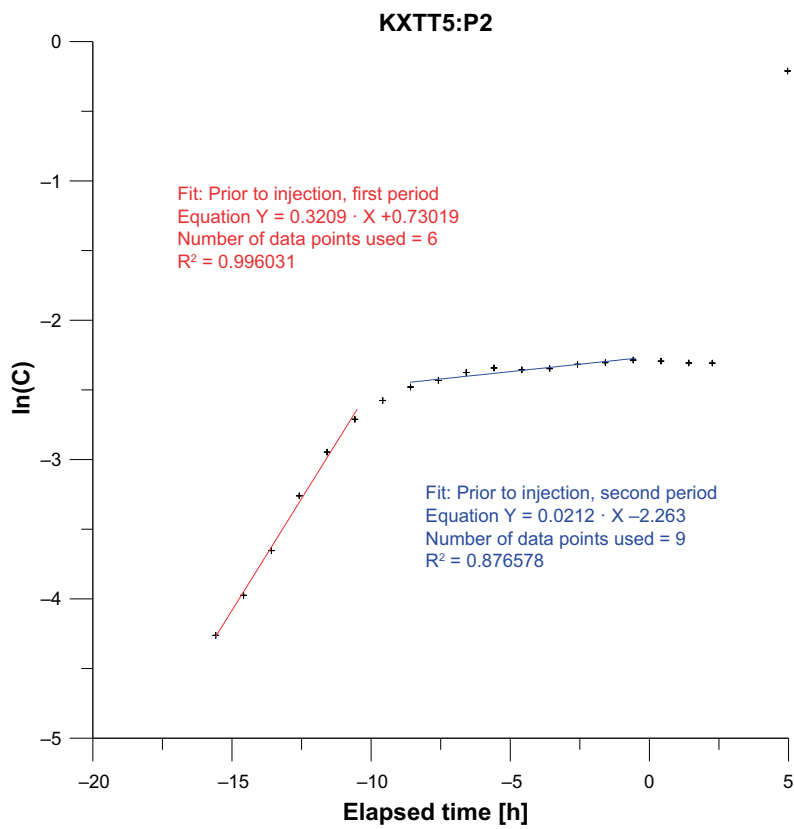**Figure A4-3.** *Rhodamine WT concentration in KXTT3:S3 after withdrawal in KXTT4:T3.*

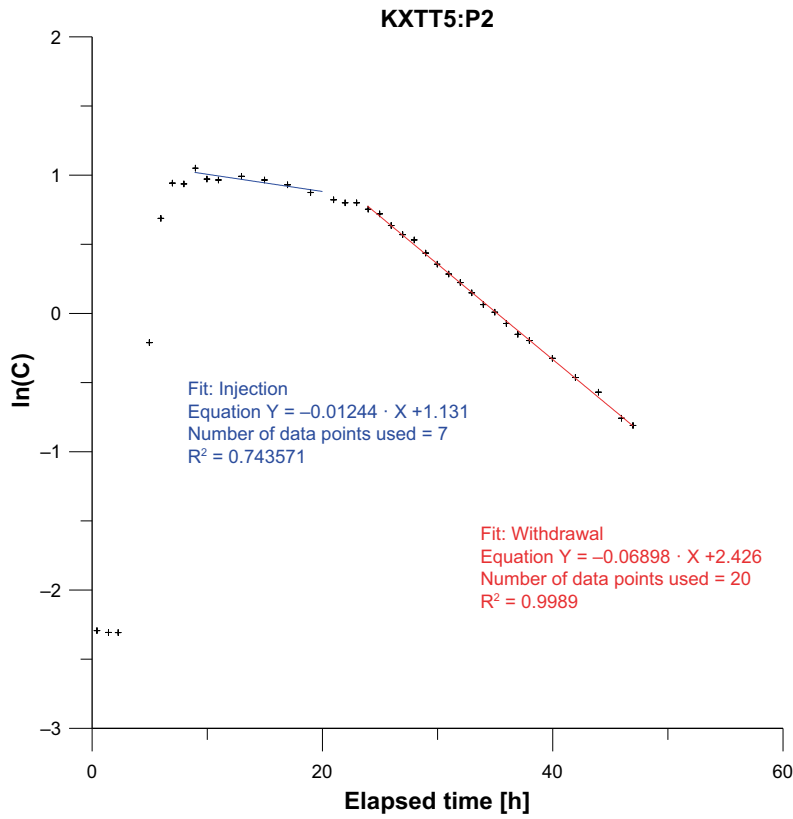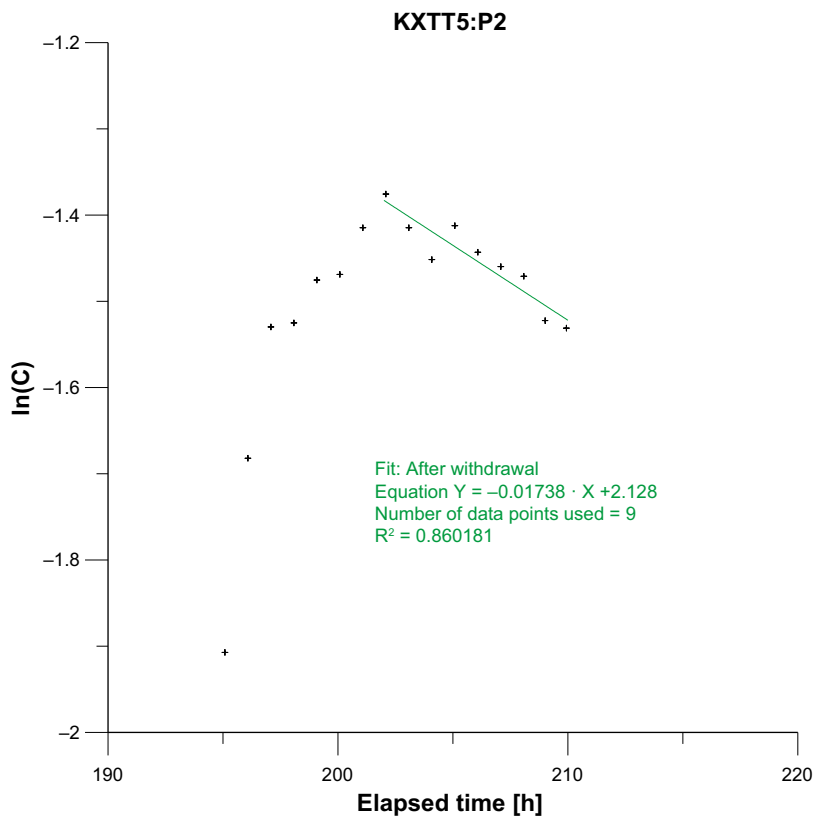**Figure A4-4.** *Rhodamine WT concentration in KXTT5:P2 prior to injection in KXTT4:T3.*

Figure A4-5. *Rhodamine WT concentration in KXTT5:P2 during injection and withdrawal in KXTT4:T3.*

Figure A4-6. *Rhodamine WT concentration in KXTT5:P2 during after withdrawal in KXTT4:T3.*
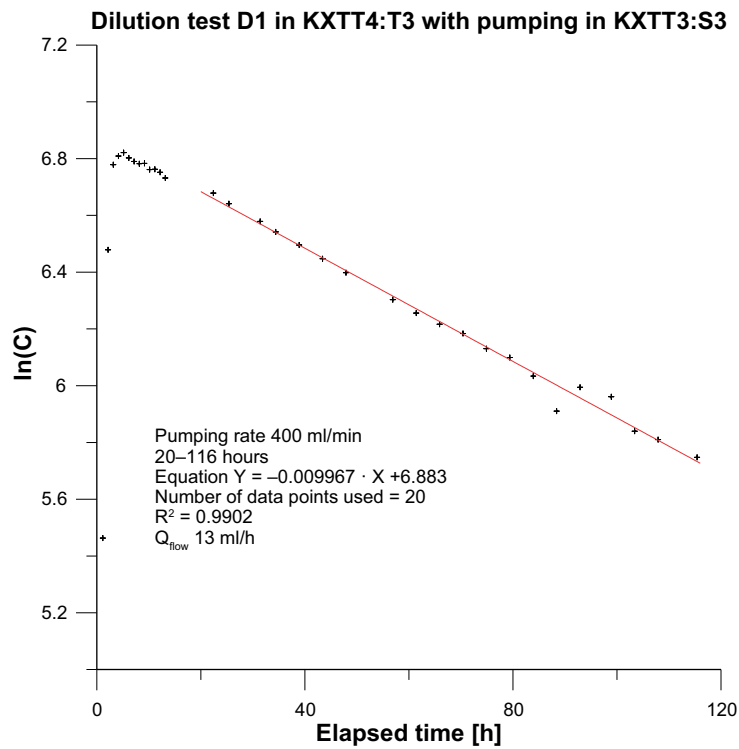
CEC pre tests D1, D2 and D3

Figure A5-1. *Dilution test D1. AminoG concentration in KXTT4:T3 while pumping in KXTT3:S3.*
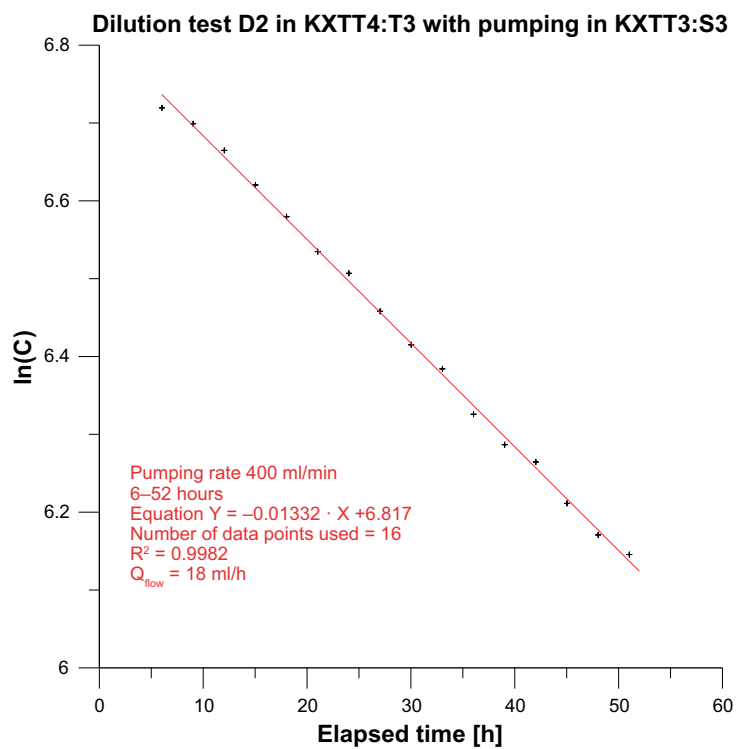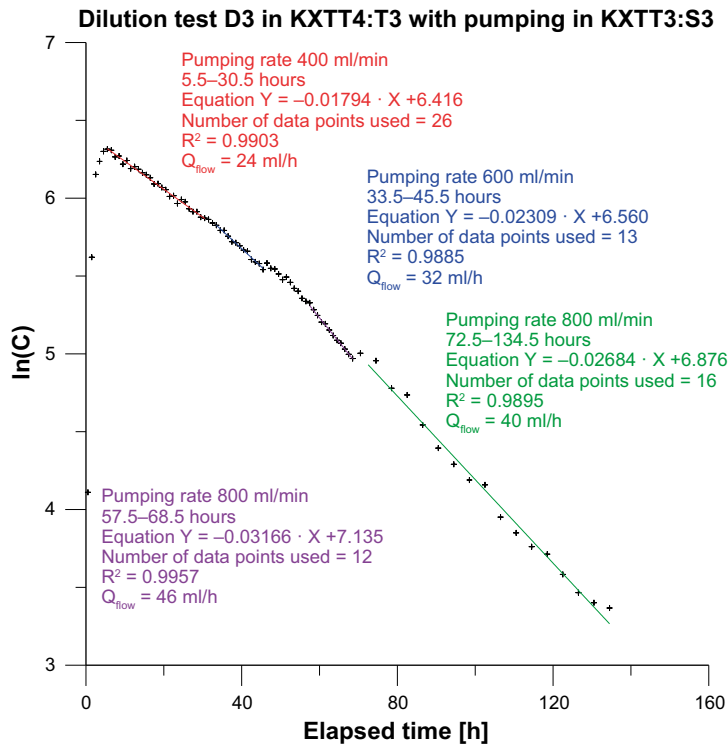

Figure A5-2. *Dilution test D2. AminoG concentration in KXTT4:T3 while pumping in KXTT3:S3.*

Figure A5-3. *Dilution test D3. Rhodamine WT concentration in KXTT4:T3 while pumping in KXTT3:S3.*